

# Nutrition's Route to Behaviour and Vice Versa: Longitudinal Links from Early Life to Adolescence



Yvonne Willemsen



# **Nutrition's Route to Behaviour and Vice Versa: Longitudinal Links from Early Life to Adolescence**

Yvonne Willemsen



This publication has been made possible by the European Union's Horizon 2020 research and innovation programme.

Author: Nishant Joshi

Title: Working Title

Radboud Dissertations Series ISSN: 2950-2772 (Online); 2950-2780 (Print)

Published by RADBOUD UNIVERSITY PRESS

Postbus 9100, 6500 HA Nijmegen, The Netherlands

[www.radbouduniversitypress.nl](http://www.radbouduniversitypress.nl)

Design: Nishant Joshi

Cover: TBD

Printing: DPN Rikken/Pumbo

ISBN: 9789493296374

DOI: 10.54195/ 9789493296374

Free download at: [www.boekenbestellen.nl/radboud-university-press/dissertations](http://www.boekenbestellen.nl/radboud-university-press/dissertations)

© Nishant Joshi, 2025

**RADBOUD  
UNIVERSITY  
PRESS**

This is an Open Access book published under the terms of Creative Commons Attribution-Noncommercial-NoDerivatives International license (CC BY-NC-ND 4.0). This license allows reusers to copy and distribute the material in any medium or format in unadapted form only, for noncommercial purposes only, and only so long as attribution is given to the creator, see <http://creativecommons.org/licenses/by-nc-nd/4.0/>.

# **Nutrition's Route to Behaviour and Vice Versa: Longitudinal Links from Early Life to Adolescence**

Proefschrift ter verkrijging van de graad van doctor  
aan de Radboud Universiteit Nijmegen  
op gezag van de rector magnificus prof. dr. J.M. Sanders,  
volgens besluit van het college voor promoties  
in het openbaar te verdedigen op

maandag 15 april 2024  
om 16:30 uur precies

door

Nishant Joshi  
geboren op 26 January 1994  
te Varanasi, India

**Promotor:**

Prof. dr. T. Celikel

**Copromotoren:**

Dr. F. Zeldenrust

**Manuscriptcommissie:**

TBD.

TBD.

TBD.

TBD.

TBD.

## **Funding**

This project has received funding from the European Union's Horizon 2020 research and innovation program under the Marie Skłodowska-Curie grant agreement No 860949.



# Table of Contents

<b>Chapter 1</b>	<b>General Introduction</b>	<b>9</b>
<b>Chapter 2</b>	<b>Neuronal Identity is Not Static—An Input-Driven Perspective</b>	<b>21</b>
<b>Chapter 3</b>	<b>Neuromodulatory Control of Cortical Function: Cell-Type Specific Reshaping of Neuronal Information Transfer</b>	<b>71</b>
<b>Chapter 4</b>	<b>Heterogeneity in delay and timescales improves task Performance</b>	<b>99</b>
<b>Chapter 5</b>	<b>General Discussion</b>	<b>105</b>
<b>Chapter 6</b>	<b>Supplementary Materials</b>	<b>121</b>
<b>Chapter 7</b>	<b>Appendices</b>	<b>167</b>



# **Chapter 1**

## **General Introduction**

## **Understanding Neuronal Function in a Dynamic Brain**

The mammalian brain is an extraordinarily complex organ, composed of an immense variety of neuronal cell types. This diversity is evident across multiple dimensions:

### **Morphology**

Neurons differ dramatically in their shapes and structures. Some, like pyramidal neurons, exhibit long apical dendrites and a characteristic triangular soma, while others, such as interneurons, display more compact and intricate branching patterns. These morphological differences are closely linked to the specific roles neurons play within neural circuits.

### **Electrophysiology**

Neuronal diversity is also reflected in the ways neurons generate and propagate electrical signals. Different neurons exhibit distinct firing patterns, action potential shapes, and responses to synaptic input. For instance, some neurons are fast-spiking, while others display adapting or bursting firing patterns. These electrophysiological properties are determined by the unique composition of ion channels and receptors expressed by each neuron.

### **Gene Expression**

Advances in molecular biology have revealed that neurons can be distinguished by their gene expression profiles. Single-cell RNA sequencing has enabled researchers to catalog the transcriptomes of individual neurons, uncovering a rich landscape of molecular identities. These profiles often correlate with, but are not strictly determined by, morphological and electrophysiological features.

## Connectivity

Neurons are further defined by their patterns of connectivity—both the sources of their inputs and the targets of their outputs. Some neurons form long-range projections across brain regions, while others participate in local microcircuits. The connectivity matrix of the brain is thus shaped by the diversity of its neuronal components.

## Traditional Classification Approaches

Historically, neuroscientists have sought to classify neurons into discrete “types” based on intrinsic, relatively stable characteristics. Early classification schemes focused on observable features such as soma size, dendritic arborization, and axonal projections. With the advent of intracellular recording techniques, electrophysiological properties like spike shape, firing rate, and synaptic integration became central to neuronal taxonomy. More recently, molecular markers—such as the expression of specific neurotransmitters, calcium-binding proteins, or transcription factors—have been used to further refine neuronal classifications.

The underlying assumption in many of these approaches is that each neuron possesses a fixed identity: a stable set of features that persists across time and context. This has led to the widespread use of terms like “cell type” and “canonical neuron,” suggesting a degree of invariance in neuronal identity.

## Large-Scale Taxonomy Initiatives

In the past decade, large-scale collaborative efforts have sought to systematically map and classify the full diversity of neurons in the brain. Notable among these are the Allen Institute for Brain Science’s Cell Types Program and the BRAIN Initiative Cell Census Network (BICCN). These projects leverage cutting-edge techniques—including high-throughput single-cell transcriptomics, large-scale electrophysiological recordings, and high-resolution imaging—to build comprehensive taxonomies of neuronal types.

While these initiatives have greatly expanded our understanding of neuronal diversity, they often operate under the assumption that neuronal identity is static and can be captured by a fixed set of features. However, emerging evidence suggests that neuronal identity may be more dynamic and context-dependent than previously thought, raising important questions about how best to define and classify the brain's myriad cell types.

## Limitations of Static Neuronal Classification

- 1. The Influence of Input and Network State on Neuronal Function** Recent experimental and computational efforts have increasingly pointed towards the idea that a neuron's functional role is not solely determined by its intrinsic static properties such as morphology, gene expression, or ion channel dynamics but also by the nature of the input it receives and its dynamic state within a circuit. Neurons operate within continuously changing environments, receiving temporally structured synaptic input that reflects sensory stimuli, behavioral demands, and ongoing internal activity. These inputs interact with intrinsic biophysical parameters in complex ways, such that the same neuron may perform different computational roles depending on the input regime or network context. Additionally, neuromodulatory systems (e.g., dopaminergic and cholinergic pathways) further reconfigure neuronal function in a cell-type- and receptor-specific manner, modulating excitability, gain, adaptation, and stimulus selectivity. This context-dependence challenges the classical view of neurons as fixed computational units.
- 2. Limitations of Static Characterization Protocols** Conventional approaches to neuronal classification typically rely on static stimulation protocols, such as step-and-hold current injections, to derive electrophysiological signatures. While these protocols offer insights into baseline excitability and passive membrane properties, they do not capture the complex temporal filtering or nonlinear input-output

transformations that neurons perform under more realistic, time-varying conditions. In naturalistic settings, neuronal input is dynamic, high-dimensional, and often stochastic features that are absent in traditional measurements. As a result, static protocols risk underestimating or mis-characterizing the functional capabilities of neurons, potentially leading to oversimplified or misleading classifications. This disconnect highlights the need for stimulus-rich paradigms, such as frozen noise inputs or *in vivo* recordings, that better approximate the computational demands faced by neurons *in situ*.

3. **Neuronal Identity as an Emergent, Dynamic Construct** Taken together, these observations point toward a new conceptual framework in which neuronal identity is not a fixed property, but rather a context-sensitive, emergent phenomenon. If neuronal function can be reshaped by synaptic input, neuromodulatory state, and network dynamics, then identity must be understood as fluid and multidimensional, rather than static and categorical. This dynamic view aligns with recent findings showing that neurons shift their classification depending on the input stimulus or modulatory condition. It also suggests that functional heterogeneity in neural populations is not simply biological variability, but may reflect adaptive specialization to a range of computational roles. In this thesis, I explore this emergent view by analyzing how neurons reorganize their functional attributes under different input regimes and neuromodulatory conditions, using high-dimensional clustering and integrative analysis across multiple feature domains. This work contributes to a growing shift in neuroscience: from static taxonomies to dynamic, functionally grounded models of neuronal identity.
4. **Rich high-dimensional functional space remains unexplored** Neurons functional space is high dimensional but most electrophysiological classification only consider one feature at a time for separability. This leads to an incomplete pic-

ture of functional heterogeneity. As we have discussed before, stimulus protocols have a strong role to play in features that can actually be extracted. For example a static input protocol doesn't expose the subthreshold potential dynamics of a neuron, similar properties related to action potential are a function of input protocol. Clustering based on these features typically involves looking at low dimensional (1-3 dimensions) feature space using a method such as K-means clustering. This approach underestimates the rich functional space in which neurons function and thus clustering based on functional properties needs methods that utilize multiple features pertaining to function simultaneously and provide a richer overview of functional heterogeneity.

5. **No consensus on properties that are the most informative about heterogeneity** While neurons have been categorized based active and passive features there is no consensus on properties or a set of properties that are the most informative about heterogeneity. While most classification studies focus on passive properties such as capacitance or conductance of the cell or active properties such as firing rates and inter-spike intervals, there are no studies that compare neuronal heterogeneity based on different sets of properties and provide a consensus for the field. Moreover, the properties extracted are limited by the stimulation protocol, therefore we must first establish the input protocol that is most suitable for studying a neuronal population and then compare properties extracted in each protocol to provide a consensus.

## Neuromodulation: Reconfiguring Neural Computation

Neuromodulatory systems particularly those involving dopamine and acetylcholine play a critical role in shaping brain states associated with attention, learning, memory, and pathology. Rather than directly triggering spikes, these modulators reshape how neurons respond to input, modulating intrinsic excitability and synaptic integration. Their

effects are often receptor and cell-type-specific, suggesting a finely tuned mechanism for reconfiguring the computational landscape of cortical networks.

Despite extensive behavioral and molecular work, the functional impact of neuromodulation on neuronal computation remains poorly understood, especially at the level of high-dimensional feature interactions. Are neuromodulatory effects isolated to individual electrophysiological features, or do they act in a coordinated manner to restructure how neurons encode information?

- **Effect of neuromodulation on computation** Much is known about molecular and excitability changes caused by dopamine and acetylcholine modulation in single neurons. Though it is still unclear how this alteration changes what neurons compute. Since neurons relay information within a network, it is unclear how dopamine and acetylcholine changes information transfer in neurons. Since activity of individual neurons determine that state of a network, it is clear that understanding alteration in transferred information due to neuromodulation would explain a lot about how cortical circuits are modulated.
- **Hetero modulation in neuronal population** A given population of neuron comprises of individuals or sub-groups of neurons that differ from each other in terms of their shape and ion-channel type and distribution. It is still unclear how this individual variability manifests itself on a circuit scale. While it is known that this heterogeneity provides flexibility to the circuit (cite), the effect of neuromodulation on this individuality is still unclear. More precisely, it is unknown if all functional parameters are altered uniformly or there exists a heterogeneity in terms of properties that are altered due to specific modulation and what are population level effects of neuromodulation.
- **Reconfiguration under the influence of dopamine and acetylcholine** Most studies that focus on neuromodulation of individual neurons, focus on how indi-

vidual active or passive properties such as firing rate or conductance is altered due to a specific receptor activation. Neuronal functional space is high dimensional, while it is important to study how individual properties are altered due to neuromodulation, it is also important to study how this high-dimensional functional space is altered due to neuromodulation, that requires looking at correlation structure between active and passive properties and how this structure changes due to neuromodulation.

## Research Objectives and Key Questions

This thesis addresses two overarching questions:

### 1. How does input context influence functional classification of neurons?

In Chapter 2, we demonstrate that neuronal identity is *not static*, but *input-dependent*, with classification outcomes varying significantly under dynamic (frozen noise) vs static (step-and-hold) stimuli. This challenges the notion of fixed electrophysiological types and highlights the role of stimulus structure in shaping neural function.

### 2. How does neuromodulation alter the functional landscape of neurons?

In Chapter 3, we explore how activation of dopaminergic (D1-R, D2-R) and cholinergic (M1-R) receptors *reconfigures information encoding*, shifting the balance between shared and private variance across feature domains. We show that *neuromodulatory effects are highly cell-type and receptor-specific*, modulating not just individual attributes but also their coordination.

## Experimental Framework and Approach

For answering the research questions stated above, this thesis utilizes single unit in-vitro recordings from the somatosensory cortex layer 2/3. These recordings were performed

in tandem, first using a static step and hold input protocol and later with a frozen noise protocol. Within each input protocol, neurons were first recorded in a vehicle control (artificial cerebral spinal fluid - aCSF) condition and a drug condition, where a specific receptor agonist is added to the bath and the recording is performed again. Some times multiple control and drug trials are performed for a single neuron.

## **Input Protocols**

### **Step and Hold**

The step-and-hold protocol is a widely used electrophysiological method for characterizing neuronal properties through controlled current injections. In this protocol, a neuron's membrane potential is maintained at a baseline value (commonly around -70 mV), and then a series of incremental current steps are injected, each lasting for a fixed duration—typically 500 ms—with recovery periods (e.g., 5.5 seconds) between steps. The current amplitude is increased in defined increments (e.g., 40 pA per step), allowing researchers to observe how the neuron responds to increasing levels of depolarizing input, including changes in firing rate, spike threshold, and other action potential characteristics. This approach enables the classification of neurons (such as distinguishing excitatory from inhibitory cells) and the assessment of properties like maximum firing frequency, spike latency, and after-hyperpolarization. The step-and-hold protocol thus provides a standardized way to probe intrinsic excitability and firing dynamics, serving as a foundational tool in cellular neurophysiology.

### **Frozen Noise**

The frozen noise protocol, introduced by (cite), is a method designed to quantify the mutual information between a neuron's input and its spike train output in electrophysiological experiments. This protocol generates a time-varying input current by simulating the activity of a presynaptic neural network of 1,000 neurons, each firing Poisson spike

trains in response to a binary "hidden state" (a Markov process representing the presence or absence of an external stimulus). The injected current is "frozen," meaning the same input sequence is used across trials or conditions, enabling direct comparison of neuronal responses. By analyzing how the recorded neuron transforms this structured input into spikes, researchers can calculate the information-theoretic relationship between the hidden state and the output spike train. This approach overcomes limitations of traditional step-and-hold protocols by mimicking naturalistic synaptic input patterns while maintaining experimental control, allowing efficient bias-free information quantification with short (3–6 minute) recordings. The protocol's output includes the injected current trace, hidden state timeline, and voltage response, facilitating both forward modeling of neuronal dynamics and reverse-engineering of coding principles.

## Extracted features

We analyze neuronal function across four distinct feature domains:

- **Action Potential (AP) Dynamics**
- **Passive Biophysical (PB) Properties**
- **Adaptation Currents (AC)** inferred via GLIF models
- **Input Feature Selectivity**, estimated using **Spike-Triggered Averages (STA)**

To dissect the structure and plasticity of neuronal encoding, we apply unsupervised clustering, cosine similarity analysis, and *Multiset Correlation and Factor Analysis (MCFA)*. These methods allow us to examine both within-domain variance and cross-domain coordination of features, offering a system-level view of functional reconfiguration.

## Summary and Outlook

This introduction has outlined the motivation and rationale for investigating neuronal identity and function through the dual lenses of input-dependence and neuromodulatory flexibility. Traditional classification approaches, though informative, fall short in capturing the high-dimensional, dynamic nature of neuronal computation. By leveraging frozen noise protocols, multivariate electrophysiological features, and modern unsupervised analysis techniques, this thesis proposes a data-driven framework to redefine neuronal identity as an emergent, context-sensitive construct. The following chapters present experimental results and theoretical insights that collectively support this paradigm shift.

## Thesis Structure

- **Chapter 2: Neuronal Identity is Not Static—An Input-Driven Perspective**

Demonstrates how different stimulation protocols yield distinct classifications, showing that neuronal identity is dynamic and shaped by input.
- **Chapter 3: Neuromodulatory Control of Cortical Function**

Examines how neuromodulators reshape the computational roles of neurons, altering both encoding capacity and feature interdependence.
- **Chapter 4: General Discussion and Future Directions**

Integrates findings across studies, discusses implications for neuroscience and artificial neural networks, and proposes directions for future research.



# Chapter 2

## Neuronal Identity is Not Static—An Input-Driven Perspective



Based on: Willemsen, Y., Beijers, R., Arias Vásquez, A., de Weerth, C., Do Breastfeeding History and Diet Quality Predict Inhibitory Control at Preschool Age? *Nutrients*, 2021, 13, 2752.

## Abstract

Neuronal classification based on morphology, electrophysiology, and molecular markers is often considered static. Here, we challenge this view, showing that functional classification depends on input patterns. Using single-cell recordings from layer 2/3 barrel cortex neurons in mice, we compared responses to step-and-hold versus dynamic frozen noise inputs that mimic presynaptic activity. Action potential and waveform-based classifications varied significantly, highlighting the dynamic nature of neuronal identity. To assess the contribution of input versus neuronal attributes toward classification, we analyzed four attribute sets, namely action potential, passive biophysical, adaptation currents, and linear input filters derived via spike-triggered averages (STA). Our findings revealed that the STA, which captures a neuron's selective responsiveness to presynaptic activity, explained the most variance within the population. This highlights input-driven dynamics as key to functional identity, emphasizing the need for physiologically relevant inputs in defining neuronal classes and shifting the focus from static properties to dynamic functional diversity.

## Introduction

Neural circuits are composed of diverse neuronal populations that exhibit variability in morphology, molecular composition, and electrophysiological properties. These neurons interact dynamically to process sensory information, support cognition, and drive behavior [Harris and Shepherd \(2015\)](#). A long-standing challenge in neuroscience has been to classify neurons into meaningful functional groups, with traditional approaches relying on intrinsic features such as molecular markers, morphological characteristics, and electrophysiological properties. However, despite significant advances, a consensus on the most informative features for neuronal classification remains elusive [Huang and Paul \(2019\)](#); [Markram et al. \(2004\)](#); [Mukamel and Ngai \(2019\)](#); [Fishell and Heintz \(2013\)](#); [Masland \(2012\)](#); [Tasic et al. \(2018\)](#); [Zeng and Sanes \(2017\)](#). An often-overlooked dimension in this classification challenge is the role of input dynamics in shaping neuronal function.

Neurons act as spatiotemporal filters, transforming incoming synaptic inputs into output firing patterns. This transformation is governed by an interplay between the structure and dynamics of the input a neuron receives, and the intrinsic membrane processes this input dynamically recruits.. Traditional classification approaches, with a focus on static properties, may therefore miss critical aspects of functional diversity that emerge from the interaction between neurons and their presynaptic partners. Recent studies suggest that electrophysiological identity is context-dependent [Gouwens et al. \(2019\)](#); [Scala et al. \(2021\)](#); [Gouwens et al. \(2020\)](#), varying as a function of the stimulation protocol used to probe neuronal function. However, a direct comparison of neuronal classification under physiologically realistic input conditions remains largely unexplored.

Recent advances in patch sequencing [Fuzik et al. \(2016\)](#); [Cadwell et al. \(2016\)](#); [Scala et al. \(2019\)](#) enable simultaneous extraction of transcriptomic, morphological,

and physiological properties, improving neuronal classification. The Allen Brain Institute dataset [Gouwens et al. \(2019\)](#); [Scala et al. \(2021\)](#); [Gouwens et al. \(2020\)](#) provides a broad classification of visual and motor cortex neurons using multi-modal features (MET types). However, classification based on electrophysiology remains challenging. Neuronal properties exist on a continuum [Markram et al. \(2004\)](#), with unclear boundaries between classes. Moreover, molecularly defined types exhibit overlapping electrophysiological properties [Gouwens et al. \(2019, 2020\)](#), and intrinsic electrophysiology varies with stimulation protocols. While multi-modal techniques improve classification, they overlook the influence of synaptic input. Neurons receive inputs from thousands of presynaptic neurons shaping their firing properties, necessitating classification under physiologically realistic conditions [Connors and Gutnick \(1990\)](#); [Steriade \(2000\)](#).

To address this gap, we investigated how neuronal identity is shaped by the nature of the input a neuron receives. We recorded from layer 2/3 neurons in the barrel cortex and compared their responses under two different stimulation paradigms: a standard step-and-hold (SH) stimulus, which provides a static, artificial input, and a frozen noise (FN) stimulus [Zeldenrust et al. \(2017\)](#), which simulates natural presynaptic activity. We hypothesized that functional classification of neurons would be stimulus-dependent, with the FN protocol revealing a distinct organization of neuronal diversity that is not captured by the SH protocol.

We analyzed four commonly used sets of electrophysiological attributes—action potential features, passive biophysical properties, adaptation currents, and linear input filters estimated via spike-triggered averaging (STA)—to assess their contributions to neuronal classification under dynamic input conditions. Using multiset correlation and factor analysis, we found that the linear input filter, which characterizes a neuron's sensitivity to specific input features, was the most informative attribute for understanding neuronal functional variance, i.e, it is the most relevant attribute to be used for clustering neurons. This finding challenges the traditional view that neuronal iden-

tity is a static property, emphasizing the importance of input dynamics on functional diversity.

By demonstrating that neuronal classification is highly dependent on input dynamics, our study highlights the need to incorporate physiologically relevant stimuli when defining neuronal types. Our findings suggest that neurons should not be categorized based solely on static features but rather on how they process and respond to dynamic synaptic input. This perspective has broad implications for both experimental and computational neuroscience, urging a paradigm shift toward input-dependent models of neuronal function.

## Materials and methods

**Ethics statement** The data used in this research was previously published and made freely available to the community da Silva Lantyer et al. (2018) and Yan et al. (2022). All the experimental work, as outlined in the cited articles, were carried out in compliance with the European directive 2010/63/EU, the national regulations of the Netherlands, and international standards for animal care and use.

**Slice electrophysiology** Data acquisition procedures, the details of the in vitro slice preparation, intracellular access to anatomically targeted neurons, data digitization, and preprocessing have been described in detail elsewhere Kole et al. (2020); Kole and Celikel (2019); da Silva Lantyer et al. (2018); kol (2017); Miceli et al. (2017). In short, Pvalbtm1(cre)Arbr (RRID:MGI:5315557) or Ssttm2.1(cre)Zjh/J (RRID:IMSR\_JAX: 013044) mice, including both females and males, were obtained from local breeding colonies and studied after the maturation of evoked neurotransmitter release in the primary somatosensory cortex (Martens et al. (2015)). Mice were anesthetized with Isoflurane (1.5 mL/mouse) before extracting tissue, and coronal slices of the primary somatosensory cortex (barrel subfield) were prepared.

The brain was removed, and 300  $\mu\text{m}$ -thick coronal slices were made. Slices were then incubated in artificial cerebrospinal fluid (aCSF) (120 mM NaCl, 3.5 KCl, 10 glucose, etc.), aerated with 95%  $O_2$ /5%  $CO_2$  at 37°C, and then at room temperature after 30 minutes.

Whole-cell electrophysiological recordings were performed with continuously oxygenated aCSF. The barrel cortex was localized, and cells in the supragranular layers were patched under 40x magnification using HEKA EPC 9 and EPC10 amplifiers with Patch Master software. Patch-clamp electrodes were pulled from glass capillaries (1.00 mm external diameter, 0.50 mm internal diameter) and used with 5–10 M $\Omega$ m resistance, filled with intracellular solution (130 mM K-Gluconate, 5 KCl, 1.5 MgCl<sub>2</sub>, etc., pH adjusted to 7.22 with KOH). Data were band-pass filtered at 0.1–3000 Hz before storage for offline analysis.

**Step and hold (SH) protocol** The Step and Hold protocol was set up in a current clamp configuration, the resting membrane potential was set to -70 mV before current injection into the soma of the neuron. In total, 10 current step injections, each 500 ms long, were performed. The steps ranged from 40 pA to 400 pA with an inter-sweep interval of 6.5s. The stimulus was repeated 1 to 3 times for neurons. The drifts encountered were not corrected for.

**Frozen Noise (FN) protocol** The Frozen Noise input protocol consisted of injecting a somatic current that is the result of an artificial neural network of 1000 neurons responding (firing Poisson spikes) to random stimuli i.e., the hidden state, the membrane potential response to the somatic input is recorded with a sampling rate of 20 kHz for a total length of 360 seconds and saved. Each raw data file consisted of a vehicle control trial (artificial Cerebrospinal fluid i.e. aCSf) and a drug trial (a specific neuromodulatory receptor agonist or antagonist was added to the bath and the recording was repeated). Some files consisted of multiple control and drug trials. See

Zeldenrust et al. (2017); da Silva Lantyer et al. (2018) for more details.

## Method details

### Feature Extraction

Feature extraction is performed separately for SH and FN protocols to classify neurons using different inputs and to determine cell class with a realistic stimulus.

For the first part, which is comparing classification across protocols, we collect waveforms and Action potential features for comparing SH and FN protocols using a subset of the data, (186 neurons). As not all cells were recorded with both types of input protocols, this subset was chosen to match the cell IDs across the two protocols. For the second part, which compares different physiological attributes for the FN protocol, we collect waveforms, spike event-based features, biophysical features, and the STA for each control (aCSF) trial for each cell in the FN dataset. We discard trials that contain recording artifacts (observed distortions or high-frequency noise), in total 11 neurons. Since there were multiple drug and control trials available for each neuron, we always took the first control trial for this study as this prevented any residual effect from the drug condition after washing. The total number of neurons used for this part of the study was 312.

**Spike waveforms** Spike waveforms were extracted for each neuron from both SH and FN protocol trials (this could not be done for all the neurons as some neuron IDs could not be matched between SH and FN protocols due to missing metadata).

Firstly, we identified the spike times in each trial in each protocol. This was done by identifying peaks in the membrane potential trace using the Scipy Findpeaks function [Virtanen et al. \(2020\)](#) with  $height = 20mV$ , and  $distance = 80ms$  as the chosen hyperparameters. Next, we cut the spike waveform by defining a window of 2 ms before and 3 ms after each spike peak to get a 5 ms long waveform for each spike. We ignored the spikes that had an ISI lower than 3 ms as we were interested in

non-bursting type spike shapes. We then average over all the waveforms for each trial to get an average waveform shape in both FN and SH protocols respectively.

Extracted Waveforms for the second part were 10 ms long (5 ms before and after the spike peak), to incorporate the subthreshold dynamic before reaching the threshold of the neuron in the waveform classification as well. We observed some variability in the baseline membrane potential values as well as the slope of membrane potential before the threshold value was reached.

**Action potential features** Action potential features were extracted to study the variability in spike-related dynamics across individual neurons. These features were designed based on their suitability for comparing neurons in FN and SH protocols. These Action potential features were divided into three categories: Spiking Dynamics, spike threshold, and Action Potential height and width.

### Spiking Dynamics

This includes the following features:

- **Current at the first spike:** We take the current amplitude when the membrane potential crosses the threshold for the first time in the trial for FN protocol. For SH protocol, it is the current step that produces the spike for the first time.
- **AP count:** We count the number of spikes over the entire trial length of 360 seconds for the FN trial and 500 milliseconds for the SH trial which is the duration for the current onset.
- **Inter spike interval:** Inter spike interval was measured as the time interval between two spikes in milliseconds. We calculate mean, median, maximum, and minimum values for each trial in SH and FN protocols. For the SH case, we measure the ISI for the maximum current amplitude (400 pA) trial.

- **Time to first spike:** We measure the time (in milliseconds) it takes for the neuron to fire the first action potential. For the SH case, we take the lowest amplitude step where a spike is observed.
- **Firing rate:** We calculate the firing rate as the number of spikes per second. For the FN case, we take the entire length of 360 seconds of the trial and for the SH case, we take the duration of the current onset which was 500 milliseconds for the highest current step (400 pA).

$$fr = \frac{N_{spikes}}{T} \quad (2.1)$$

where  $N_{spikes}$  is the total number of spikes in the trial and T is the total length of the trial.

- **Interspike Interval:** Interspike interval is the duration between two spikes  $t_{spike_{n+1}} - t_{spike_n}$ , where  $t_{spike_{n+1}}$  and  $t_{spike_n}$  are spike times for spikes n+1 and n. We take the interspike interval for all the spikes in the trial for both FN and SH protocols and calculate the mean, median, minimum, and maximum values.
- **Instantaneous rate:** Instantaneous rate is defined as the reciprocal of the average of the Interspike interval.

$$inst.firing\_rate = \frac{1}{t_{spike_{n+1}} - t_{spike_n}} \quad (2.2)$$

## Spike threshold

- We measure the threshold of each spike from the trial as described in [Fontaine et al. \(2014\)](#). The threshold is defined as the voltage V at the spike onset when the first derivative of the membrane potential  $dV/dt$  reaches 25 mV/ms for the first time. We take the first threshold value of the trial as well as the mean,

median, maximum, and minimum values of the thresholds from the entire trial length.

### Action Potential height and width

- **Width:** Spike width is calculated as the time it takes between when the membrane potential reaches the AP threshold and when the membrane voltage goes below the threshold after the spike peak. We calculate the width for each spike in the trial for both FN and SH protocols. We calculate the mean, median, maximum, and minimum for all the values obtained from a trial.
- **Amplitude:** Spike amplitude is calculated as the difference between AP peak and AP threshold value. We calculate the amplitude for each spike in the trial for both FN and SH protocols. We calculate the mean, median, maximum, and minimum for all the values obtained from a trial.

### Biophysical Feature extraction using GLIF model

Since it is not possible to empirically observe the biophysical properties of the cell just using the membrane potential, we fit a Generalized Leaky Integrate and fire model (GLIF) to the recordings, which can capture universal spiking and sub-threshold dynamics [Pozzorini et al. \(2015\)](#). The following equations define the GLIF model:

$$C\dot{V}(t) = -g_L(V(t) - E_L) - \sum_{t_j < t} \eta(t - \hat{t}_j) + I(t), \quad (2.3)$$

where  $V(t)$  is the membrane potential,  $C$  is the membrane capacitance,  $g_L$  is the leak conductance,  $E_L$  is the resting potential, and  $\eta(t)$  is the adaptation current triggered by a spike event. Spikes are stochastically produced by a point process that represents conditional firing intensity  $\lambda(t|V, V_t)$  that is dependent on the instantaneous difference between the membrane potential and voltage threshold given by:

$$\lambda(t|V, V_t) = \lambda_0 * \exp\left(\frac{V(t) - V_T(t)}{\Delta V}\right), \quad (2.4)$$

where  $\lambda_0$  is the base firing rate in Hz,  $V(t)$  is the membrane potential, and  $V_T(t)$  is the moving spike threshold and  $\Delta V$  controls the sharpness of the exponential threshold function. The probability of a spike  $\hat{t}$  between a time interval  $t$  and  $\Delta t$  is given by the following equation (based on [Gerstner et al. \(2014\)](#)):

$$P(\hat{t} \in [t, t + \Delta t]) = 1 - \exp(-\int_t^{t+\Delta t} \lambda(s) ds) \approx 1 - \exp(-\lambda(t)\Delta t), \quad (2.5)$$

The dynamics of the firing threshold  $V_T(t)$  are given by:

$$V_T(t) = V_T^* + \sum_{\hat{t}_j < t} \gamma(t - \hat{t}_j), \quad (2.6)$$

where  $\gamma$  is the stereotypical movement of the spike threshold after a spike and  $V_T^*$  is the threshold baseline.

The method for fitting this neuron model to a membrane potential recording is divided into the following steps:

**Preparation step:** A 100-second window from the initial part of the trial is taken as the training set for the fitting, [Pozzorini et al. \(2015\)](#) shows that a longer trial length doesn't improve the fit. Spike times and waveforms are also extracted for the preparation step of the fitting procedure.

**Step 1. Fitting the reset voltage:** The waveforms extracted in the preparation step were averaged, and then the Reset voltage  $V_{reset}$  was extracted using the averaged waveform by setting an arbitrary refractory period  $t_{ref}$  and taking the membrane potential value at  $t_i + t_{ref}$ , where  $t_i$  is the spike peak. The refractory

period is chosen to be always lower than the minimum inter-spike interval, we chose the refractory period of  $t_{ref} = 4ms$  in this case.

**Step 2. Fitting sub-threshold dynamics :** The voltage dynamics in eq (2.3) are given by parameter set  $\theta_{sub} = \{C, g_L, \eta, \text{ and } E_L\}$ , by fitting the temporal derivative of the data  $\dot{V}_{data}$  in the model, we can extract the set of passive parameter set  $\theta_{sub}$  for the data. Firstly, we can write the adaptation current  $\eta$  as a linear sum of rectangular basis functions Mensi et al. (2012).

$$\eta(t) = \sum_{k=1}^K a_k f^{(k)}(t), \quad (2.7)$$

Using the fact that the voltage dynamics are approximately linear in the sub-threshold regime,  $\theta_{sub}$  parameter set can be extracted using a multi-linear regression between  $\dot{V}_{data}$  and  $\dot{V}_{model}$ . For this, we created a training set  $V_{data}^{sub}$  where we removed the spike waveforms from  $V_{data}$ ,  $V_{data}^{sub} = \{V_{data}(t) | t \notin (t_i - 5ms, t_i + t_{ref})\}$ , where  $t_i$  is the spike times. The regression problem can be stated as:

$$\theta_{sub} = (X^T X)^{-1} X^T \dot{V}_{data}^{sub}, \quad (2.8)$$

where  $X^T$  is a matrix representing parameter values at different time points, its row elements  $x_t^T$  are of the following form

$$x_t^T = [V_{data}^{sub}, 1, f^{(1)}(t), f^{(2)}(t), \dots, f^{(K)}(t)], \quad (2.9)$$

**Step 3. Fitting the spike probability:** For fitting the spiking probability to the data, we need to extract parameters defining the dynamics of the threshold eq (2.6). The stereotypical shape of the adaptation current threshold movement can be

expanded as a sum of rectangular basis functions as follows ([Mensi et al. \(2012\)](#)):

$$\gamma(t) = \sum_{p=1}^P \gamma_p f^{(p)}(t), \quad (2.10)$$

We use the parameters obtained in the previous steps to compute the subthreshold membrane potential of the model using numerical integration of eq (2.3). We set  $\lambda_0 = 1$  Hz and all the threshold parameters  $\theta_{thr} = \{\Delta V, V_T^*, \text{ and } \gamma(t)\}$  are extracted by maximizing the likelihood function of the following form based on the experimental spike train:

$$\hat{\theta}_{thr} =_{\theta_{thr}} \left[ \sum_{t \in [t_j]} y_t^T \theta_{thr} - \Delta T \sum_{t \in \Omega} \exp(y_t^T \theta_{thr}) \right], \quad (2.11)$$

Where  $\Omega = \{t | t \notin (\hat{t}_j, \hat{t}_j + t_{ref})\}$ ,

The subthreshold fit is examined by comparing the variance explained  $R^2$  of the subthreshold membrane potential trace  $V$  between the data and the model. All the models chosen for clustering had an  $R^2$  value  $> 0.7$ . The sets  $\theta_{clustering} = \{g_L, \Delta V, C, V_T^*, E_L, V_{reset}\}$  are the parameters that are extracted from the model that is used in the clustering procedures.

**Spike Triggered Average** The spike-triggered average (STA) is the average shape of the stimulus that precedes each spike. We extracted the STA using the following equation given by [Schwartz et al. \(2006\)](#):

$$STA = \frac{1}{N} \sum_{n=1}^N \vec{s}(t_n), \quad (2.12)$$

where  $t_n$  is the  $n^{th}$  spike time,  $s$  is the stimulus vector preceding the spike for a fixed time window of 100 ms, and  $N$  is the total number of spikes. Before clustering, we

standardize (i.e. z score) and then normalize the STA vector with an  $L_2$  norm. We didn't use any kind of whitening or regularization to calculate the STA.

## **UMAP + Louvain clustering**

Conventional clustering algorithms such as K-means do not perform well in high dimensional spaces ( $p > N$ , where  $p$  is the dimension of data and  $N$  is the number of samples) due to the curse of dimensionality [Aggarwal et al. \(2001\)](#), and therefore need a pre-processing dimensionality reduction step. Addressing this issue, a non-linear dimensionality reduction algorithm such as UMAP [McInnes et al. \(2018a\)](#) creates a high-dimensional graph representation of the data which can be utilized for clustering using a graph-based clustering method such as Louvain clustering [Blondel et al. \(2008\)](#) or ensemble clustering [Poulin and Théberge \(2019\)](#). This method utilizes the high dimensional space of the data for clustering. As shown by [Lee et al. \(2021\)](#) using the WaveMAP algorithm, the UMAP+Louvain community detection algorithm has been successful in finding neuron types based on extracellular recordings.

## **UMAP**

Universal Manifold Approximator (UMAP) is a non-linear dimensionality reduction technique that preserves local and global relationships between data in high dimensional space [McInnes et al. \(2018a\)](#). It is divided into two steps, the first step is creating a k-nearest neighbor graph and the second step is to generate a low-dimensional representation that is similar to the high-dimensional graph structure.

We used the Scikit-learn UMAP-learn software package [McInnes et al. \(2018b\)](#) to extract the embedding and the graphs.

### Louvain Community detection

The Louvain community detection algorithm [Blondel et al. \(2008\)](#) maximizes modularity amongst the identified groups in a graph. Modularity can be defined by the following equation:

$$Q = \frac{1}{w} \sum_{i,j} \left[ A_{i,j} - \gamma \frac{d_i^+, d_i^-}{w} \right] \delta(c_i, c_j) \quad (2.13)$$

where  $A_{i,j}$  is the adjacency matrix,  $k_i = \sum_j A_{ij}$  is the sum of the weights of the edges attached to the vertex  $i$ ,  $c_i$  is the community for vertex  $i$ ,  $d_i$  is the degree of node  $i$ ,  $d_i^+$  and  $d_i^-$  are the in degree and out degree for node  $i$ ,  $\delta(u, v)$ , Kronecker symbol, is 1 if  $u=v$  and 0 otherwise,  $w = \sum_{i,j} A_{i,j}$  and  $\gamma > 0$  is the resolution parameter. For Louvain graph-based clustering we used the implementation from the Scikit-network software package [Bonald et al. \(2020\)](#).

The clustering approach can be summarized in the following steps:

1. The high dimensional k-neighbor graph is obtained by the first step of the UMAP algorithm using data vectors that are first standardized and then normalized using the  $L_2$  norm. The nearest neighbor and distance parameters for UMAP were 20 and 0.1 respectively. This is to ensure a compact embedding and a clear clustering.
2. Using the graph obtained in the first step, we perform Lovain community-based clustering, using the resolution parameter  $\gamma$  that maximizes the modularity score, and the corresponding community/partition is chosen as the final cluster labels.
3. Using the cluster labels found in the second step, we color the individual points in distinct colors on the low-dimensional UMAP representation.

This unsupervised clustering approach was effective in capturing the global structure of the high dimensional space across attributes such as waveforms, adaptation

current, and Spike Triggered average. The clusters found using this method were robust even when clustering was repeated with a sub-sample of the data and while iteratively removing the features.

**Cluster Stability and Parameter Selection** Cluster stability is tested by clustering a 90% sub-sample of the data chosen at random and repeating the procedure 25 times for each resolution parameter, varying from 0 to 5 with a step of 0.5. The modularity score is calculated for each resolution parameter and finally, the resolution parameter is chosen for which the modularity score is maximal. Variation in the number of clusters is observed for each resolution parameter and is contrasted with the modularity score. Clustering robustness is also tested by repeating the procedure above while excluding one feature at a time for Action potential feature clustering and passive biophysical clustering.

**Cluster Likelihood comparison** Cluster likelihood between two sets of labels was calculated in two steps, firstly we created a contingency matrix such that  $C_{i,j}$  contained the number of times neurons classified in cluster  $i$  in the SH protocol classified as cluster  $j$  in the FN protocol, such that each row contains the division of elements of cluster  $i$  in the SH protocol into all the clusters of the FN protocol. Secondly, to get the likelihood, we divided each row by the total count of neurons in cluster  $i$  in the SH protocol.

$$P(j|i) = \frac{C_{i,j}}{\sum_j C_{i,j}} \quad (2.14)$$

Here  $P(j|i)$  is the probability of the neuron classifying into FN cluster  $j$  given it is classified in SH cluster  $i$ .

**Cluster Similarity Measures** We measured the similarity between two given cluster assignments using the Adjusted Random Index (ARI) and Adjusted Mutual

Information (AMI) Score. Both of these measures amount to change agreements between two clusters. The ARI (range -1-1) measures the pairwise relationships between clusters and the AMI (range 0-1) measures the overall information shared between the two clusters.

We used the scikit-learn Python package [Pedregosa et al. \(2011\)](#) to calculate the ARI and AMI measures.

### Ensemble Clustering for Graphs (ECG)

We used Ensemble Clustering for Graph algorithm [Poulin and Théberge \(2019\)](#) to validate the clusters found using the Louvain Community detection algorithm. It is a two-step algorithm, the first step called the generation step consists of producing a  $k$ -level 1 partition  $P = \{P_1, P_2, \dots, P_k\}$  by running the first pass of the Louvain clustering algorithm with random vertices on the initial graph  $G = (V, E)$ . The second step, also known as the integration step, consists of running the Louvain algorithm on a weighted version of the initial graph. Where the weights are the weight of an edge given by

$$W_p(u, v) = \begin{cases} w_* + (1 - w_*) * \left( \frac{\sum_{i=1}^k v_{p_i}(u, v)}{k} \right) & , \text{if } (u, v) \text{ is in 2-core of } G \\ w_* & , \text{otherwise} \end{cases} \quad (2.15)$$

where  $0 < w_* < 1$  is the minimum ECG weight and  $v_{p_i}(u, v) = \sum_{j=1}^{l_i} 1_{C_i^j}(u) \cdot 1_{C_i^j}(v)$  shows if the vertices  $u$  and  $v$  co-cluster in the same cluster of  $P_i$  or not. Thus it takes advantage of multiple instances of the Louvain clustering algorithm to make a clustering based on consensus. We used the implementation provided by [\(Lee et al. \(2021\)\)](#) for comparing the waveform clustering for SH and FN protocols. The graph used for Ensemble clustering was the same as in the original clustering using the

UMAP algorithm.

## Quantification and statistical analysis

**MANOVA** We measured the significance between excitatory and inhibitory action potential and passive biophysical feature vectors using a one-sided MANOVA. We present the following statistics: Wilk's lambda, Pillai's trace, Hotelling-Lawley trace, and Roy's greatest root using the Stats Model python package [Perktold et al. \(2024\)](#).

**Canonical Correlation Analysis** To perform a post-hoc analysis on Action potential and Passive biophysical features, to find the importance of each feature, we used a Canonical Correlation analysis. Which is a method to find a linear combination of features between two datasets that maximizes the correlation between them. It is a deterministic method that results in canonical variates of the two datasets that are maximally correlated. Since the excitatory/inhibitory populations were different in numbers, we repeated the SHA procedure 10 times with random sampling from the larger group to make the population size equal between excitatory and inhibitory groups. We then obtain loadings for each dataset by averaging over the 10 repetitions, which represents the correlation of a feature with the canonical variate. We used the Scikit learn python package ([Pedregosa et al. \(2011\)](#)) for performing the SHA procedure.

**Welch's ANOVA** To compare the significance of cosine similarity measures for excitatory and inhibitory populations, we first calculated the cosine similarity matrix comparing the excitatory and inhibitory populations separately and a third matrix comparing excitatory with inhibitory populations. We take the upper triangular part of the excitatory and inhibitory within-population comparison matrix and the entire excitatory vs inhibitory matrix for the significance test. The Welch's ANOVA test was used to compare the three groups of cosine similarity for each attribute with one

categorical variable namely, excitatory or inhibitory. This test was chosen because the populations for each attribute were heterodrastic and of unequal size. We performed a post-hoc Games-Howell test to determine which group was significantly different, this was done because the variances across groups were heterodrastic. The significance levels are reported in the figures based on the p-values obtained by the post-hoc test. We used the Stats model python package [Perktold et al. \(2024\)](#) for calculating Welch's ANOVA.

## Multi-set Correlation and Factor Analysis

The Multi-set Correlation and Factor Analysis (MCFA) was performed using the procedure as described by [Brown et al. \(2023\)](#), and the accompanying software was used for the analysis [Brown and collinwa \(2023\)](#). The problem can be stated as follows, let  $\{Y^m\}_{m=1}^M$  be a set of M attributes extracted from the electrophysiological data, each with dimension  $N \times P_m$ , where N is the number of samples and  $P_m$  is the dimension of each attribute (Action potential parameters ( $P_1 = 22$ ), passive biophysical parameters ( $P_2 = 6$ ), Spike triggered Average ( $P_3 = 2000$ ), and Spike triggered current ( $\eta$ ) ( $P_4 = 10000$ )). Each attribute set can be modeled as having a contribution from two factors, a shared and a private factor respectively, as shown below.

$$z_n \sim N(0, I_d) \quad (2.16)$$

$$x_n^m \sim N(0, I_{k_m}) \quad (2.17)$$

$$y_n^m \sim N(W_m z_n + L_m x_n^m, I_{k_m}, \Psi_m) \quad (2.18)$$

Here  $z_n$  is the shared factor of dimension d, and  $W_m$  is the shared space loading matrix of shape  $P_m \times d$ .  $k_m$  is the dimension of each private mode.  $x_n^m$  is the private space for each attribute m of dimension  $k_m$ ,  $L_m$  is the private space loading of shape

$P_m \times k_m$ .  $\Psi_m = diag(\psi_m^1, \dots, \psi_m^{k_m})$  are the diagonal residual covariance matrices. Given  $Y$ ,  $d$ , and  $k_m$  the goal is to find hidden factors  $z_n$ ,  $x_n^m$ , and loading matrices  $W_m$ ,  $L_m$ . This is achieved by the Expectation Minimization (EM) method Brown et al. (2023).

We center and scale all variables as in Brown et al. (2023) and initialize the loading matrices similarly to the original method, using the pairwise correlations with average variance constraint initialization. To model the shared latent space  $z_n$ , we chose the most informative PCA components based on Marchenko Pasteur Law to control over-fitting Brown et al. (2023), which states for any normalized dataset ( $\mu = 0$ ,  $\sigma = 1$ ), the principal components with eigenvalues above  $\lambda_m = 1 + \sqrt{p_m/N}$  are considered non-noise. We set the size of the private space  $k_m = 1$  for passive biophysical parameters due to its relatively lower dimension and  $k_m = 2$  for the other attributes. After initializing all the variables, we run the expectation minimization (EM) algorithm to obtain  $z_n$ ,  $x_n^m$ ,  $W_m$ , and  $L_m$  matrices.

For feature  $j$  of mode  $m$ , the variance explained by a shared feature  $d$  is given by  $W_m^{(j,d)^2}$ . Similarly, the variance explained by the  $k^{th}$  private factor of feature  $j$  of mode  $m$  is given by  $L_m^{(j,k_m)^2}$ . The total variance explained for a mode by a shared factor is given by  $\sum_j W_m^{(j,d)^2}$ , similarly, the total variance explained by the private factor  $k_m$  is  $\sum_j L_m^{(j,k_m)^2}$ . Hence, the total variance explained by all shared and all private factors is given by  $\sum_{j,d} W_m^{(j,d)^2}$  and  $\sum_{j,k_m} L_m^{(j,k_m)^2}$ .

The relative feature importance is given by the cross-correlation of columns of the posterior mean of  $Z$  on observing a single mode denoted by  $\hat{Z}_m$  Brown et al. (2023)

$$\hat{Z}_m = E[Z|W_m, \Psi_m, L_m, Y_m] = Y_m (W_m W_m^T + L_m L_m^T \Psi_m)^{-1} W_m \quad (2.19)$$

$$S_d = cor(\hat{Z}_1^{(:,d)}, \dots, \hat{Z}_m^{(:,d)}) \quad (2.20)$$

## Results

We aimed to observe the contribution of the input type in explaining functional classification and to explore what a physiologically realistic stimulus reveals about the functional classification of a neuron. For the first aim, we researched the stimulus dependence of neural classification using two different sets of classification features: 1) action potential waveforms and 2) other action potential attributes, such as the spike threshold and spiking dynamics. Next, to research the second aim, we investigated which attributes are the most informative about neuronal heterogeneity under a physiologically realistic stimulation protocol. Therefore, We performed classifications based on four different attribute sets that capture 1) action potential attributes, 2) Passive biophysical attributes, 3) Adaptation current, and 4) linear input filter through a Spike Triggered Average (STA). Finally, we used a method known as Multi-set correlation and Factor Analysis (MCFA) to compare the variance explained by the shared structure across these four attribute sets.

### Stimulus dependence of neural classification

We first aim to understand the role of a neuron's input in the functional classification of neural populations. For this, we analyze single-cell patch-clamp recordings (da Silva Lantyer et al. (2018); Yan et al. (2022)) recorded with two different input conditions: 1) a Step and Hold (SH) and 2) a Frozen Noise (FN) protocol (see Methods). We want to understand the influence of a physiologically realistic FN input on classification using commonly used features in contrast to SH input. To contrast the heterogeneity between SH and FN input conditions, we compare compare classification in these two input conditions using the neuronal spike waveforms and action potential attribute sets and also measure the similarity in the waveforms and action potential attributes between each cluster across the two input protocols.

### Stimulus dependence of neural classification using intracellular action potential waveforms

To understand if waveform-based classification differs under FN and SH input conditions, we analyzed control (aCSF) trials from a total of 186 in-vitro whole-cell patch-clamp neural recordings that consist of the same cell recorded under 2 different input protocols, namely Step and Hold (SH) and Frozen Noise (FN) (Fig. ?? **c-d**, see methods). Using extracted waveforms of the same length (5 ms) from both FN and SH trials, we standardize (subtracting the mean and scaling to unit variance) the waveforms and then normalize the data using an L2 norm. Next, we apply an unsupervised high dimensional clustering algorithm that combines UMAP and Louvain Community detection (see methods) and found 7 clusters for SH trials as well as 7 clusters for FN trials (Fig. ?? **a-b**) respectively. We also measured the stability of the clusters (see Methods) against changing the hyperparameter (resolution parameter) for the unsupervised method. We found the clusters to be stable (low standard deviation) for the chosen resolution parameter (chosen at a value of 1.0) (Fig. ??**g**).

From inspecting the two-dimensional UMAP projection, we found that the manifold representing the waveforms in the FN protocol (Fig. ??**a**) consists of two broad subdivisions, whereas the SH protocol manifold seems much more connected and spread out (Fig. ??**b**). We compared waveform shapes across clusters by creating a pairwise cosine similarity matrix between FN and SH protocols and then taking the average of the submatrix for each SH and FN cluster pair. The average similarity across clusters is summarized using a heatmap (Fig. ??**e-f**). We first perform this comparison for each protocol separately and find that some cluster waveform shapes are similar (cosine similarity  $> 0.9$ ) to their immediate neighbors (e.g. cluster 7, 3, and 4 in SH and cluster 6, 3, and 4 in FN in (Fig. ??**e**) for both FN and SH protocols. Similarly, comparing the waveform shapes between SH and FN, we find that narrow-width clusters for the SH

protocol (4, 3, and 7) are highly similar to narrow-width clusters for the FN protocol (6, 2, and 3). We also project all the SH and FN waveforms together on a single embedding space and observed they were distinct (Appendix. ??a), suggesting that waveform shapes are not fixed across protocols. We then test if there exists a drift in the recordings by dividing the 360-second trial into two parts and comparing the waveforms between the first and the second trial by projecting the waveforms on the same 2D UMAP space. Both halves are overlapping suggesting that waveform shapes are similar between the two halves of the trail.

Finally, we calculate the likelihood for neurons in one of the SH clusters to be clustered together in one of the FN clusters (see methods and Fig. ??h). We find that for each SH cluster, the likelihood of clustering in one of the FN clusters is spread without a strong majority, suggesting that neurons grouping in the SH protocol do not group in the FN protocol. We further quantify the clustering agreement between the SH and FN clusters using an adjusted random score (ARI) and adjusted mutual information score (AMI) between FN and SH clusters. Both measures show low values ( $ARI = 0.085$ ,  $AMI = 0.133$ ). This confirms that neurons cluster differently between SH and FN protocols. To verify if the found clusters don't have a bias as a result of the method that we use, we repeat the analysis using the Ensemble clustering method (Appendix. ??) to cluster the SH and FN waveforms. Taking the average of the highest values for each row in the co-clustering matrix, we find 84% correspondence for FN waveforms between wave map and ensemble clustering and 96% correspondence for SH waveforms between wave map and ensemble clustering. Comparing the ensemble clustering with Louvain clustering using an adjusted mutual information score (AMI Louvain vs Ensemble (FN) = 0.765, AMI Louvain vs Ensemble (SH) = 0.736), we find a high level of similarity for both SH and FN protocols. In conclusion, we find that clustering neurons into cell classes based on their waveforms results in different cell classes in the SH and FN input protocols, resulting from differences in the waveform

shapes due to the stimulation protocol. This shows that waveform-based neuronal identity is stimulus-dependent.

### **Stimulus dependence of neural classification using action potential attributes**

It has been found that excitability measures such as total spike count and AMPA conductance threshold (dynamic) vs rheobase (static) have a low correlation between static and dynamic stimulus conditions Hernáth et al. (2019); Szabó et al. (2021). As we found in the previous section that cell clustering based on waveforms depend critically on the stimulation protocol. This intrigued us to investigate if neuronal classification based on action potential attributes (see Methods), that incorporate among others spiking dynamics, spike threshold and action potential height and width (a total of 22 attributes), is also input-specific. We designed a set of features to allow for comparisons across input protocols. This choice of attributes is based on previous literature that clusters neurons based on electrophysiological attributes. The attribute list is not exhaustive but rather confined as features can be input specific. The properties included in the spiking dynamics set incorporate the firing statistics such as inter-spike interval (ISI), firing rate, and action potential count among others that are commonly studied. Next, we design a spike threshold attribute set to capture spike threshold-related parameters for the trial. The spike thresholds were calculated for each action potential in each trial for the analysis (see Methods). Finally, we measure the action potential height and width parameters, even though we have clustered based on average waveforms in the previous section. We do this for two reasons, first, height and width parameters are electrophysiological parameters commonly used in the clustering literature and second, the average waveforms studied previously do not capture the change in the height and width of the waveform within each trial. We used descriptive statistics such as mean, median, minimum and maximum values for some of the features to capture the distribution of these features in each trial.

We use the unsupervised UMAP+Louvain clustering method (explained in the previous section) on the 22-dimensional feature set that we extracted from the SH and FN trials for 186 neurons. We find 7 classes for SH and 7 classes for FN protocol respectively (Fig. ?? **a-b**). Unlike in the waveform-based clustering, the UMAP representation is more continuous for the FN trials than for the SH protocols (Fig. ?? **a and b**). We visualize the differences attributes between the classes using a radar plot to investigate this further. We consider features based on spiking dynamics (such as firing rate, ISI, etc.), spike threshold, and action potential height and width separately for both SH and FN protocols (Fig. ?? **d-e** and methods for a list of all features and their sub-classification). We plot these features for each trial (thin line) along with the mean for each class (thick line). On visual inspection, we observe that the means for each cluster (thick line) in both SH and FN protocols are non-overlapping for all the 3 attribute sets (spiking dynamics, spike threshold, and AP height and width) respectively. Suggesting that each cluster has distinct action potential attributes. We measure the stability of the clusters (see methods) as a result of changing the hyperparameters (resolution parameter) for the unsupervised clustering method. We find the clusters to be stable (low standard deviation) for the chosen hyperparameter (resolution parameter = 1.0) (Fig. ??**c**).

We want to compare action potential attribute sets across SH and FN trials, so we quantify the differences across clusters for the FN and SH protocols using the cosine similarity between the feature vectors. We calculate the pairwise cosine similarity matrix between all SH and FN trials and take the means of the sub-matrix for neurons in each SH and FN cluster pair. This gives a cosine similarity matrix comparing each SH cluster with each FN cluster. We observe that none of the SH clusters show a high similarity ( $> 0.9$ ) with FN clusters, suggesting that action potential attributes differ drastically as a result of input protocol (Fig. ??**f**). We also overlay the UMAP embedding for each feature vector for the SH and FN protocol (Appendix. ??**c**) and found that the

SH and FN feature manifolds are entirely different.

To understand the role of input in overall action potential attributes based cluster assignment, we calculate the likelihood (see Methods) for a neuron in one of the SH clusters to be clustered in one of the FN clusters (Fig. ??g). We find that for each SH cluster, the likelihood for clustering in one of the FN clusters is spread over the FN clusters without a strong majority for a specific FN cluster. We further quantify the correspondence between SH and FN clusters using an adjusted random index score (ARI) and adjusted mutual information score (AMI), both values were found to be low (ARI = 0.149 and AMI = 0.206). This shows neurons cluster differently between SH and FN protocols based on Spike Event-based features. These results suggest that action potential attributes based clustering of neuronal populations is input dependent.

## **Functional classification of neurons stimulated by the FN protocol based on different feature sets**

We have shown in the previous section that neuronal classification based on waveforms and action potential attributes is input-dependent. We want to expand our understanding of which features result in distinctive functional classifications within the FN-stimulated neurons. To understand the variance in the neuronal population captured by different attribute sets, we perform classifications based on four different attribute sets that capture 1) the commonly used action potential attributes, 2) passive biophysical attributes, 3) adaptation attributes, and 4) linear input filters approximated using the Spike Triggered Average (STA), to assess input feature selectivity.

Ample experimental evidence suggests that cortical neurons can be divided into two broad functional categories [Avermann et al. \(2012\)](#), namely excitatory (glutamatergic) and inhibitory (GABAergic), based on the type of effect (either excitation or inhibition) they have on their post-synaptic neurons [Zeng and Sanes \(2017\)](#). Excitatory and inhibitory neurons have also been found to have distinct electrophysiological properties

and thus are known to perform different functions. We therefore subdivide our data into excitatory and inhibitory groups to study the diversity within and across populations. Previous studies have associated neuronal waveform shapes with functional identity Trainito et al. (2019); Lee et al. (2021). The broad and narrow spike-width neurons have also been found to have a characteristic firing statistic, i.e. neurons with narrow-width waveforms were found to have a high firing rate (putatively inhibitory), and neurons with broad-width waveforms were found to have lower firing rates (putatively excitatory) Connors and Gutnick (1990); Bean (2007); Kiritani et al. (2023) in the barrel cortex. This suggests that inhibitory neurons can be putatively characterized by narrow width and high firing rate and that excitatory neurons can be putatively characterized by broad width and low firing rate. Also, barrel cortical excitatory neurons are more adaptive compared to inhibitory neurons Heiss et al. (2008). Based on this reasoning, we partitioned our data into a putative excitatory and an inhibitory population.

We extract the average intracellular waveforms from the entire dataset, 312 cells in total. Note that the number of neurons under analysis is much larger than in the previous sections because more FN than SH experiments were performed. We then apply the UMAP+Louvain algorithm to classify intracellular waveforms and find 8 clusters. (Fig. ??a) shows the UMAP projection of all waveforms with their corresponding cluster label colors. Next, we plot the distribution of the firing rates and half-widths for each cluster with matching colors using a violin plot (Fig. ??b-c). We observe clusters 1,5 and 6 to have a narrow width and high firing rate relative to the rest of the clusters; therefore, we categorize these clusters as putatively inhibitory (I) and the rest as putatively excitatory (E). We compare the average cosine similarity between E/I populations. We find that the excitatory and inhibitory populations are significantly different (Welch's ANOVA,  $F(2,49135)=19148.00$ , \*\*\* $p= 0.0$ ; Post-hoc Games-Howell test, E vs I (\*\* $p=0.001$ ), I vs Exl (\*\* $p=0.001$ ), and E vs Exl (\*\* $p=0.001$ ), Fig. ??d), but

the excitatory population is more heterogeneous than the inhibitory one, based on the average similarity of the waveforms within the E/I population (Fig. ??d).

### Action potential attributes based neuron profiles using the FN protocol

As pointed out in the previous section, we aimed to understand and compare the usefulness of commonly used physiological attributes in uncovering functional classification in neuronal populations when neurons receive a physiologically realistic FN input. For that aim, we study commonly used action potential attributes for excitatory and inhibitory populations separately to discern if action potential attributes sufficiently capture within-population heterogeneity in excitatory and inhibitory groups. We also aim to unravel the differences between excitatory and inhibitory populations regarding their action potential attributes. For this, we extract 22 attributes (see Methods) subdivided into spiking dynamics, Spike threshold, and action potential height and width attributes with their descriptive statistics incorporating the mean, median, minimum, and maximum values.

We cluster the E/I populations separately based on the features and find 7 clusters for excitatory cells (shaded in red) and 6 clusters for inhibitory cells (shaded in blue). The UMAP representation of the spike-based properties for E/I populations with unique colors for each cluster for the chosen cluster parameter is shown in (Fig. ??a-b). We show the cluster stability (see Methods) in (Fig. ??c), the number of clusters is stable (low standard deviation) for the chosen resolution parameter (black arrow). We also test the stability of the clusters by excluding one attribute at a time and repeating the stability analysis (see Methods) and find the inhibitory clusters to be more stable to attribute exclusion (Appendix. ??a-b). We compare the means of action potential attributes simultaneously between excitatory and inhibitory populations and find them to be significantly different (one-sided MANOVA (see Methods), Wilks' lambda;  $F(21, 290.0) = 35.1841$ ;  $p = 0.000***$ , Pillai's trace;  $F(21, 290.0) = 35.1841$ ;

$p = 0.000^{***}$ , Hotelling-Lawley trace;  $F(21,290.0) = 35.1841$ ;  $p = 0.000^{***}$ , Roy's greatest root;  $F(21,290.0) = 35.1841$ ;  $p = 0.000^{***}$ ). To identify the relative importance of each attribute in the separation of excitatory and inhibitory populations, we perform a canonical correlation analysis (CCA) (see Methods) between the excitatory and inhibitory action potential attributes and calculate the loading (structure correlation) for each attribute (Fig. ??d). We find that spiking dynamics attributes have the most influence on the inhibitory canonical variates suggesting that these variables have the most influence on separating the inhibitory population apart from the excitatory population. Alternatively, AP height and width attributes strongly influence the excitatory population canonical variate, suggesting that AP height and width are the most discriminatory. These results also show that individual action potential attributes contribute differently to the canonical variate (i.e., the latent structure) for excitatory and inhibitory populations respectively.

Next, we want to compare the level of heterogeneity within excitatory (E-E) and inhibitory (I-I) populations as well as across (I-E) populations using the action potential attributes. We visualize the action potential attributes using a radar plot shown in (Fig. ??e-f). It shows the diversity of spiking dynamics, spike threshold, and AP height and width for each neuron in each cluster (with the same color as in the UMAP projection (Fig. ??a-b) along with the mean for the cluster (thick line). We observe that spiking dynamics attributes differ between excitatory and inhibitory clusters. The spiking threshold profiles were also found to be different across E/I clusters. Comparing the AP height and width attributes, however, show a similar profile across E/I clusters. We quantify the heterogeneity in the E/I clusters using a cosine similarity measure. The excitatory population had a significantly higher cosine similarity measure within the population than the inhibitory population (Welch's ANOVA,  $F(2,49135)=3626998.65$ ,  $p= 0.0$ ; Post-hoc Games-Howell test, E-E vs I-I ( $**p=0.001$ ), I-I vs I-E ( $**p=0.001$ ), and E-E vs I-E ( $**p=0.001$ )), (Fig. ??g)), suggesting that inhibitory action potential

attributes are more heterogeneous than their excitatory counterparts. The mean cosine similarity score between excitatory and inhibitory populations are significantly lower than the within-population cosine similarity score for both excitatory and inhibitory populations respectively, suggesting that excitatory and inhibitory feature action potential attribute vectors are different from each other, reiterating the MANOVA results. The results above demonstrate that action potential attributes are different between excitatory and inhibitory populations. The inhibitory population is more heterogeneous in its action potential attributes than the excitatory population.

### **Passive biophysical feature and adaptation-based profile using the FN protocol**

As we describe in the last two sections, we aim to compare neuronal attribute sets to find the attribute(s) most informative about heterogeneity in excitatory and inhibitory populations and try to understand how neurons cluster based on these properties. The passive biophysical attributes (i.e., membrane resistance, capacitance, etc.) shape the response properties of a neuron. Moreover, it has been reported that adaptation current which captures the adaptation properties of the membrane is another important neuron property that can determine cell classes with noisy input [Mensi et al. \(2012\)](#). We, therefore, consider the passive biophysical attributes and the adaptation current as potential candidates that capture heterogeneity within the neuronal population. To understand the heterogeneity of passive biophysical properties and adaptation parameters across the excitatory and inhibitory populations, we extract both a set of passive parameters (see methods) and an adaptation current by fitting a Generalized Leaky Integrate and Fire (GLIF) model on the first 100 seconds of each FN trial, using the automated method described by [Pozzorini et al. \(2015\)](#) (see methods). (Fig. ??a) shows an example of a 10s instance of a GLIF-fitted model and one of the original recordings. We characterized the goodness of fit by measuring the explained variance (EV) between the subthreshold membrane potential of the original data and the model.

(Fig. ??b) shows the distributions of the EV and  $\Gamma$  for the entire dataset. We eliminate the models with an EV value below 0.7 and obtain a set of 307 samples (out of 312 samples).

We cluster the recordings into cell classes based on a set of passive biophysical parameters along with threshold adaptation constants (in total 6 features, see Fig. ??a-b) using the UMAP+Louvain clustering method explained in the previous sections, we find 7 clusters for the excitatory population and 6 clusters for the inhibitory population. We examine the stability of the clusters (Fig. ??c) with different hyperparameters (resolution parameters, see Methods) and choose (black arrow) the resolution parameter with the maximum modularity score. The clusters for the chosen hyperparameter for both excitatory and inhibitory populations were stable (low standard deviation). We also test the stability of the clusters by excluding one attribute at a time and repeating the stability analysis (see Methods) and found the inhibitory clusters to be more stable to attribute exclusion (Appendix. ??c-d). (Fig. ?? d-e) shows the UMAP representation of the feature set (inset) for excitatory (red background) and inhibitory (blue background) populations, the radar plot shows the individual biophysical parameter values for each neuron and each thin line in the radar plot represents a single neuron and are color matched to respective clusters, the mean for each cluster is plotted with a thick line. We compare the means of all the passive biophysical attributes simultaneously between excitatory and inhibitory populations and find them to be significantly different (one-sided MANOVA, Wilks' lambda;  $F(6,301) = 23.2629$ ;  $p = 0.000***$ , Pillai's trace;  $F(6,301) = 23.2629$ ;  $p = 0.000***$ , Hotelling-Lawley trace;  $F(6,301) = 23.2629$ ;  $p = 0.000***$ , Roy's greatest root;  $F(6,301) = 23.2629$ ;  $p = 0.000***$ ). To identify the relative importance of each passive biophysical attribute in the separation between excitatory and inhibitory populations, we perform a canonical correlation analysis (CCA) (see Methods) between the excitatory and inhibitory passive biophysical attributes and calculate the loading (structure correlation) for each attribute (Fig. ??h). We find dis-

similar contributions from excitatory and inhibitory passive parameters towards their respective canonical variate, suggesting that each passive biophysical attribute contributes differently to the excitatory-inhibitory latent structure and therefore sets the excitatory-inhibitory populations apart. Next, we compare the level of heterogeneity between the passive feature vectors across the E/I populations (Fig. ??i) using the cosine similarity measure within and across excitatory populations and find no significant difference between the mean cosine similarity measure within excitatory and inhibitory populations as well as across excitatory-inhibitory population (due to low effect size) (Welch's ANOVA,  $F(2,66792)=0.16777$ ;  $p= 0.84$ , Fig. ??i). These results suggest that even though the mean of the excitatory and inhibitory passive biophysical attributes are significantly different from each other (measured using MANOVA), the level of heterogeneity within excitatory-inhibitory populations respectively based on biophysical parameters is quite low. Therefore the passive biophysical attributes are not so informative about the neuronal heterogeneity.

As we saw above, passive biophysical features are not informative about population heterogeneity, this result is consistent with Mensi et al. (2012), which finds that passive biophysical features do not distinguish between neuron types. The adaptation current is more useful in putting neuron types apart. Therefore we classify the neurons using the adaptation current ( $\eta$ ) extracted from the fitted GLIF model for the E/I population separately. We find 6 classes for the excitatory population (red) and 5 classes for the inhibitory population (blue). In (Fig. ??f-g) we show the UMAP representation of the adaptation current and the corresponding average normalized shapes for each cluster (inset) each cluster has its respective color in the UMAP as well as shape plots. We observe that the excitatory adaptation currents have a stronger negative amplitude than their inhibitory counterparts. Moreover, the adaptation currents of the inhibitory population relax back to their resting values at earlier times than for the excitatory population.

We quantify the heterogeneity of adaptation currents within excitatory and inhibitory populations using the cosine similarity measure. The heatmap in (Fig. ??j) shows that the excitatory adaptation currents have a significantly higher average cosine similarity compared to the inhibitory adaptation currents, suggesting that the inhibitory adaptation current is more heterogeneous than the excitatory population (Welch's ANOVA;  $F(2,46968) = 2796.77$ ,  $**p = 0.0$ ; Post-hoc Games-Howell test E vs I ( $**p = 0.001$ ), I vs ExI ( $p = 0.75$ ), and E vs ExI ( $**p = 0.001$ ), Fig. ??j). The similarity measure is not significantly different between the inhibitory (I) population and across the inhibitory and excitatory (I vs E) population. This suggests that inhibitory adaptation currents are as different from each other as they are different from the excitatory adaptation currents. These results suggest that adaptation current profiles are different between excitatory and inhibitory populations. These results also show that adaptation currents are useful for understanding the heterogeneity within the inhibitory population but not so much for the excitatory populations.

### **Neuronal classification based on linear input filter approximated using a Spike Triggered Average (STA) in the FN protocol**

In last two sections, we explored neuronal heterogeneity based on action potential, passive biophysical, and adaptation attributes in neurons while responding to an FN input. We found that except for passive biophysical attributes, other properties show both within population across population heterogeneity for both excitatory and inhibitory populations. We observe a higher level of heterogeneity for inhibitory populations. Since we aim at understanding the extent to which various neuronal properties help uncover neuronal diversity, in this section we focus on the linear input filter of neurons and aim to understand the neuronal diversity based on this attribute. We consider this attribute important as neurons respond strongly to specific features in the input Sharpee (2014), making linear input filter an important property to study the functional diversity of the

neuronal population.

The spike-triggered average (STA) method, as described in Schwartz et al. (2006), estimates a neuron's linear input filter by identifying the features in the input that trigger the neuron to spike. It does this by averaging the input signal over a specific time window preceding each spike, using data from all observed spikes. This makes the STA a useful method to approximate the linear input filter of a neuron. We want to investigate the STA diversity across the E/I population, for this, we extract the STA from all the neurons (see Methods). For calculating the STA, we use the injected current which is the result of shifting a theoretical dimensionless input with a constant baseline and scaling it by a factor as explained by Zeldenrust et al. (2017); da Silva Lantyer et al. (2018).

We cluster the excitatory and inhibitory population STAs separately using an unsupervised UMAP+Louvain clustering method (see Methods). We find 7 clusters for the excitatory population STAs (red) and 8 for the inhibitory population STAs. The STAs were normalized and standardized before clustering (see Methods). The UMAP representation and the corresponding averaged and normalized STAs for each cluster are shown in (Fig. ??a-b). A visual inspection shows that inhibitory and excitatory STA shapes differ in their peak amplitudes and in the maximum slope of their initial rise (Fig. ??a-b inset), this difference is shown more clearly in (Fig. ??d). The stability of the clustering algorithm for the chosen parameters is shown in (Fig. ??c). To quantify the heterogeneity within the excitatory and inhibitory population as a result of that linear input filters, we first calculate the STA shape similarity between clusters, using a cosine similarity between excitatory and inhibitory STA clusters (Fig. ??e-f). The values shown in the heatmap in Fig. ??e-f were calculated by averaging the cosine similarity matrices between STAs of each cluster pair and within each cluster (for the within-cluster comparison, only the upper triangular values were included in the average). The average cosine similarity value between excitatory STA clusters shows

higher values ( $> 0.9$ ) with each other except for clusters IDs 2 and 6, which show a low similarity with every other cluster except for itself. On average, each excitatory cluster shows a high similarity ( $>0.9$ ) with more than 2 other clusters. On the other hand, the average cosine similarity values between inhibitory clusters is low ( $<0.9$ ), with some exceptions such as cluster IDs (2, 8), (3, 6), (5, 4), (6, 5) and (8, 6). On average, the STA of each inhibitory cluster is highly similar to approximately 1 other cluster. The average cosine similarity value is high between STAs within each inhibitory cluster. We summarize the STA similarities within the excitatory (E-E) and inhibitory populations (I-I) as well as across the two populations (I-E) in the heatmap in (Fig. ??g). This is done by averaging the cosine similarity matrices between STAs within excitatory (E-E) and inhibitory (I-I) populations as well as across excitatory and inhibitory (I-E) populations, these matrices are shown in (Appendix. ??b). For within-population averages (E-E and I-I), we only take the upper-triangular portion of the matrix. The average cosine similarity value within the inhibitory population is significantly lower than that of within the excitatory population (Fig. ??g Welch's ANOVA,  $F(2,48825)=1005.90$ ,  $**p= 0.0$ ; Post-hoc Games-Howell test, E vs I ( $**p=0.001$ ), I vs ExI ( $**p=0.001$ ), and E vs ExI ( $**p=0.001$ )), suggesting that inhibitory STAs are more heterogeneous than excitatory ones. Also, the STA shape similarity between excitatory and inhibitory populations is significantly lower than the within excitatory and inhibitory similarity, suggesting that excitatory and inhibitory STAs are different. We can see that on average inhibitory neurons respond to more diverse features in the input than excitatory neurons.

### **Comparing Physiological Heterogeneity across attribute sets using Multi Correlation and Factor Analysis**

We aim to explore what a physiologically realistic stimulus reveals about the functional heterogeneity of a neural population. For this aim, we need to compare FN-based neu-

ronal attribute sets and find out which attribute set is the most informative about neuronal heterogeneity under the dynamic FN stimulation protocol. This is a complicated problem, as the four attribute sets are of varying dimensions. To perform this comparison, we use a method known as Multi Correlation and Factor Analysis (MCFA) Brown et al. (2023), which is an unsupervised multi-set integration method based on probabilistic Principal Component Analysis (pPCA) and Factor Analysis (FA), that can help to understand the common and shared factors across multi-modal data (see methods & Brown et al. (2023)). We use this method to compare the private and shared variance explained by the 4 attribute sets we examined in the previous sections (i.e., action potential attributes, passive biophysical attributes, adaptation currents, and linear input filters (STA)). We use the pPCA space to model the shared structure across attributes (see Methods), and the residuals are modeled as a private structure for each attribute set using factor analysis (see methods).

Comparing the variance explained by the shared structure across attributes, we found that the excitatory population which is inferred by a 4-dimensional shared structure, explains almost 50% of the variance in action potential and passive biophysical attributes (Fig. ??a top), this is higher than linear input filter (STA) (32.9 %) and adaptation current attribute (19.7 %). Most importantly, we see that the linear input filters (STAs) explain the highest private variance (57.2 %), followed by adaptation current (41.2 %). The action potential and passive biophysical attributes have a relatively lower private variance (35.7 %). We can further investigate the contribution to the most important shared factor by each attribute, through which we find that action potential and passive biophysical features explain the most variance for the most important shared dimension (Fig. ??a(middle, bottom)). Similarly, for the inhibitory population, explained by a 3 dimensional shared structure, we find that the linear input filter (STA) explains the most amount of private variance (80.6 %), much higher than the excitatory population (Fig. ??b (top)), followed by adaptation current (29.4

%), action potential features (35.7 %), and passive biophysical features (17.1 %) respectively. The action potential features and Passive biophysical features explain the most and almost equal amount of shared variance (33.8 % and 33.85 % respectively) (Fig. ??b (middle)), followed by adaptation Current (29.4 %) and linear input filter (9.9 %) (Fig. ??b (top)). We find that the adaptation current and passive features explain the largest amount of variance for the most important shared dimension (Fig. ??b (bottom)) for the inhibitory population. It is important to observe that the linear input filter explains more than 85% of the total variances (shared+private) for both excitatory and inhibitory populations, higher than the other 3 attribute sets.

The high values of private variance explained by the linear input filters (STAs) in both excitatory and inhibitory cases show that passive biophysical, action potential, and adaptation currents are not highly correlated with the linear input filter of a neuron. Therefore, the linear input filter contains unique information about the excitatory and inhibitory population that is not shared with the other 3 attribute sets. Most importantly, the high value of private variance for the linear input filter, along with low residual values compared to other attribute sets indicates that linear input filters are likely to be the most informative attributes for explaining neuronal heterogeneity compared to passive biophysical, action potential, and adaptation current attributes. On the contrary, high values of shared variance for passive biophysical attributes and action potential attributes show that these attributes share a common structure, and can be a good predictor of one another. It is also important to observe that the total variance explained (shared + private) by adaptation currents is lower than action potential attributes for both excitatory and inhibitory populations, suggesting that action potential attributes are more informative about neuronal heterogeneity than adaptation currents.

## Discussion

In this work, we aimed to study the effect of input protocol (SH vs FN) on neuronal functional classification as well as to draw consensus on the attribute that are most informative about functional heterogeneity. For this, we first looked at the effect of the input protocol on neuronal classification based on two feature sets: waveforms and action potential features, while neurons were stimulated using two stimulus protocols: a static Step and Hold (SH) and a physiologically realistic Frozen Noise (FN) input. We found neuronal classification based on FN and SH protocols to be inconsistent when comparing the similarity in the cluster assignment in both input conditions using the co-cluster likelihood and cluster similarity indices (ARI and AMI). This highlights the importance of using a physiologically realistic input for studying functional heterogeneity of a neuronal population. We then aimed to determine which attribute(s) is/are the most informative about the neuronal functional heterogeneity when neurons are stimulated with a physiologically realistic FN input. We first explored the functional diversity of cells using 4 attribute sets (action potential, passive biophysical, adaptation current, and linear input filter (STA) attributes) for putative excitatory and inhibitory populations. To infer which attribute(set) is most informative about neuronal heterogeneity, we compared the private and shared variance across the four attribute sets. We found that the linear input filters (STAs) explain the most variance, especially private variance across the excitatory and inhibitory neurons, and thus, contains unique information about neuronal functional heterogeneity compared to other attributes and is the most informative about neuronal functional heterogeneity.

### The role of input in neuronal functional diversity

In the present work, we found that neuronal functional classification changes as a function of the input the neurons receive, this point is still undiscussed in neuronal clustering literature. Our results fill an important gap in the literature, the effect of in-

put on physiological classification, by showing that waveforms and electrophysiological attributes-based classifications are different when neurons are stimulated with static versus dynamic inputs. Previous studies that combined electrophysiological, morphological, and molecular attributes for neuronal classification (Gouwens et al. (2019); Scala et al. (2019); Gouwens et al. (2020)), hypothesized that electrophysiological classification of a neuron can potentially change when using a different stimulus protocol. Our classification results confirm this hypothesis, by showing that clustering based on intracellular waveforms and action potential attributes are inconsistent across SH and FN-based inputs.

Our results showcase the importance of considering the functional dimension of neuronal identity that emerges from the interaction between input characteristics and intrinsic neuronal properties. These results do not only showcase how neurons cluster differently as a result of changing input protocol, which is an important and novel finding in the context of neuronal classification, but they also show that spiking dynamics, spike threshold, and AP height and width attributes were distinct between FN and SH protocols, as shown by the consistently low cosine similarities between FN and SH clusters and the radar plots comparing the spiking dynamics, spike threshold, and AP height and width attributes for each neuron. This is in agreement with earlier results of Szabó et al. (2021); Hernáth et al. (2019); Szücs and Huerta (2015), which have already shown that firing intensity measures (AP count and AMPA conductance) are weakly correlated between static and dynamic stimuli (dynamic clamp) conditions. We extended these results by showing that the commonly studied action potential attributes span different latent manifolds as a result of input protocol (Appendix ??). Therefore, these classical action potential features do not encode a signature of the neurons that is invariant to the input, but are susceptible to the input the neurons receive. Since the conventionally used step and hold protocol does not represent an input a neuron receives *in vivo*, our findings advocate for using a physiologically realis-

tic dynamic inputs such as the FN input for studying functional diversity. Our results therefore establish that input dynamics and its effects on functional classification and need to be considered even before molecular and morphological markers.

We used an unsupervised UMAP+Louvain clustering method in this study which has already been shown to distinguish neuronal classes based on extracellular waveforms ([Lee et al. \(2021\)](#)) and also has been shown to improve upon classifications based on a low number of features extracted from waveforms. We capitalized on this idea by using UMAP+Louvain clustering to cluster SH and FN intracellular waveforms and action potential attributes and then compared the cluster assignments across the two protocols. Since the Louvain community method clusters on the high-dimensional graph structure provided by the UMAP algorithm, rather than projecting the data on a low dimensional space [Druckmann et al. \(2013\)](#); [Gouwens et al. \(2019\)](#), which often leads to a loss of information about the latent structure [Druckmann et al. \(2013\)](#), the clusters using the UMAP graphs were more robust than found either using a dimensional feature set or a low dimensional projection of the original high dimensional feature set. A second important advantage of using a non-linear dimensionality reduction technique like UMAP is that it allows for a manifold comparison between the two input conditions (see Appendix ??(a-b)).

## **Neuronal classification using frozen noise input-based attributes**

We have established that neuronal functional classification is a result of the type of input that neurons receive, therefore a physiologically realistic input is important to understand neuronal functional diversity. A new question emerges: which attribute sets are the most informative about neuronal functional heterogeneity when neurons are presented with a dynamic stimuli? A similar question has been raised by ([Zeng and Sanes \(2017\)](#)). We attempted to provide a schema for answering this question. We did not intend to suggest a definitive number of classes of neurons, nor did we want to match

our findings with previously established MET type classification, but we rather aimed to delineate a framework for drawing a consensus about which attribute(s) are the most informative about neuronal functional heterogeneity. An array of previous classification studies have relied upon variants of action potential and passive biophysical features Contreras (2004); Halabisky et al. (2006); McGarry et al. (2010); Casale et al. (2015), without any consensus about the informativeness of the attributes selected. Also, these studies have conventionally been reliant on feature extraction based on step stimulus protocols, which we demonstrate to produce cell classes that are different from when the neurons are stimulated with a dynamic input.

Although Hernáth et al. (2019); Szabó et al. (2021) provide a comparison between neurons responding to static and dynamic inputs, an active recommendation for which parameters are the most discriminatory was still missing. We supersede this by offering an alternative classification paradigm, based on the physiologically realistic frozen noise input. We tried to fill this gap by dividing the neuronal population into putative excitatory and inhibitory groups, then clustering neurons using the unsupervised UMAP+Louvain method, using four different sets of attributes separately. We found that neuronal clusters are subjective to feature selection. There was little consistency in comparing cluster assignments across the four attribute sets (see Appendix ??a-b): the number of classes as well as the cluster assignments were found to be inconsistent across the four attribute sets.

We divided the neuronal population into putative excitatory and inhibitory classes based on the waveform shapes and firing rates, which is rather different from using molecular and morphological labels for E/I classification. Still, the goal of this study is not to align the neuronal identities to their ME-type markers, but rather to highlight the importance of input stimuli in functional classification. We show this by demonstrating that the firing properties of the narrow-width and broad-width neurons, which are conventionally categorized into inhibitory and excitatory classes respectively, change

as a result of changing input type.

Parallel to investigating how putative E/I populations cluster based on different features, we also estimated the within-population variance for each feature set within E/I populations, which is representative of population heterogeneity based on a said feature. For action potential and passive biophysical attribute sets, we calculated the differences in the means of cosine similarity between E/I populations. We found that action potential attributes significantly differed between excitatory and inhibitory populations, consistent with previous findings Connors and Gutnick (1990). We also found that the action potential attributes for the inhibitory population was more heterogeneous than the excitatory population, which is also consistent with previous findings Gouwens et al. (2019, 2020). It is important to highlight that the number of clusters found in our analysis is similar across excitatory and inhibitory populations, which might result from our dataset containing more excitatory than inhibitory neurons. The clustering based on the second feature set, that of passive biophysical properties extracted by fitting a GLIF model to the neural recordings, showed that passive parameters were also significantly different between excitatory and inhibitory neurons, but within-population heterogeneity was not significantly different between excitatory and inhibitory neurons. This suggests that passive parameters do not drive functional heterogeneity. This result is consistent with Mensi et al. (2012), which suggests that passive properties are not sufficiently discriminatory within E and I populations. Moreover, the authors claim that adaptive properties extracted using the GLIF model, such as the adaptation current, are more discriminatory than passive parameters. Our findings confirm this: adaptation currents show low similarity between excitatory and inhibitory populations, we found that the absolute maximum amplitude of all the adaptation current of the inhibitory neurons is smaller than that of the excitatory ones. We also found that inhibitory neurons have a significantly more heterogeneous adaptation profile than the excitatory population. This result provides data for designing and studying heterogeneous adap-

tive network models to further enhance our understanding of neural circuits' functional underpinnings.

Neurons can be functionally classified based on their input response features [Famulare and Fairhall \(2010\)](#); [Sharpee \(2014\)](#); [Chéreau et al. \(2020\)](#). We analyzed the linear input filters of neurons using the Spike Triggered Averages (STAs). This technique has been extensively used in studying the stimulus preference of neurons in the visual cortex [Chichilnisky \(2001\)](#); [Rathbun et al. \(2018\)](#). Our results show that the STA features are effective for estimating neuronal functional heterogeneity. We found that on average the STA shapes between the excitatory and inhibitory populations were different, based on comparing the average cosine similarity values between E and I populations, showing the difference in linear input filter between the two populations. We also found that the STA heterogeneity within the inhibitory population is significantly higher than the excitatory population. It has been shown [Cardin et al. \(2007\)](#) that visual cortical fast-spiking (putatively inhibitory) and regular-spiking (putatively excitatory) neurons have distinct levels of feature selectivity due to differences in passive biophysical attributes, such as the membrane time constant and input resistance. Since fast-spiking neurons have higher membrane leak conductance, therefore lower resistance it results in sharpening of neuronal selectivity to its preferred input as shown in previous studies such as [Li et al. \(2020\)](#). Conversely, regular spiking neurons were found to have lower conductance and thus, lower sensitivity to preferred stimuli. Previous computational studies have found that physiological and passive biophysical have degenerative relationships with STA kernels [Jain and Narayanan \(2020\)](#), this study has shown that the same STA shape can be achieved by multiple difference values of the passive biophysical properties. This kind of degeneracy has been observed at the ion channel level as well [Prinz et al. \(2004\)](#); [Marder and Taylor \(2011\)](#). On the contrary, we observed a limited variability in biophysical features giving rise to a higher heterogeneity (comparing the within-population similarity matrices) in the STAs, i.e.

in the functional linear input filter. We expect that the measured passive biophysical parameters from our data would be a good starting point to study the relationship between STA shape differences and the range of passive biophysical attributes, this needs further computational modeling efforts. Since the diversity of feature preference by single neurons in the barrel cortex is not completely understood, a quantification of the functional heterogeneity observed in the linear input filter provided by our results is important for creating biophysically realistic models of cortical circuits and for a better understanding of circuit characteristics.

### **MCFA-based variance comparison across attribute sets**

To determine which attribute set is most informative about neuronal functional heterogeneity, we compared the amount of neuronal population heterogeneity showcased by each attribute set by comparing the amount of private and shared variance explained by each attribute set. To our knowledge, the multi-attribute set comparison has not been done with physiological attributes before. This method provides a structured pathway to understand the limitations of commonly used electrophysiological features in cluster studies and helps to reach a consensus about the choice of attributes to be used for functional classification. We found that linear input filter explained the highest amount of private variance of all the attribute sets, for both excitatory and inhibitory neuronal populations. This is a clear indication of the usefulness of a linear input filter (STA) as an attribute to explore functional heterogeneity. Contrarily, we found that passive biophysical attributes and action potential attributes explain the most shared variance for excitatory and inhibitory populations, suggesting that these attributes are correlated and contain similar latent structures. This is an important result that can aid in the debate around selecting a feature that is the most informative about neuronal functional heterogeneity. We expect our approach to provide a framework for comparing heterogeneity across other brain regions as well.

## Limitations

There are several limitations to our study. Firstly, the sample size for the shared FN and SH comparison set was 186 cells, which might not be enough to capture all variability across the somatosensory cortex layer 2/3. For the second part of the study, the sample size was 312 neurons. We expect an increased sample size would increase confidence in functional neuronal clusters. It would be insightful to sample from all layers of the barrel cortex and compare the linear input filter across layers, to gain a complete insight into the barrel cortical functional diversity. It has been argued that the activity of a large population of neurons that captures a certain behavior can be approximated by a low-dimensional representation from a few neurons ([Gao and Ganguli \(2015\)](#)) and therefore that the number of recorded neurons should depend on the neural task complexity. Even though the Frozen Noise is a better approximation of the synaptic input than a Step-and-Hold stimulus, it might not be representative of the full dimensionality of the input that a neuron receives *in vivo*, as the FN input is based on somatic current injection. We understand that a somatic current injection doesn't represent the full range of non-linear dendritic integration but it is quite helpful in estimating the linear input filter of a neuron which is found to be the most varying across neural populations and is sufficient for understanding the functional heterogeneity. We also lack the morphological and transcriptomic labels of the neurons, which makes the clusters found in this study incomparable to the commonly known types [Zeng \(2022\)](#). We expect a dynamic clamp-like setup using the frozen noise input along with morphological and transcriptomic labels to provide more clarity. Our study is also limited in providing a mechanistic relationship between the attribute sets we use, such as how the input changes the passive biophysical features and ultimately the linear input filter. Although the point GLIF model is quite helpful for extracting passive features, it does not provide a mechanistic description at ion channel level resolution for the

variability in adaptation current and the feature selectivity. As explained above, we expect that a more detailed single neuron model, when studied with a physiologically realistic input, would provide a more elaborate picture of how the passive biophysical properties give rise to action potential and adaptation properties, which eventually result in the linear input filter. However, more detailed neuron models are difficult to fit and often do not produce unambiguous model properties Gonçalves et al. (2020); Nandi et al. (2022).

## Conclusion

In conclusion, we show that neuronal functional classification is a function of the input protocol and therefore, a physiologically realistic input should be preferred for functional classification. We also established that linear input filters are the most distinguishing property, compared to action potential, passive biophysical, and adaptation current attributes, for understanding the functional diversity of neurons when stimulated with a physiologically realistic input. These results provide an important recommendation for neural taxonomists and electrophysiologists: to consider a neuron's physiological input when defining neural identity. We expect computational single neuron as well as cortical network modeling efforts to discover the implications of the heterogeneity found in the 4 attribute sets of the excitatory and inhibitory neuronal populations we studied.

## References

- (2017). Proteomic landscape of the primary somatosensory cortex upon sensory deprivation. *GigaScience*, 6(10):gix082.
- Aggarwal, C. C., Hinneburg, A., and Keim, D. A. (2001). On the surprising behavior of distance metrics in high dimensional space. In *Database theory—ICDT 2001: 8th international conference London, UK, January 4–6, 2001 proceedings* 8, pages 420–434. Springer.
- Avermann, M., Tomm, C., Mateo, C., Gerstner, W., and Petersen, C. C. (2012). Microcircuits of excitatory and inhibitory neurons in layer 2/3 of mouse barrel cortex. *Journal of neurophysiology*, 107(11):3116–3134.
- Bean, B. P. (2007). The action potential in mammalian central neurons. *Nature Reviews Neuroscience*, 8(6):451–465.
- Blondel, V. D., Guillaume, J.-L., Lambiotte, R., and Lefebvre, E. (2008). Fast unfolding of communities in large networks. *Journal of statistical mechanics: theory and experiment*, 2008(10):P10008.
- Bonald, T., de Lara, N., Lutz, Q., and Charpentier, B. (2020). Scikit-network: Graph analysis in python. *Journal of Machine Learning Research*, 21(185):1–6.
- Brown, B. and collinwa (2023). collinwa/mcfa: First pypi release.
- Brown, B. C., Wang, C., Kasela, S., Aguet, F., Nachun, D. C., Taylor, K. D., Tracy, R. P., Durda, P., Liu, Y., Johnson, W. C., et al. (2023). Multiset correlation and factor analysis enables exploration of multi-omics data. *Cell Genomics*, 3(8).
- Cadwell, C. R., Palasantza, A., Jiang, X., Berens, P., Deng, Q., Yilmaz, M., Reimer, J., Shen, S., Bethge, M., Tolias, K. F., et al. (2016). Electrophysiological, transcriptomic and morphologic profiling of single neurons using patch-seq. *Nature biotechnology*, 34(2):199–203.
- Cardin, J. A., Palmer, L. A., and Contreras, D. (2007). Stimulus feature selectivity in excitatory and inhibitory neurons in primary visual cortex. *Journal of Neuroscience*, 27(39):10333–10344.
- Casale, A. E., Foust, A. J., Bal, T., and McCormick, D. A. (2015). Cortical interneuron subtypes vary in their axonal action potential properties. *Journal of Neuroscience*, 35(47):15555–15567.
- Chéreau, R., Bawa, T., Fodoulian, L., Carleton, A., Pagès, S., and Holtmaat, A. (2020). Dynamic perceptual feature selectivity in primary somatosensory cortex upon reversal learning. *Nature communications*, 11(1):3245.
- Chichilnisky, E. (2001). A simple white noise analysis of neuronal lightresponses. *Network: computation in neural systems*, 12(2):199.
- Connors, B. W. and Gutnick, M. J. (1990). Intrinsic firing patterns of diverse neocortical neurons. *Trends in neurosciences*, 13(3):99–104.
- Contreras, D. (2004). Electrophysiological classes of neocortical neurons. *Neural Networks*, 17(5–6):633–646.
- da Silva Lantyer, A., Calcini, N., Bijlsma, A., Kole, K., Emmelkamp, M., Peeters, M., Scheenen, W. J., Zeldenrust, F., and Celikel, T. (2018). A databank for intracellular electrophysiological mapping of the adult somatosensory cortex. *GigaScience*, 7(12):giy147.
- Druckmann, S., Hill, S., Schürmann, F., Markram, H., and Segev, I. (2013). A hierarchical structure of cortical interneuron electrical diversity revealed by automated statistical analysis. *Cerebral Cortex*, 23(12):2994–3006.
- Famulare, M. and Fairhall, A. (2010). Feature selection in simple neurons: how coding depends on spiking dynamics. *Neural computation*, 22(3):581–598.
- Fishell, G. and Heintz, N. (2013). The neuron identity problem: form meets function. *Neuron*, 80(3):602–612.
- Fontaine, B., Peña, J. L., and Brette, R. (2014). Spike-threshold adaptation predicted by membrane potential dynamics in vivo. *PLoS computational biology*, 10(4):e1003560.

- Fuzik, J., Zeisel, A., Máté, Z., Calvignoni, D., Yanagawa, Y., Szabó, G., Linnarsson, S., and Harkany, T. (2016). Integration of electrophysiological recordings with single-cell rna-seq data identifies neuronal subtypes. *Nature biotechnology*, 34(2):175–183.
- Gao, P. and Ganguli, S. (2015). On simplicity and complexity in the brave new world of large-scale neuroscience. *Current opinion in neurobiology*, 32:148–155.
- Gerstner, W., Kistler, W. M., Naud, R., and Paninski, L. (2014). *Neuronal dynamics: From single neurons to networks and models of cognition*. Cambridge University Press.
- Gonçalves, P. J., Lueckmann, J.-M., Deistler, M., Nonnenmacher, M., Öcal, K., Bassetto, G., Chintaluri, C., Podlaski, W. F., Haddad, S. A., Vogels, T. P., et al. (2020). Training deep neural density estimators to identify mechanistic models of neural dynamics. *Elife*, 9:e56261.
- Gouwens, N. W., Sorensen, S. A., Baftizadeh, F., Budzillo, A., Lee, B. R., Jarsky, T., Alföldi, L., Baker, K., Barkan, E., Berry, K., et al. (2020). Integrated morphoelectric and transcriptomic classification of cortical gabaergic cells. *Cell*, 183(4):935–953.
- Gouwens, N. W., Sorensen, S. A., Berg, J., Lee, C., Jarsky, T., Ting, J., Sunkin, S. M., Feng, D., Anastassiou, C. A., Barkan, E., et al. (2019). Classification of electrophysiological and morphological neuron types in the mouse visual cortex. *Nature neuroscience*, 22(7):1182–1195.
- Halabisky, B., Shen, F., Huguenard, J. R., and Prince, D. A. (2006). Electrophysiological classification of somatostatin-positive interneurons in mouse sensorimotor cortex. *Journal of neurophysiology*, 96(2):834–845.
- Harris, K. D. and Shepherd, G. M. (2015). The neocortical circuit: themes and variations. *Nature neuroscience*, 18(2):170–181.
- Heiss, J. E., Katz, Y., Ganmor, E., and Lampl, I. (2008). Shift in the balance between excitation and inhibition during sensory adaptation of sI neurons. *Journal of Neuroscience*, 28(49):13320–13330.
- Hernáth, F., Schlett, K., and Szűcs, A. (2019). Alternative classifications of neurons based on physiological properties and synaptic responses, a computational study. *Scientific reports*, 9(1):13096.
- Huang, Z. J. and Paul, A. (2019). The diversity of gabaergic neurons and neural communication elements. *Nature Reviews Neuroscience*, 20(9):563–572.
- Jain, A. and Narayanan, R. (2020). Degeneracy in the emergence of spike-triggered average of hippocampal pyramidal neurons. *Scientific reports*, 10(1):374.
- Kiritani, T., Pala, A., Gasselin, C., Crochet, S., and Petersen, C. C. (2023). Membrane potential dynamics of excitatory and inhibitory neurons in mouse barrel cortex during active whisker sensing. *Plos one*, 18(6):e0287174.
- Kole, K. and Celikel, T. (2019). Neocortical microdissection at columnar and laminar resolution for molecular interrogation. *Current Protocols in Neuroscience*, 86(1):e55.
- Kole, K., Zhang, Y., Jansen, E. J., Brouns, T., Bijlsma, A., Calcini, N., Yan, X., Lantyer, A. d. S., and Celikel, T. (2020). Assessing the utility of magneto to control neuronal excitability in the somatosensory cortex. *Nature neuroscience*, 23(9):1044–1046.
- Lee, E. K., Balasubramanian, H., Tsolias, A., Anakwe, S. U., Medalla, M., Shenoy, K. V., and Chandrasekaran, C. (2021). Non-linear dimensionality reduction on extracellular waveforms reveals cell type diversity in premotor cortex. *Elife*, 10:e67490.
- Li, B., Routh, B. N., Johnston, D., Seidemann, E., and Priebe, N. J. (2020). Voltage-gated intrinsic conductances shape the input-output relationship of cortical neurons in behaving primate v1. *Neuron*, 107(1):185–196.
- Marder, E. and Taylor, A. L. (2011). Multiple models to capture the variability in biological neurons and networks. *Nature neuroscience*, 14(2):133–138.
- Markram, H., Toledo-Rodriguez, M., Wang, Y., Gupta, A., Silberberg, G., and Wu, C. (2004). Interneurons of the neocortical inhibitory system. *Nature reviews neuroscience*, 5(10):793–807.
- Martens, M. B., Celikel, T., and Tiesinga, P. H. (2015). A developmental switch for hebbian plasticity. *PLoS Computational Biology*, 11(7):e1004386.

- Masland, R. H. (2012). The neuronal organization of the retina. *Neuron*, 76(2):266–280.
- McGarry, L. M., Packer, A. M., Fino, E., Nikolenko, V., Sippy, T., and Yuste, R. (2010). Quantitative classification of somatostatin-positive neocortical interneurons identifies three interneuron subtypes. *Frontiers in neural circuits*, 4:1284.
- McInnes, L., Healy, J., and Melville, J. (2018a). Umap: Uniform manifold approximation and projection for dimension reduction. *arXiv preprint arXiv:1802.03426*.
- McInnes, L., Healy, J., Saul, N., and Grossberger, L. (2018b). Umap: Uniform manifold approximation and projection. *The Journal of Open Source Software*, 3(29):861.
- Mensi, S., Naud, R., Pozzorini, C., Avermann, M., Petersen, C. C., and Gerstner, W. (2012). Parameter extraction and classification of three cortical neuron types reveals two distinct adaptation mechanisms. *Journal of neurophysiology*, 107(6):1756–1775.
- Miceli, S., Nadif Kasri, N., Joosten, J., Huang, C., Kepser, L., Proville, R., Selten, M. M., van Els, F., Azarfar, A., Homberg, J. R., et al. (2017). Reduced inhibition within layer iv of sert knockout rat barrel cortex is associated with faster sensory integration. *Cerebral Cortex*, 27(2):933–949.
- Mukamel, E. A. and Ngai, J. (2019). Perspectives on defining cell types in the brain. *Current opinion in neurobiology*, 56:61–68.
- Nandi, A., Chartrand, T., Van Geit, W., Buchin, A., Yao, Z., Lee, S. Y., Wei, Y., Kalmbach, B., Lee, B., Lein, E., et al. (2022). Single-neuron models linking electrophysiology, morphology, and transcriptomics across cortical cell types. *Cell reports*, 40(6).
- Pedregosa, F., Varoquaux, G., Gramfort, A., Michel, V., Thirion, B., Grisel, O., Blondel, M., Prettenhofer, P., Weiss, R., Dubourg, V., Vanderplas, J., Passos, A., Cournapeau, D., Brucher, M., Perrot, M., and Duchesnay, E. (2011). Scikit-learn: Machine learning in Python. *Journal of Machine Learning Research*, 12:2825–2830.
- Perktold, J., Seabold, S., Sheppard, K., ChadFulton, Shadden, K., jbrockmendel, j grana6, Quackenbush, P., Arel-Bundock, V., McKinney, W., Langmore, I., Baker, B., Gommers, R., yogabonito, s scherrer, Zhurko, Y., Brett, M., Giampieri, E., yl565, Millman, J., Hobson, P., Vincent, Roy, P., Augspurger, T., tvanzyl, alexbrc, Hartley, T., Perez, F., Tamiya, Y., and Halchenko, Y. (2024). statsmodels/statsmodels: Release 0.14.2.
- Poulin, V. and Théberge, F. (2019). Ensemble clustering for graphs. In *Complex Networks and Their Applications VII: Volume 1 Proceedings The 7th International Conference on Complex Networks and Their Applications COMPLEX NETWORKS 2018* 7, pages 231–243. Springer.
- Pozzorini, C., Mensi, S., Hagens, O., Naud, R., Koch, C., and Gerstner, W. (2015). Automated high-throughput characterization of single neurons by means of simplified spiking models. *PLoS computational biology*, 11(6):e1004275.
- Prinz, A. A., Bucher, D., and Marder, E. (2004). Similar network activity from disparate circuit parameters. *Nature neuroscience*, 7(12):1345–1352.
- Rathbun, D., Ghorbani, N., Shabani, H., Zrenner, E., and Hosseinzadeh, Z. (2018). Spike-triggered average electrical stimuli as input filters for bionic vision—a perspective. *Journal of neural engineering*, 15(6):063002.
- Scala, F., Kobak, D., Bernabucci, M., Bernaerts, Y., Cadwell, C. R., Castro, J. R., Hartmanis, L., Jiang, X., Laturnus, S., Miranda, E., et al. (2021). Phenotypic variation of transcriptomic cell types in mouse motor cortex. *Nature*, 598(7879):144–150.
- Scala, F., Kobak, D., Shan, S., Bernaerts, Y., Laturnus, S., Cadwell, C. R., Hartmanis, L., Froudarakis, E., Castro, J. R., Tan, Z. H., et al. (2019). Layer 4 of mouse neocortex differs in cell types and circuit organization between sensory areas. *Nature communications*, 10(1):4174.
- Schwartz, O., Pillow, J. W., Rust, N. C., and Simoncelli, E. P. (2006). Spike-triggered neural characterization. *Journal of vision*, 6(4):13–13.
- Sharpee, T. O. (2014). Toward functional classification of neuronal types. *Neuron*, 83(6):1329–1334.
- Steriade, M. (2000). Corticothalamic resonance, states of vigilance and mentation. *Neuroscience*, 101(2):243–276.

- Szabó, A., Schlett, K., and Szücs, A. (2021). Conventional measures of intrinsic excitability are poor estimators of neuronal activity under realistic synaptic inputs. *PLOS Computational Biology*, 17(9):e1009378.
- Szücs, A. and Huerta, R. (2015). Differential effects of static and dynamic inputs on neuronal excitability. *Journal of Neurophysiology*, 113(1):232–243.
- Tasic, B., Yao, Z., Graybuck, L. T., Smith, K. A., Nguyen, T. N., Bertagnolli, D., Goldy, J., Garren, E., Economo, M. N., Viswanathan, S., et al. (2018). Shared and distinct transcriptomic cell types across neocortical areas. *Nature*, 563(7729):72–78.
- Trainito, C., von Nicolai, C., Miller, E. K., and Siegel, M. (2019). Extracellular spike waveform dissociates four functionally distinct cell classes in primate cortex. *Current Biology*, 29(18):2973–2982.
- Virtanen, P., Gommers, R., Oliphant, T. E., Haberland, M., Reddy, T., Cournapeau, D., Burovski, E., Peterson, P., Weckesser, W., Bright, J., van der Walt, S. J., Brett, M., Wilson, J., Millman, K. J., Mayorov, N., Nelson, A. R. J., Jones, E., Kern, R., Larson, E., Carey, C. J., Polat, I., Feng, Y., Moore, E. W., VanderPlas, J., Laxalde, D., Perktold, J., Cimrman, R., Henriksen, I., Quintero, E. A., Harris, C. R., Archibald, A. M., Ribeiro, A. H., Pedregosa, F., van Mulbregt, P., and SciPy 1.0 Contributors (2020). SciPy 1.0: Fundamental Algorithms for Scientific Computing in Python. *Nature Methods*, 17:261–272.
- Yan, X., Calcini, N., Safavi, P., Ak, A., Kole, K., Zeldenrust, F., and Celikel, T. (2022). A whole-cell recording database of neuromodulatory action in the adult neocortex. *bioRxiv*, pages 2022–01.
- Zeldenrust, F., de Knecht, S., Wadman, W. J., Denève, S., and Gutkin, B. (2017). Estimating the information extracted by a single spiking neuron from a continuous input time series. *Frontiers in computational neuroscience*, 11:49.
- Zeng, H. (2022). What is a cell type and how to define it? *Cell*, 185(15):2739–2755.
- Zeng, H. and Sanes, J. R. (2017). Neuronal cell-type classification: challenges, opportunities and the path forward. *Nature Reviews Neuroscience*, 18(9):530–546.

# Chapter 3

## Neuromodulatory Control of Cortical Function: Cell-Type Specific Reshaping of Neuronal Information Transfer



Based on: Willemsen, Y., Beijers, R., Gu, F., Arias Vásquez, A., Schols, H.A., de Weerth, C. Fucosylated Human Milk Oligosaccharides during the First 12 Postnatal Weeks are Associated with Better Executive Functions in Toddlers. *Nutrients*, 2023, 15, 1463.

## Abstract

Neuromodulatory systems modulate circuit flexibility by acting on neuronal properties, yet their cell-type-specific influence on functional identity and stimulus encoding remains unresolved. Here, we assess how dopaminergic (D1R, D2R) and cholinergic (M1R) receptor activation alters the physiology and information processing of excitatory and inhibitory neurons in the mouse somatosensory cortex. Using whole-cell recordings under a Frozen Noise protocol, we measured four core functional domains —action potential dynamics, passive membrane properties, adaptation currents, and spike-triggered input filters. Receptor activation reorganized correlations among these features, with excitatory neurons exhibiting reduced coupling and inhibitory neurons showing increased coherence. Unsupervised clustering revealed that neuromodulation reshaped the distribution of functional neuron types. Critically, receptor activation modulated the transfer of stimulus information in a receptor- and cell-type-specific manner, reducing fractional information transfer in excitatory neurons. Our findings demonstrate that neuromodulators restructure the computational landscape of cortical circuits, tuning both functional identity and encoding fidelity.

## Introduction

Neuromodulators such as dopamine has been known to play a role in memory, learning and other higher cognitive function in the brain and has also been implicated with diseases such as Parkinson's and schizophrenia (Durstewitz and Seamans (2008); Arnsten and Rubia (2012); Winterer and Weinberger (2004)), similarly acetylcholine has been implicated with brain function such as learning, sleep and attention Dalley et al. (2004); Hasselmo et al. (2006); Sarter et al. (2009). These neuromodulators are known to affect the excitability of neurons in various parts of the brain Bargmann (2012); Bargmann and Marder (2013); Marder (2012); Taghert and Nitabach (2012). Dopamine and acetylcholine alter the intrinsic and tuning properties of neurons by activating G-protein-coupled receptors (GPCRs) such as Dopamine D1 and D2 receptors and muscarinic acetylcholine M1 receptors Dascal (2001), which differs from neuron to neuron due to the distribution of these receptor types Nusser (2009) in each neuron. Activation/inactivation of these receptors have long been known to modulate excitability and firing properties (for example, D1R activation has been found to increase firing rate of excitatory neurons in PFC Seong and Carter (2012), similar effects have been recorded for D2R Cousineau et al. (2020) and M1R). However, despite ion-channel and behavioral understanding of receptor-specific modulation, it is still unknown how functional properties, which ranges from passive to filtering properties of individual neurons are altered by the activation of specific receptors in a population.

Since response to synaptic input depends upon the passive properties such as conductance of the neuron Häusser (2000) which ultimately depends on activation level of active ion channels at any given instant, modulation of passive properties ultimately modulates the response to synaptic input i.e, the receptive field Ferguson and Cardin (2020); Salinas and Sejnowski (2001). Although, these neuromodulators change the action potential dynamics of the cell through the activation/inactivation of ion channels,

that results in changing the broad scope properties including information transferred to the postsynaptic neuron. Traditional approaches that study neuromodulation have largely focused on gross excitability measures such as firing rate or spike frequency adaption [Nadim and Bucher \(2014\)](#); [Marder \(2012\)](#); [Shine et al. \(2021\)](#). Although these measures are informative, it under represents the high dimensional space in which neurons operate. Neurons integrate inputs over time, encode information via complex nonlinear transformations of the synaptic input, and exhibit diverse passive and active membrane properties. It is still not completely understood how high-dimensional functional properties such as action potential dynamics, adaptation, passive biophysical attributes and input feature selectivity is altered by specific neuromodulatory signal. More specifically, it is still unknown how these functional properties change as a result of Dopamine (D1R and D2R activation) and acetylcholine (M1R activation) and how this high-dimensional modulation varies on cellular and population level and how it ultimately affects the amount of information transferred by a neuron to its postsynaptic neuron.

In this study we address the question: how high-dimensional neuronal functional landscape is altered by Dopamine and Acetylcholine and what is the implication of this modulation on encoding properties of neurons? In order to understand how activation of D1R, D2R and M1R alters the functional properties and ultimately information transfer in a population of neurons, we analyzed in-vitro single neuron electrophysiological recordings under a Frozen Noise protocol from layer 2/3 in the somatosensory cortex in mice in sequence, first under a control (artificial cerebral spinal fluid (aCSF)) and then with a receptor agonist trial. We extracted four sets of functional features namely 1.) action potential (AP), 2.) passive biophysical (PB), 3.) adaptation current (AC) and 4.) linear input filter via a spike triggered average (STA).

To address the question we first compared the coordinated change in passive and input driven as a result of neuromodulation using a multi-set correlation and factor

analysis (MCFA). We further employ (UMAP) combined with Louvain clustering to explore how neurons reorganize into distinct functional subgroups depending on the neuromodulatory context. Since our final aim was to understand the consequence of neuromodulation on function, we measured the amount of transferred information about input in the spike train during control and agonist trials and compared it across E/I cell types to understand the heterogeneous effect of modulation. In summary, our results provide a broad understanding of neuromodulation on functional properties of neurons in somatosensory cortex. By bridging the gap between receptor-level neuromodulation and high-dimensional functional phenotyping, these results provide a framework for modeling and studying neural circuits and for further exploring how information processing is affected as a result of cell-type specific neuromodulation and modeling disorders.

To address the question we first studied the population level reorganization by neuromodulation by comparing how D1, D2 and M1 agonist alters classification using an unsupervised high-dimensional UMAP+Louvain clustering approach based on AP, PB, AC and STA compared to a control (aCSF). This allowed us to study if neuronal population is heterogeneously modulated or classify into subgroups or uniformly with specific receptor activation. We then compared the coordinated change in passive and input driven as a result of neuromodulation using a multi-set correlation and factor analysis (MCFA). To finally understand the functional affect of specific neuromodulator we compared the transferred information about the stimulus in the somatic input and the spike train in control and agonist trials for excitatory and inhibitory neurons. In summary, our findings provide a systems-level view of how neuromodulation reorganizes intrinsic and input-driven properties of neurons. By linking receptor-specific activation to high-dimensional changes in neuronal function and information encoding, this work offers a principled framework for modeling neuromodulatory effects in neural circuits and understanding how such modulation might contribute to dynamic brain states and

disease phenotypes.

## Methods

**Ethics statement** The data used in this research was previously published and made freely available to the community [da Silva Lantyer et al. \(2018\)](#) and [Yan et al. \(2022\)](#). All the experimental work, as outlined in the cited articles, were carried out in compliance with the European directive 2010/63/EU, the national regulations of the Netherlands, and international standards for animal care and use.

**Slice electrophysiology** Data acquisition procedures, the details of the in vitro slice preparation, intracellular access to anatomically targeted neurons, data digitization, and preprocessing have been described in detail elsewhere [Kole et al. \(2020\)](#); [Kole and Celikel \(2019\)](#); [da Silva Lantyer et al. \(2018\)](#); [kol \(2017\)](#); [Miceli et al. \(2017\)](#). In short, Pvalbtm1(cre)Arbr (RRID:MGI:5315557) or Ssttm2.1(cre)Zjh/J (RRID:IMSR\_JAX: 013044) mice, including both females and males, were obtained from local breeding colonies and studied after the maturation of evoked neurotransmitter release in the primary somatosensory cortex ([Martens et al. \(2015\)](#)).

Mice were anesthetized with Isoflurane (1.5 mL/mouse) before extracting tissue, and coronal slices of the primary somatosensory cortex (barrel subfield) were prepared.

The brain was removed, and 300 µm-thick coronal slices were made. Slices were then incubated in artificial cerebrospinal fluid (aCSF) (120 mM NaCl, 3.5 KCl, 10 glucose, etc.), aerated with 95%  $O_2$ /5%  $CO_2$  at 37°C, and then at room temperature after 30 minutes.

Whole-cell electrophysiological recordings were performed with continuously oxygenated aCSF. The barrel cortex was localized, and cells in the supragranular layers were patched under 40x magnification using HEKA EPC 9 and EPC10 amplifiers with Patch Master software. Patch-clamp electrodes were pulled from glass

capillaries (1.00 mm external diameter, 0.50 mm internal diameter) and used with 5–10 M $\Omega$  resistance, filled with intracellular solution (130 mM K-Gluconate, 5 KCl, 1.5 MgCl<sub>2</sub>, etc., pH adjusted to 7.22 with KOH). Data were band-pass filtered at 0.1–3000 Hz before storage for offline analysis.

**Frozen Noise (FN) protocol** The Frozen Noise input protocol consisted of injecting a somatic current that is the result of an artificial neural network of 1000 neurons responding (firing Poisson spikes) to random stimuli i.e., the hidden state, the membrane potential response to the somatic input is recorded with a sampling rate of 20 kHz for a total length of 360 seconds and saved. Each raw data file consisted of a vehicle control trial (artificial Cerebrospinal fluid i.e. aCSF) and a drug trial (a specific neuromodulatory receptor agonist or antagonist was added to the bath and the recording was repeated). Some files consisted of multiple control and drug trials. See Zeldenrust et al. (2017); da Silva Lantyer et al. (2018) for more details.

## Method details

### Feature Extraction

We extracted waveform, action potential, passive biophysical and spike triggered average from single neuron recordings recorded under Frozen Noise input protocol, these recordings were performed first under a vehicle control (aCSF) and then repeated with a receptor agonist added to the bath. In total 288 neurons (Table. 3.1) were analyzed, we discarded recordings with high levels of noise.

Condition	Trials
aCSF	288
D1	54
D2	59
M1	41

Table 3.1. Number of neurons with agonist applied

**Spike waveforms** As explained in [Joshi et al. \(2024\)](#), we identified peaks from the membrane potential traces and kept the hyperparameter and ISI threshold criteria the same as in [Joshi et al. \(2024\)](#). The length of waveforms used in this study is 10ms (5ms before and after the peak).

**Action potential features** The action potential features were extracted to study the dynamics, threshold and waveforms related features throughout a trial via descriptive statistics. The action potential features were extracted for aCSF and agonist trials as described in [Joshi et al. \(2024\)](#).

### Biophysical Feature extraction using GLIF model

In order to extract passive biophysical attributes as well as adaptation current from aCSF and agonist trials, we fit a Generalized Leaky Integrate and Fire (GLIF) neuron model [Pozzorini et al. \(2015\)](#) as described in detail in [Joshi et al. \(2024\)](#). We take the 100 second instance from trial as the training set extract passive features as well as adaptation current from the trial.

**Spike Triggered Average** The spike-triggered average (STA) is the average shape of the stimulus that precedes each spike. We extracted the STA using the following equation given by [Schwartz et al. \(2006\)](#):

$$STA = \frac{1}{N} \sum_{n=1}^N \vec{s}(t_n), \quad (3.1)$$

where  $t_n$  is the  $n^{th}$  spike time,  $s$  is the stimulus vector preceding the spike for a fixed time window of 100 ms, and  $N$  is the total number of spikes. Before clustering, we standardize (i.e. z score) and then normalize the STA vector with an  $L_2$  norm. We didn't use any kind of whitening or regularization to calculate the STA.

## UMAP + Louvain clustering

Universal Manifold Approximator (UMAP) is a non-linear dimensionality reduction algorithm which is advantageous for preserving global structure of the data [McInnes et al. \(2018\)](#) in lower dimensions, this makes it more suitable for visualization especially for high dimensional datasets ( $p >> N$ , where  $p$  is the dimensionality of the data and  $N$  is number of samples) compared to other methods such as PCA which fail to perform due to curse of dimensionality [Aggarwal et al. \(2001\)](#). As explained in [Lee et al. \(2021\)](#); [Joshi et al. \(2024\)](#) the high-dimensional graph obtained during the intermediate step in the UMAP algorithm can be exploited to perform clustering using Louvain community detection [Blondel et al. \(2008\)](#). We chose the hyperparameter based on cluster stability criteria and the corresponding number of clusters based on the same heuristic as explained in [Joshi et al. \(2024\)](#).

For measuring clustering similarity between aCSF and drug conditions, we calculate a cluster similarity matrix as explained in [Joshi et al. \(2024\)](#). For quantifying the similarity between labels assigned to aCSF versus drug trials, we used cluster similarity measure such as adjusted random index and adjusted mutual information score using scikit-learn Python package [Pedregosa et al. \(2011\)](#).

## Information transfer protocol

We used the information transfer protocol described in detail in [Zeldenrust et al. \(2017, 2024\)](#), this method involves calculating entropy of the hidden state  $x$  which can be a stimuli that is observed by the network. Further steps involves calculation of mutual information between the hidden state and the input current  $MI_I$  and again between the hidden state and the spike times  $MI_{spiketimes}$  for a given neuron. The fraction of mutual information, referred to as fraction of information ( $FI$ ) gives a measure of how much information is transferred by the spikes about the hidden state for a given

neuron.

$$FI = \frac{MI_{spiketimes}}{MI_I} \quad (3.2)$$

Since the entropy of the hidden state will always be greater or equal to mutual information values. The value of FI will always be between 0 and 1. This calculation works under the assumption of ergodicity, therefore, an average over samples is the same as an average over time. This method also assumes that spike trains are Poissonian. The method still works, if there are minor deviations from Poisson distribution.

## Quantification and statistical analysis

We used the non-parametric Wilcoxon test to test significance difference in information transfer (FI) between paired aCSF and drug trials . We also used one sided Student's T-test to test significance change between aCSF and agonist condition for passive biophysical and action potential attributes. Significance value was set to  $p < 0.05$  in both cases. We performed Kruskal-Wallis H test and a post-hoc Mann-Whitney U test with Bonferroni correction for multiple comparisons for comparing cosine similarity between aCSF and agonist trials. All statistical tests were performed using `scipy-stats` package [Virtanen et al. \(2020\)](#).

## Multi-set Correlation and Factor Analysis

In order to assess the correlation between AP, PB, AC and STA attribute sets extracted from the electrophysiological recordings, and to further analyze how the correlation changes as a result of the application of agonists we used Multi-set correlation and factor analysis (MCFA) [Brown et al. \(2023\)](#) as explained previously in [Joshi et al. \(2024\)](#). It is an unsupervised integration method designed to analyze multiple high dimensional data types from the same sample. This method is a combination of multi-set canonical correlation and factor analysis. The outcome is a joint model of the shared and private space between these high dimensional datasets. We used this method

to extract the shared and private variance for each dataset and compare how these variances change as a result of the application of a certain agonist compared to a control condition.

We center and scale all datasets and initialize the loading matrices similar to the Brown and collinwa (2023); Joshi et al. (2024), the number of principal components for aCSF condition were chosen based on the Marchenko Pasteur Law and the size of private space  $k_m$  for AP, AC and STA datasets were chosen to be 2 and 1 for the PB dataset. For agonist condition, instead of choosing the PCA components using the Marchenko Pasteur Law, we chose the number of principal components to be 2 and  $k_m$  to 1 for all four datasets. This was done due to relatively small sample size for excitatory and inhibitory agonist sets. The fit is performed using an expectation minimization algorithm in order to obtain the shared and private loading matrices as well as shared and private spaces as described in Joshi et al. (2024).

## Results

To understand how neuromodulation affects the high dimensional functional landscape dynamics of neuronal population we extracted four attributes from single neuron in-vitro somatic recordings Yan et al. (2022), performed using the frozen noise protocol (see 3), namely action potential (AP), passive biophysical (PB), adaptation current (AC) and linear input filter approximated using a spike triggered average (STA) as described in (see Joshi et al. (2024) and 3), we extracted these features from 296 distinct sets of neural recordings and divided them into excitatory and inhibitory subsets based on their waveform shapes and firing rates as described in Joshi et al. (2024). We then separated the recording sets based on the receptor agonists applied and the corresponding aCSF trials. Here we present the analysis based on D1-agonist, D2-agonist and M1-agonist trials.

Functional Attributes	Description
Action Potential (AP)	An ensemble of descriptive statistics of action potential shapes and dynamics.
Passive Biophysical (PB)	Attributes related to the non-active properties of cells, such as membrane capacitance and resistance.
Adaptation Current (AC)	Refers to the ionic currents in neurons that change in response to prolonged stimuli. Extracted via fitting a GLIF model.
Spike Triggered Average (STA)	The average of signal features occurring before neuron spikes, used to understand stimulus-response relations. It is an approximation of the linear input filter of a neuron.

Table 3.2. Functional Attributes and their Descriptions

### **Neuromodulation changes structured correlation between functional attributes in a cell-type as well as receptor type specific manner**

We wanted to understand how neuromodulation (dys)regulate AP, PB, AC and STA attributes which represent distinct modalities of functional landscape. To study the conjoint effect of neuromodulation on active and input driven functional attributes and how the correlation between attribute sets change as a result of specific receptor activation, we applied multi-set correlation and factor analysis (MCFA) to our dataset, first on aCSF (control) trials and each agonist trial set respectively. We summarized the results of shared, private and residual variance using stacked histogram (Fig. ??). In this analysis, when individual feature sets exhibit high shared variance, this indicates that the features are functionally coordinated: changes in one set tend to co-vary with changes in others. In contrast, when feature sets exhibit high private variance, it suggests that the features are relatively independent, meaning changes in one set do not systematically correspond to changes in the others. Or a feature with high private variance varies independently from the other features. A high residual signifies either noise or a complex non-linear relationship not captured by a linear method such as

MCFA.

It can be seen from Fig. ?? that the relationship between functional attributes is cell-type specific. Comparing the histograms for aCSF trials (Fig. ??A) between excitatory and inhibitory population, we can see that the private variance for Linear Input Filter attribute (STA) is higher for inhibitory neurons (see Table.??) compared to excitatory neurons (see Table.??), this shows that STA in inhibitory population is not strongly correlated with other functional attributes, therefore STA in the inhibitory population is not coordinated with other functional properties. The passive biophysical and action potential attributes show a high shared variance for excitatory neurons compared to inhibitory neurons. This shows a high level of coordination between AP and PB attributes between excitatory neurons compared to inhibitory neurons.

It can be seen from fig. ?? that private variance for excitatory population vanishes for AP, PB and AC sets except for STA, for which it increases drastically compared to aCSF trials (see Table.?? and Figure ?? A-B) upon D1 receptor activation. The shared variance reduces sharply compared to aCSF for AC and STA sets for the excitatory population. This suggests that D1R activation makes STA less functionally coordinated with other attributes. While the shared variance for AP and PB are slightly reduced suggesting that the coordination level between these two properties remain intact. We observe a dramatically different effect in inhibitory population compared to the excitatory counterpart. Private variance decreases sharply for AC and STA sets (see Figure. ??A-B and Table. ??), while drastically increasing the shared variance for these attributes, suggesting that AC and STA become functionally coordinated with the latent space, therefore AP and PB properties. In summary, effect of D1R is cell-type specific and nuanced. Increasing coordination between properties in inhibitory neurons while decreasing coordination for excitatory linear-input filter. In a similar manner, in order to study the effect of D2R activation, we analyzed D2 trials using MCFA and present in comparison with aCSF trials (see Fig. ??C and Table. ??). We observe that

D2 modulates the coordination between functional attributes in more subtle manner for excitatory neurons, the shared variance for PB and STA decreases, while opposite effect is seen in case of AC and AP attribute sets. Private variance on the other hand decreases drastically for AP and AC attributes as also observed in case of D1 and increases for STA and PB. The stark increase in private variance in case of STA needs to be highlighted. This suggests that D2 makes AP and AC properties more coordinated, while decreasing coordination between STA and PB attributes. In case of inhibitory neurons, the modulation is rather straight forward. The private variance for all the four attributes decreases and the shared variance increases for all the attributes except for AP attributes. This suggests that D2R overall makes the functional properties more coordinated for inhibitory similar to D1. In case of M1, we observe an entirely different functional landscape. The shared variance increases for AC and AP properties similar to D2 for excitatory neurons and decreases for PB and STA. This suggests that AC and AP attributes become coordinated and PB and STA properties become more independent as a result of M1R activation. On the other hand, private variance decreases for all the attributes except for PB. For inhibitory neurons, the shared variance increases for all sets except for AC, suggesting a stronger functional coordination. Surprisingly, the private variance increases sharply for AC suggesting a decoupling with the rest of the attributes set.

For a broader understanding of neuromodulation, specifically D1R, D2R and M1R activation, how it affects the coordination structure between functional attribute sets, we calculated the average shared over private variance for each agonist as well as aCSF conditions, we observe that the fraction of shared over private variance increases for D1R, D2R and M1R trials compared to aCSF trials for both excitatory and inhibitory populations (Fig. ??E). This suggest that on average functional attributes become more coordinated as a result of specific receptor activation.

In summary, we observed that neuromodulation changes the coordination structure

between functional properties in a cell type as well as agonist specific way. For excitatory neurons the individual variability diminishes compared to their inhibitory counterparts as seen in Fig. ??E. In case of inhibitory population, on average the neuromodulation increases coordination between functional attributes.

### **Specific receptor activation alters functional classification**

Neuromodulators are known to affect the intrinsic properties as well as excitability of neurons. Such as, it well understood that D2-R activation modulates excitability in motor cortex [Cousineau et al. \(2020\)](#). Neuronal functional classification which is classically studied using action potential and passive biophysical features, has been shown to change as a function of input to the neuron [Joshi et al. \(2024\)](#); [Hernáth et al. \(2019\)](#). Also, we have shown in the previous section that neuromodulation (D1, D2 and M1) changes the correlation structure (measured using shared variance) between functional attributes as well as individual private variance for each functional attribute set in a cell-type specific manner. Therefore it is important to understand how functional attributes (intrinsic, excitability as well as dynamics) are altered by D1-R, D2-R and M1-R activation as well as how neuronal clustering based on functional attributes changes, if at all, as a result of neuromodulation.

To this aim we first wanted to check if there is a recoding drift present in the data as result of experimental setup when performing multiple trial, for this we extracted the 4 functional attribute sets along with their waveforms from experiments with multiple aCSF trials and compared the clustering between aSCF trial 1 with trial 2. The histogram in Fig. ?? show that there is a high level of correspondence between aCSF trial 1 and trial 2 for waveform and passive biophysical features. The low level of correspondence for the AP, AC and STA results from the differences in inputs that cells receive in the two trials. We also show the manifold overlap between trial 1 and trial 2 for all properties (see Fig. ??).

We clustered D1-R, D2-R and M1-R agonist group trials as well as their corresponding aCSF trials separately using UMAP+Louvain clustering (see Methods as well as [Joshi et al. \(2024\)](#)) and measured the similarity in clustering using adjusted mutual information score (AMI) see [3](#). We summarized the clustering for excitatory neurons in case of D1-R activation in histogram (Fig. ?? **A.1**), it can be seen that AMI scores are consistently low for AP, PB, AC and STA, suggesting that functional attribute based clustering is altered as a result of D1-R activation. We further explored how each attribute set is altered as a result of D1-R activation, for passive biophysical properties (Fig. ?? **A.2**) we found that conductance ( $gL$ ) (One Sided t-test:  $p < 0.001$ ) and reset voltage ( $V_r$ ) (One Sided t-test:  $p < 0.05$ ) are significantly reduced as a result of D1-R activation. We then explored how adaptation current and linear input filter (STA) are altered as a result of D1R modulation shown in Fig. ?? **A.3** and Fig. ?? **A.4**, the red curves represent D1 trials and black curves represent aCSF trials. To quantify the differences between D1 and aCSF trials, we calculated the rise time and peak values (see [3](#)) for both adaptation currents and STA. The joint plot Fig. ?? shows the rise time and peak differences between D1 and aCSF trials for adaptation current and Fig. ?? shows rise time and peak value for STA. The peak and rise time for adaptation current (AC paired t-test (decay time):  $p = 0.4341$ , AC paired t-test (peak):  $p = 0.2444$ ) and STA (STA paired t-test (rise time):  $p = 0.758$ , STA paired t-test (peak):  $p = 0.0514$ ) were found to not be significantly different between aCSF and D1 trials for excitatory neurons. This suggest that STA and adaptation currents are not altered significantly as a result of D1-R activation. We also performed a cosine similarity measurement within and across the aCSF and D1 trials for AC curves, we performed a Kruskal–Wallis H test on three groups: within-aCSF, within-agonist, and across-aCSF and agonist conditions. The test revealed a significant effect of group on similarity distributions ( $H(2) = 15.3953$ ,  $p = 4.53e - 4$ ). Post hoc comparisons using Mann–Whitney U tests (Bonferroni-corrected for multiple comparisons) showed that:

- Similarity scores were significantly higher within aCSF compared to across-pair comparisons ( $U = 120654.00, p = 3.17e - 4$ ),
- D1 also showed significantly lower similarity than across-pair comparisons ( $U = 153267.00, p = 0.0217$ ),
- We didn't observe a significant difference between aCSF and D1 mean cosine similarity distributions ( $U = 135299.00, p = 1.0$ ).

These findings indicate that neural representations are more consistent within conditions than across conditions, suggesting that D1 modulation significantly alters the AC consistently across the population.

Similar to AC, we also performed a cosine similarity measurement within and across the aCSF and D1 trials for STA curves, we performed a Kruskal–Wallis H test on three groups: within-aCSF, within-agonist, and across-aCSF and agonist conditions. The test revealed a significant effect of group on similarity distributions ( $H(2) = 14.3199, p = 7.77e - 4$ ).

Post hoc comparisons using Mann–Whitney U tests (Bonferroni-corrected for multiple comparisons) showed that:

- Similarity scores were significantly higher within aCSF compared to across-pair comparisons ( $U = 142428.00, p = 7.44e - 3$ ),
- D1 also showed significantly lower similarity than across-pair comparisons ( $U = 134285.50, p = 1.95e - 3$ ),
- We didn't observe a significant difference between aCSF and D1 mean cosine similarity distributions ( $U = 142204.00, p = 1.0$ ).

These findings indicate that neural representations are more consistent within conditions than across conditions, suggesting that D1 modulation significantly alters the STA consistently across the population.

Finally, we assessed the effect of D1-R activation on action potential attributes (Fig. ?? **A.5**) which incorporates spiking dynamics, spiking threshold and AP height and width attributes for excitatory population. We found that max ISI (one sided t-test:  $t = 3.148$ ,  $p = 4.49e-3$ ), mean ISI (one sided t-test:  $t = 2.283$ ,  $p = 0.0319$ ), instantaneous firing Rate (one sided t-test:  $t = -3.826$ ,  $p = 8.64e-4$ ) form the spiking dynamics are significantly altered as a result of D1-R activation. We performed similar analysis for D2 and M1 agonist trials and summarized the results in Fig. ?? and Fig. ??.

For inhibitory neurons, the effect on clustering in case of D1-R activation is shown in histogram (Fig. ?? **B.1**), it can be seen that AMI scores are consistently low for AP, PB, AC and STA, suggesting that functional attribute based clustering is altered as a result of D1R activation. We further explored how each attribute set is altered as a result of D1-R activation, for passive biophysical properties (Fig. ?? **B.2**) we found that conductance ( $gL$ ) and reset voltage ( $V_r$ ) are significantly reduced (One sided t-test:  $p < 0.001$ ,  $p < 0.05$ ) as a result of D1-R activation. We then explored how adaptation current and linear input filter (STA) are altered as a result of D1-R modulation shown in Fig. ?? **B.3** and Fig. ?? **B.4**. As for excitatory population, we calculated the rise time and peak values (see 3) for both adaptation currents and STA. The joint plot Fig. ?? shows the rise time and peak differences between D1 and aCSF trials for adaptation current and Fig. ?? shows rise time and peak value for STA. The peak (paired t-test:  $t = -1.195$ ,  $p = 0.244$ ) and decay time (paired t-test:  $t = 0.7966$ ,  $p = 0.4341$ ) for adaptation current were not found to be significantly different. For STA, the rise time was found to be significantly different between aCSF and D1 trials (paired t-test:  $t = 2.454$ ,  $p = 0.0208$ ) but the peak current was not significantly different for inhibitory neurons (paired t-test:  $t = 1.834$ ,  $p = 0.077$ ). This suggest that STA and adaptation currents are not altered significantly as a result of D1-R activation. We also performed a cosine similarity measurement within and across the aCSF and D1 trials for AC curves,

we performed a Kruskal–Wallis H test on three groups: within-aCSF, within-agonist, and across-aCSF and agonist conditions. The test revealed a non-significant effect between aCSF and D1 trials on similarity distributions ( $H(2) = 2.0098, p = 0.3660$ ). These findings indicate that AC is not altered as a result of D1 modulation. Similarly, we performed a cosine similarity measurement within and across the aCSF and D1 trials for STA curves. The test revealed a significant effect of group on similarity distributions ( $H(2) = 3.2486, p = 0.1970$ ). These findings indicate that AC is not altered as a result of D1 modulation. Finally, we assessed the effect of D1-R activation on action potential attributes (Fig. ?? **B.5**) which incorporates spiking dynamics, spiking threshold and AP height and width attributes for inhibitory population. We found that firing rate (one sided t-test:  $t = 3.627511899, p = 0.0011$ ) from spiking dynamics subset are significantly altered, also mean threshold (one sided t-test:  $t = 4.1205, p = 3.038e-4$ ), median threshold (one sided t-test:  $t = 4.361, p = 1.582e-4$ ) and minimum threshold (one sided t-test:  $t = 2.443, p = 0.021$ ) from the spiking threshold set were significantly altered as result of D1-R activation.

We wanted to further understand if there are sub groups of neurons that are altered differently in their action potential and passive biophysical attributes as a result of D1R activation. For this, we clustered the change in AP and PB attributes between aCSF and D1 trials for both excitatory and inhibitory neurons and summarize our finding using polar plots with each set of attributes Fig. ??, each curve represents a single neuron, colored with its respective cluster identity and the mean is represented with a thick line. It can be seen that there are 3 clusters of AP attributes for excitatory neurons and 4 clusters for inhibitory neurons. Similarly, we find 3 clusters each of PB attributes for both excitatory and inhibitory neurons. We also compared the overall similarity between clustering results based on aCSF trials and clustering the difference between aCSF and D1 trials for the 4 attribute sets using the AMI score between cluster labels. We summarized our findings in histogram shown in Fig. ???. It can be

seen that AMI score for both excitatory and inhibitory neurons consistently low for all 4 attributes for both excitatory and inhibitory neurons. We performed similar analysis for D2 and M1 agonist trials and summarized our findings in Fig. ?? and Fig. ??.

## **Effect of neuromodulation on information transfer capability in single neurons**

In order to assess the impact of neuromodulation on neuronal function, we first examined the relationship between firing rate changes and information transfer (fractional information, FI) across different recording conditions. Fig. ?? A shows a scatter plot comparing the change in firing rate versus change in FI between two consecutive aCSF recordings, the values are normalized in order to be compared to agonist trials. We find that excitatory neurons mostly lie on the 3rd quadrant which means that firing rate and FI lowers as a result of consecutive aCSF trials. Inhibitory neurons on the other hand show much more heterogeneous response in change in firing rate and FI with mean centered around zero as seen from the size of the violin plots for both FI and firing rate between two aCSF trials suggesting heterogeneous trial to trial variability.

We next investigated the effects of respective receptor activation on transferred information in a cell-type specific manner, as shown using box plot in Fig. ?? B. We observed that D1-R activation resulted in a significant reduction in FI for excitatory neurons compared to inhibitory neurons (students t-test:  $t = -3.1667$ ,  $p = 2.707e-3$ ), underscoring a pronounced cell-type specific effect. In contrast, D2 receptor activation did not significantly alter FI in either neuronal population (students t-test:  $t = -1.5401$ ,  $p = 0.1291$ ). M1 receptor activation also produced a cell-type specific modulation, with excitatory neurons displaying a significant reduction in FI relative to inhibitory neurons (students t-test:  $t = -2.9521$ ,  $p = 5.38e-3$ ). Furthermore, the change in FI between consecutive aCSF trials was significantly lower in excitatory neurons than in inhibitory neurons (students t-test:  $t = -2.5738$ ,  $p = 0.0118$  ), reinforcing the idea

that inhibitory neurons exhibit a broader trial to trial variability.

To further examine the effect of specific receptor activation, we plotted the normalized change in firing rate against FI for each neuromodulator compared to aCSF. The scatter plots in Fig. ?? C (left panels) demonstrates that D1 activation alters the relationship between firing rate and FI, we can see that excitatory neurons show a much larger variance for change in firing rate and FI compared to inhibitory neurons. This suggest that excitatory neurons are modulated much more strongly than inhibitory neurons. The kernel density estimation (KDE) plots (right panels) compared the distribution of FI values between aCSF and D1 conditions. The KDE plot show a significant shift to the right in FI distribution under D1 activation for excitatory neurons, indicating that D1 receptor activation is significantly increases (Wilcoxon signed-rank test: stat = 110.0, p = 0.0190 ) the information transfer in excitatory neurons. Similarly, the scatter plots in Fig. ?? C-D (left panels) demonstrates that D2-R and M1-R activation alters the relationship between firing rate and FI as well, we can see that excitatory neurons show a much larger variance for change in firing rate and FI compared to inhibitory neurons in case of D2. This suggest that excitatory neurons are modulated much more strongly than inhibitory neurons in case of D2-R activation. In case of M1-R activation, the difference in variance between excitatory and inhibitory neurons is much less pronounced. The kernel density estimation (KDE) plots (right panels) compared the distribution of FI values between aCSF and D1 conditions. For both M1-R (Wilcoxon signed-rank test: statistic = 22.0, p = 2.02e-3) and D2-R (Wilcoxon signed-rank test: stat = 225.0 , p = 0.01201) activation the FI distribution was significantly lowered for excitatory neurons, indicating that both M1 and D2 receptor activation significantly modulates the information transfer capabilities of excitatory neurons.

Together, these results demonstrate that neuromodulation exerts cell-type specific effects on information transfer in neurons. D1 and M1 receptor activations significantly reduce FI in excitatory neurons compared to inhibitory neurons, while the effects of D2

activation are not significant. On the other hand, D1 receptor activation significantly increases information transfer for inhibitory neurons, while D2-R and M1-R significantly reduces information transfer for excitatory neurons. The differential changes observed in excitatory versus inhibitory populations, both under baseline conditions and following neuromodulatory interventions, suggest that neuromodulators play a critical role in redefining neuronal functional identity and information processing within neural circuits.

## Discussion

In this study, we aimed to investigate how neuromodulation, specifically through dopamine (D1R, D2R) and acetylcholine (M1R) receptor activation, alters the functional properties of cortical neurons beyond traditional measures of excitability. Using frozen noise stimulation based single-cell in-vitro somatic recordings from layer 2/3 of the mouse somatosensory cortex, we extracted four functional feature sets comprising action potential (AP), passive biophysical (PB), adaptation currents (AC), and linear input filter via a spike-triggered average (STA). This approach enabled us to study the impact of neuromodulation across multiple physiological domains within and across neuronal subtypes.

### **Receptor-Specific Neuromodulation Reshapes Functional Architecture in Distinct Cell Types**

Our analyses revealed that dopaminergic and cholinergic receptor activation altered the correlation structure among functional attributes, and these effects were excitatory/inhibitory cell-type specific. For inhibitory neurons, D1R and D2R activation increased inter-attribute correlations, suggesting a convergence of functional attributes under neuromodulatory influence. In contrast, excitatory neurons displayed decreased correlations under D1R activation, indicating a decoupling of intrinsic and encoding

features. This suggests that dopaminergic modulation sharpens functional coherence in inhibitory neurons while increasing functional independence in excitatory neurons.

These results extend previous findings that D1R activation increases firing in both excitatory and inhibitory neurons in prefrontal and motor cortices [Seamans and Yang \(2004\)](#); [Tritsch and Sabatini \(2012\)](#); [Anastasiades et al. \(2019\)](#), by showing that in the sensory cortex, such modulation also reorganizes functional coupling between key electrophysiological domains. Inhibitory neurons, under D1R and D2R activation, exhibited stronger coupling between passive properties, AP dynamics, and linear input filtering; suggesting that neuromodulation may reduce heterogeneity and impose a more unified computational role. This aligns with the hypothesis that dopamine can increase synchronization and gain control within inhibitory networks, potentially sharpening their influence on local circuits [Gao and Goldman-Rakic \(2003\)](#); [Morozova et al. \(2016\)](#); [Seamans et al. \(2001\)](#).

Interestingly, we observed similar coupling effects under M1R activation, pointing to a convergent mechanism across dopaminergic and cholinergic systems in shaping the internal structure of inhibitory neuron function. The decoupling observed in excitatory neurons, particularly under D1R, may reflect a shift toward greater computational flexibility or specialization, allowing for more diverse input-output transformations. These effects may be a substrate for dynamic control of cortical processing modes, such as switching between attentive and exploratory states.

### **Functional Clustering and Heterogeneous Modulation of Neuronal Identity**

To examine how these neuromodulatory changes reorganize functional neuron types, we applied UMAP-Louvain clustering to the high-dimensional feature sets before and after receptor activation. Our results show that agonist application drastically alters functional clustering, suggesting that receptor-specific modulation reshapes neuronal identities in both excitatory and inhibitory populations.

Importantly, the modulatory effects were not uniform, but heterogeneous within cell types, implying that neuromodulation acts in a subtype-specific manner. This is consistent with recent work showing volume transmission and receptor expression gradients as mechanisms for differential modulation across cell types [Özçete et al. \(2024\)](#). By clustering neurons based on their change vectors (difference between agonist and control), we identified distinct subpopulations exhibiting coordinated shifts in AP and passive properties, reinforcing the idea that neuromodulation reconfigures the functional state space of neurons rather than simply scaling their excitability.

We also found that adaptation currents and STAs became more homogeneous in excitatory neurons compared to inhibitory neurons following neuromodulation. This suggests that although both populations undergo modulation, excitatory neurons may be pushed toward a more constrained encoding regime, possibly to provide stability in coding under varying network conditions. Nonetheless, the core distinction between excitatory and inhibitory populations remained intact, highlighting the robustness of intrinsic identity despite substantial functional plasticity. We speculate that a modeling effort superimposing neuromodulatory affects on a balanced networks would reveal the implication of neuromodulatory alteration on the balance excitation-inhibition and therefore the shift that neuromodulation can cause.

### **Neuromodulation Selectively Alters Information Transfer**

While neuromodulators are known to affect neuronal excitability, less is known about how such changes impact information transmission. Using the frozen noise protocol [Zeldenrust et al. \(2017\)](#), we estimated fractional information (FI) between stimulus and spike train for each neuron under different receptor conditions.

Our key finding is that neuromodulation alters information transfer in a cell-type and receptor-specific manner. Specifically, D1R and M1R activation significantly decreased FI in excitatory neurons, while D2R activation increased FI in inhibitory neu-

rons. This suggests that excitatory and inhibitory neurons are differentially engaged by neuromodulators to redistribute information processing roles. Moreover, FI variance increased in excitatory neurons under D1R, implying a diversification of encoding strategies, whereas inhibitory neurons exhibited more stable and coordinated changes.

These findings underscore an important result that modulation of biophysical and spike-generating properties has direct consequences on the information transfer and encoding of neurons. Neuromodulators do not simply shift the gain of neurons, they reconfigure how inputs are integrated and transformed into outputs, thus shaping the flow of information through cortical networks. This raises exciting new questions about how neuromodulatory systems shape perceptual inference, attention, and learning by dynamically allocating information processing across cell types.

### **Limitations and Future Directions**

Our study, while comprehensive, has several important limitations. First, our recordings were limited to the soma, whereas neuromodulation often targets synaptic and dendritic compartments, which could substantially influence neuronal input-output transformations. Second, our analysis is constrained by sample size and cortical region, necessitating broader recordings across layers and brain areas to validate the generality of our findings.

Most critically, neuromodulatory systems are highly degenerate: the same ion channel can be targeted by multiple modulators, and a single neuromodulator can affect many channels and cellular processes. Thus, our receptor-specific results represent only a partial view of the underlying modulatory landscape. Future work should incorporate multi-receptor interactions, consider temporal dynamics of modulation, and examine how these single-cell changes propagate to network-level phenomena such as synchrony, attractor stability, and behavioral output.

## Conclusion

Together, our findings reveal that D1, D2, and M1 receptor activation differentially reorganizes the biophysical, adaptive, and encoding properties of excitatory and inhibitory neurons in layer 2/3 of the somatosensory cortex. Neuromodulation can couple or decouple domains of neuronal function, alter functional classification, and modulate information transmission in a subtype-specific manner. These effects likely support context-dependent reconfiguration of cortical computation and offer a new window into how global modulatory signals dynamically orchestrate diverse local circuit functions.

## References

- (2017). Proteomic landscape of the primary somatosensory cortex upon sensory deprivation. *Giga-science*, 6(10):gix082.
- Aggarwal, C. C., Hinneburg, A., and Keim, D. A. (2001). On the surprising behavior of distance metrics in high dimensional space. In *Database theory—ICDT 2001: 8th international conference London, UK, January 4–6, 2001 proceedings* 8, pages 420–434. Springer.
- Anastasiades, P. G., Boada, C., and Carter, A. G. (2019). Cell-type-specific d1 dopamine receptor modulation of projection neurons and interneurons in the prefrontal cortex. *Cerebral cortex*, 29(7):3224–3242.
- Arnsten, A. F. and Rubia, K. (2012). Neurobiological circuits regulating attention, cognitive control, motivation, and emotion: disruptions in neurodevelopmental psychiatric disorders. *Journal of the American Academy of Child & Adolescent Psychiatry*, 51(4):356–367.
- Bargmann, C. I. (2012). Beyond the connectome: how neuromodulators shape neural circuits. *Bioessays*, 34(6):458–465.
- Bargmann, C. I. and Marder, E. (2013). From the connectome to brain function. *Nature methods*, 10(6):483–490.
- Blondel, V. D., Guillaume, J.-L., Lambiotte, R., and Lefebvre, E. (2008). Fast unfolding of communities in large networks. *Journal of statistical mechanics: theory and experiment*, 2008(10):P10008.
- Brown, B. and collinwa (2023). collinwa/mcfa: First pypi release.
- Brown, B. C., Wang, C., Kasela, S., Aguet, F., Nachun, D. C., Taylor, K. D., Tracy, R. P., Durda, P., Liu, Y., Johnson, W. C., et al. (2023). Multiset correlation and factor analysis enables exploration of multi-omics data. *Cell Genomics*, 3(8).
- Cousineau, J., Lescouzères, L., Taupignon, A., Delgado-Zabalza, L., Valjent, E., Baufreton, J., and Le Bon-Jégo, M. (2020). Dopamine d2-like receptors modulate intrinsic properties and synaptic transmission of parvalbumin interneurons in the mouse primary motor cortex. *eneuro*, 7(3).
- da Silva Lantyer, A., Calcini, N., Bijlsma, A., Kole, K., Emmelkamp, M., Peeters, M., Scheenen, W. J., Zeldenrust, F., and Celikel, T. (2018). A databank for intracellular electrophysiological mapping of the adult somatosensory cortex. *GigaScience*, 7(12):giy147.
- Dalley, J. W., Theobald, D. E., Bouger, P., Chudasama, Y., Cardinal, R. N., and Robbins, T. W. (2004). Cortical cholinergic function and deficits in visual attentional performance in rats following 192 igg–saporin-induced lesions of the medial prefrontal cortex. *Cerebral Cortex*, 14(8):922–932.
- Dascal, N. (2001). Ion-channel regulation by g proteins. *Trends in Endocrinology & Metabolism*, 12(9):391–398.
- Durstewitz, D. and Seamans, J. K. (2008). The dual-state theory of prefrontal cortex dopamine function with relevance to catechol-o-methyltransferase genotypes and schizophrenia. *Biological psychiatry*, 64(9):739–749.
- Ferguson, K. A. and Cardin, J. A. (2020). Mechanisms underlying gain modulation in the cortex. *Nature Reviews Neuroscience*, 21(2):80–92.
- Gao, W.-J. and Goldman-Rakic, P. S. (2003). Selective modulation of excitatory and inhibitory microcircuits by dopamine. *Proceedings of the national academy of sciences*, 100(5):2836–2841.
- Hasselmo, M. E., Giocomo, L. M., et al. (2006). Cholinergic modulation of cortical function. *Journal of Molecular Neuroscience*, 30(1-2):133–136.
- Häusser, M. (2000). The hodgkin-huxley theory of the action potential. *Nature neuroscience*, 3(11):1165–1165.
- Hernáth, F., Schlett, K., and Szücs, A. (2019). Alternative classifications of neurons based on physiological properties and synaptic responses, a computational study. *Scientific reports*, 9(1):13096.

## Chapter 3. Neuromodulatory Control of Cortical Function: Cell-Type Specific Reshaping of Neuronal Information Transfer

---

- Joshi, N., van der Burg, S., Celikel, T., and Zeldenrust, F. (2024). Understanding neuronal diversity: Role of input dynamics and filtering. *bioRxiv*, pages 2024–10.
- Kole, K. and Celikel, T. (2019). Neocortical microdissection at columnar and laminar resolution for molecular interrogation. *Current Protocols in Neuroscience*, 86(1):e55.
- Kole, K., Zhang, Y., Jansen, E. J., Brouns, T., Bijlsma, A., Calcini, N., Yan, X., Lantyer, A. d. S., and Celikel, T. (2020). Assessing the utility of magneto to control neuronal excitability in the somatosensory cortex. *Nature neuroscience*, 23(9):1044–1046.
- Lee, E. K., Balasubramanian, H., Tsolias, A., Anakwe, S. U., Medalla, M., Shenoy, K. V., and Chandrasekaran, C. (2021). Non-linear dimensionality reduction on extracellular waveforms reveals cell type diversity in premotor cortex. *Elife*, 10:e67490.
- Marder, E. (2012). Neuromodulation of neuronal circuits: back to the future. *Neuron*, 76(1):1–11.
- Martens, M. B., Celikel, T., and Tiesinga, P. H. (2015). A developmental switch for hebbian plasticity. *PLoS Computational Biology*, 11(7):e1004386.
- McInnes, L., Healy, J., and Melville, J. (2018). Umap: Uniform manifold approximation and projection for dimension reduction. *arXiv preprint arXiv:1802.03426*.
- Miceli, S., Nadif Kasri, N., Joosten, J., Huang, C., Kepser, L., Proville, R., Seltén, M. M., van Eijs, F., Azarfar, A., Homberg, J. R., et al. (2017). Reduced inhibition within layer iv of sert knockout rat barrel cortex is associated with faster sensory integration. *Cerebral Cortex*, 27(2):933–949.
- Morozova, E. O., Zakharov, D., Gutkin, B. S., Lapish, C. C., and Kuznetsov, A. (2016). Dopamine neurons change the type of excitability in response to stimuli. *PLoS Computational Biology*, 12(12):e1005233.
- Nadim, F. and Bucher, D. (2014). Neuromodulation of neurons and synapses. *Current opinion in neurobiology*, 29:48–56.
- Nusser, Z. (2009). Variability in the subcellular distribution of ion channels increases neuronal diversity. *Trends in neurosciences*, 32(5):267–274.
- Özçete, Ö. D., Banerjee, A., and Kaeser, P. S. (2024). Mechanisms of neuromodulatory volume transmission. *Molecular Psychiatry*, pages 1–14.
- Pedregosa, F., Varoquaux, G., Gramfort, A., Michel, V., Thirion, B., Grisel, O., Blondel, M., Prettenhofer, P., Weiss, R., Dubourg, V., Vanderplas, J., Passos, A., Cournapeau, D., Brucher, M., Perrot, M., and Duchesnay, E. (2011). Scikit-learn: Machine learning in Python. *Journal of Machine Learning Research*, 12:2825–2830.
- Pozzorini, C., Mensi, S., Hagens, O., Naud, R., Koch, C., and Gerstner, W. (2015). Automated high-throughput characterization of single neurons by means of simplified spiking models. *PLoS computational biology*, 11(6):e1004275.
- Salinas, E. and Sejnowski, T. J. (2001). Book review: gain modulation in the central nervous system: where behavior, neurophysiology, and computation meet. *The Neuroscientist*, 7(5):430–440.
- Sarter, M., Parikh, V., and Howe, W. M. (2009). Phasic acetylcholine release and the volume transmission hypothesis: time to move on. *Nature Reviews Neuroscience*, 10(5):383–390.
- Schwartz, O., Pillow, J. W., Rust, N. C., and Simoncelli, E. P. (2006). Spike-triggered neural characterization. *Journal of vision*, 6(4):13–13.
- Seamans, J. K., Durstewitz, D., Christie, B. R., Stevens, C. F., and Sejnowski, T. J. (2001). Dopamine d1/d5 receptor modulation of excitatory synaptic inputs to layer v prefrontal cortex neurons. *Proceedings of the National Academy of Sciences*, 98(1):301–306.
- Seamans, J. K. and Yang, C. R. (2004). The principal features and mechanisms of dopamine modulation in the prefrontal cortex. *Progress in neurobiology*, 74(1):1–58.
- Seong, H. J. and Carter, A. G. (2012). D1 receptor modulation of action potential firing in a subpopulation of layer 5 pyramidal neurons in the prefrontal cortex. *Journal of Neuroscience*, 32(31):10516–10521.

## Chapter 3. Neuromodulatory Control of Cortical Function: Cell-Type Specific Reshaping of Neuronal Information Transfer

---

- Shine, J. M., Müller, E. J., Munn, B., Cabral, J., Moran, R. J., and Breakspear, M. (2021). Computational models link cellular mechanisms of neuromodulation to large-scale neural dynamics. *Nature neuroscience*, 24(6):765–776.
- Taghert, P. H. and Nitabach, M. N. (2012). Peptide neuromodulation in invertebrate model systems. *Neuron*, 76(1):82–97.
- Tritsch, N. X. and Sabatini, B. L. (2012). Dopaminergic modulation of synaptic transmission in cortex and striatum. *Neuron*, 76(1):33–50.
- Virtanen, P., Gommers, R., Oliphant, T. E., Haberland, M., Reddy, T., Cournapeau, D., Burovski, E., Peterson, P., Weckesser, W., Bright, J., van der Walt, S. J., Brett, M., Wilson, J., Millman, K. J., Mayorov, N., Nelson, A. R. J., Jones, E., Kern, R., Larson, E., Carey, C. J., Polat, I., Feng, Y., Moore, E. W., VanderPlas, J., Laxalde, D., Perktold, J., Cimrman, R., Henriksen, I., Quintero, E. A., Harris, C. R., Archibald, A. M., Ribeiro, A. H., Pedregosa, F., van Mulbregt, P., and SciPy 1.0 Contributors (2020). SciPy 1.0: Fundamental Algorithms for Scientific Computing in Python. *Nature Methods*, 17:261–272.
- Winterer, G. and Weinberger, D. R. (2004). Genes, dopamine and cortical signal-to-noise ratio in schizophrenia. *Trends in neurosciences*, 27(11):683–690.
- Yan, X., Calcini, N., Safavi, P., Ak, A., Kole, K., Zeldenrust, F., and Celikel, T. (2022). A whole-cell recording database of neuromodulatory action in the adult neocortex. *bioRxiv*, pages 2022–01.
- Zeldenrust, F., Calcini, N., Yan, X., Bijlsma, A., and Celikel, T. (2024). The tuning of tuning: How adaptation influences single cell information transfer. *PLOS Computational Biology*, 20(5):e1012043.
- Zeldenrust, F., de Knecht, S., Wadman, W. J., Denève, S., and Gutkin, B. (2017). Estimating the information extracted by a single spiking neuron from a continuous input time series. *Frontiers in computational neuroscience*, 11:49.



# Chapter 4

## Heterogeneity in delay and timescales improves task Performance



Based on: Willemsen, Y.\* , Ou, Y.\* , Belzer, C., Arias Vásquez, A., Smidt, H., Beijers, R., and de Weerth, C. A longitudinal study of the gut microbiota during the first three years of life: Links with problem behavior and executive functions at preschool age. *Development and Psychopathology*, 2023, 1-17. \*Authors contributed equally

## **Abstract**

## Introduction

## Results

## **Discussion**



# **Chapter 5**

## **General Discussion**



Executive functions (EF) and inhibitory control (IC) are essential skills that are important for executing goal-directed behaviours (?). Early life nutrition is suggested to have a pivotal role in explaining inter-individual differences in these behaviours (?). The general goal of this thesis was to uncover unknown links between nutrition and behaviour in early life. We investigated this by means of three aims. The **first aim** was to investigate the relations between early life nutrition-related predictors and future cognitive and behavioural outcomes. The **second aim** was to investigate potential mechanisms underlying the relations between early life nutrition and cognitive and behavioural outcomes. Because of the important role of the microbiota-gut-brain axis on behaviour (???), we focused on the gut bacteria in early as well as later life (two weeks to three years of age). Lastly, as nutrition is important for the development of many physiological, and likely psychological systems (?), it is important to study predictors of healthy nutritional behaviours, especially in phases of life where risk for unhealthy nutritional behaviours is heightened, such as adolescence. The **third aim** was therefore to investigate the role of maternal caregiving behaviour on adolescent nutritional behaviours.

In light of **aim 1**, we investigated whether the duration of breastfeeding predicted better toddler EF and IC, and if this was mediated by toddler diet quality (**Chapter 2**), and whether the human milk oligosaccharide (HMO) composition in breast milk at two, six, and 12 weeks predicted better toddler EF and IC (**Chapter 3**). We found that duration of breastfeeding, and toddler diet quality did not predict toddler IC and EF (**Chapter 2**). However, we did find a relation between longer breastfeeding duration and better toddler diet quality (**Chapter 2**). Furthermore, in **Chapter 3**, we found that higher concentrations of 2'FL and grouped fucosylated HMOs in mother milk predicted better toddler EF in exclusively breastfed toddlers. These relations were not found for 3'SL, 6'SL, and grouped sialylated HMOs.

For **aim 2**, gut microbiota composition at ages two, six, and 12 weeks, and one and three years, were assessed in relation to EF, IC, and problem behaviour in toddlerhood (**Chapter 4**). One of the most important findings was the association between higher relative abundances of *Streptococcus* throughout the first three years of life and worse EF at age three years.

Lastly, for **aim 3**, we investigated the relation between maternal caregiving quality, measured from the early postnatal period until adolescence, and adolescent diet quality and emotional eating behaviour, and whether adolescent IC mediated these potential relations (**Chapter 5**). We found that higher diet quality was associated with better IC in adolescence. However, adolescent emotional eating behaviour was not related to adolescent IC. Finally, we did not find support for a relation between maternal caregiving quality (at all ages) and adolescent inhibitory control or diet quality and emotional eating behaviour.

Figure 5.1 shows a summary of the results found. The following paragraphs discuss how these findings contribute to research on early life and development, as well as their limitations and directions for future research.

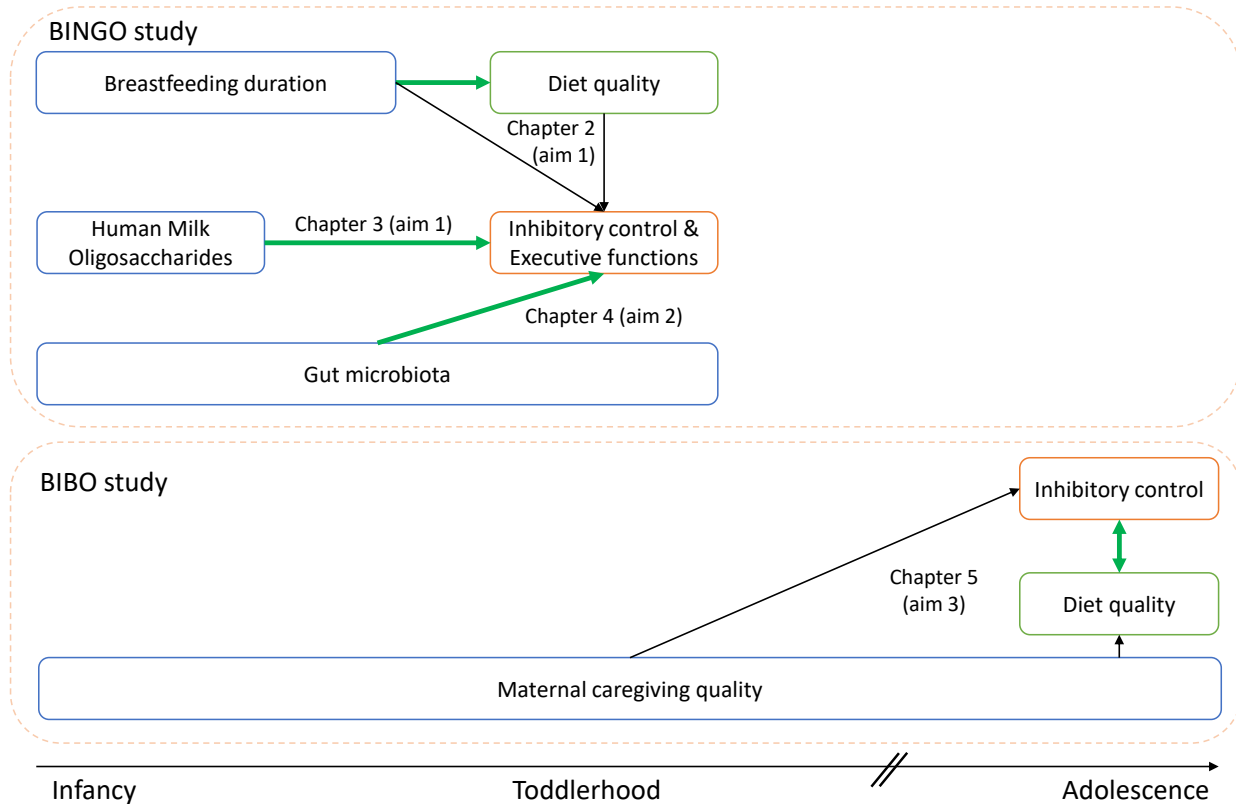


Figure 5.1. Overview of the research topics per chapter. Blue boxes indicate the expected predictors. The orange and green boxes indicate the outcome measures. Light orange dotted lines indicate the cohorts used. The black arrows indicate the expected direction of the association, as causality could not be determined in the present data. The bold green arrows indicate the associations found.

## The impact of early life nutrition on future behaviour

Early life has been shown to be an extremely important phase predicting future development (?). In line with this, many studies investigating early life factors, such as early life stress and early life nutrition, have found impactful health consequences on children's future physiological and psychological wellbeing (??). In the current studies, we also found that early life nutrition predicted future child health outcomes. First, we found that longer exclusive breastfeeding duration predicted higher diet quality in toddlers (**Chapter 2**). This is in line with the results of many studies that found longer (exclusive and total) breastfeeding duration to be related to higher intake of vegetables and fruits in toddlers, contributing to a higher toddler diet quality (see reviews by ? and ?). A potential mechanism underlying these findings could be that the mother shapes healthier food preferences in the child through breastfeeding (??). Mother milk is the first exposure to flavours for most infants. The flavour of mother milk changes depending on the maternal diet. Specifically, compounds of garlic, carrot, anise, mint, eucalyptus, alcohol, and molecular structures of fruit and vegetables are transferred to human milk (?). An infant responds to this flavour change by increasing or decreasing sucking time and number of sucks (?). Long-term studies show that during solid food consumption, young children show greater preferences (defined as greater duration of mouthing behaviour) for the flavours they have been exposed to through breast milk, with lasting effects until at least ten years of age (e.g., maternal diet with higher vegetable intake is associated with greater child preferences for, and intake of vegetables) (????). This explanation falls under the Lactocrine Programming hypothesis, which states that milk constituents can have long term effects on an infant's development (??, for a review, see ?). In this case, the effect would be a programming of the child's food preferences. Note that this proposed explanation is plausible under the assumption that mothers who breastfeed longer have healthier diets than mothers

who breastfeed for shorter times (??). An alternative and most probable complementary explanation for our findings is that mothers who breastfeed longer also provide and feed their children healthier foods in toddlerhood.

A clear result in this thesis that is supported by the Lactocrine Programming hypothesis is the evidence we found for higher levels of fucosylated HMOs in mother milk predicting better toddler EF (**Chapter 3**). This is in line with rodent studies that confirmed a causal relation between early life HMOs and better cognition (?). The review by ? described rodent studies that administered HMOs in early life and assessed their behaviour in adulthood. In addition, several human studies also found relations between HMOs and better cognitive outcomes (???). When comparing the results of **Chapters 2** and **3**, they suggest that breastfeeding duration independently does not predict EF or IC, but that the constituents of mother's milk, i.e., HMOs, may be important for predicting cognitive outcomes. As there are still unclear relations between breastfeeding duration and child and toddler EF (???), both breastfeeding duration and milk-borne bioactive factors should be considered in future research to obtain a clear view on how Lactocrine Programming predicts toddler behaviour. Note, however, that causality cannot be established with observational longitudinal studies. Animal studies that include early life manipulations in experimental trials can unveil causal relations between early life nutrition and cognition, though results are still difficult to translate to humans (?). Hence, a combination of these methods (i.e., longitudinal observational human studies, experimental animal studies, randomised controlled trials), as well as replication studies to confirm previous results (to allow for performing meta-analyses), are necessary to determine whether and how early life nutrition causally affects future cognitive and behavioural outcomes in human children.

## The microbiota-gut-brain axis: mechanism underlying the relations between nutrition and behaviour?

We found that early life fucosylated HMOs predicted better toddler EF (**Chapter 3**). Interestingly, the main functions of HMOs are to serve as nutrition for the gut microbiota (???). Indeed, in the same BINGO cohort, HMO levels were positively related to higher levels of specific gut microbiota (e.g., high levels of 2'FL were related to higher levels of *Bifidobacteria*) (?). In addition, animal studies as well as human studies have observed an interplay between the gut microbiota and brain functioning (?????). Because of the potential regulatory function of the gut microbiota on the brain (e.g., through production of short chain fatty acids that affect the central nervous system (?)), the microbiota-gut-brain axis is a strong candidate for explaining the relations found between early life nutrition and cognition. In line with previous findings (???), we found that high levels of *Veillonella* and *Bacteroides* in early life were related to better toddler IC (**Chapter 4**). In addition, findings came forth that were not seen in previous literature, e.g., we found that higher levels of gut *Streptococcus* in early life as well as throughout the first three years of life, predicted worse toddler EF (**Chapter 4**). Although we speculated about potential pathways through which these gut microbiota may regulate behaviour, we were unable to confirm these pathways in the current thesis. To discover the causal role of gut microbiota in the relation between behaviour and cognition, future research should aim at identifying the function of bacteria, involving a multi-omics approach (?), as explained below.

Metagenomics, including marker gene analyses (16S rRNA in bacteria) and shotgun sequencing, have allowed us to reveal the composition of bacteria in a stool sample (?). Many studies identify the relative abundance of bacteria and infer on the relations found with the health outcome, leading to insightful discoveries, such as that bacterial composition between depressed, and anxious individuals differ significantly from healthy

controls (?). Note, however, that interpretation of relative abundance data could lead to false discovery rates (?), and correlation biases (?). This is due to the fact that an increase in abundance of one taxa is equal to a decrease in all other taxa, meaning that relative abundance of one taxa is dependent on the abundance of the remaining taxa (?). Identifying absolute bacterial abundances (measured by e.g., quantitative PCR or flow cytometry) may aid in the interpretation of biological mechanisms regarding the microbiota-gut-brain axis. Importantly, as gut microbiota composition is subject to day-to-day, and within-person variation (?), it is advisable to include repeated measures of stool sampling. To increase the reliability of earlier findings, replication studies are necessary (?). When consistency in results is found over multiple studies, the next step is to explore the mechanism behind the relations.

Nonetheless, assessing relative or absolute abundance of bacteria does not reveal their transcriptional activities (???). Metatranscriptomics, which is the identification of microbial mRNA, allows for identification of bacterial metabolic activities. Interestingly, this technique has helped uncover different functions of the same bacterial species. For example, in patients with Crohn's disease, *Ruminococcus gnavus* is able to produce inflammatory glucorhamnan that induces production of inflammatory cytokines in the gut (?). This same bacterium was also found to modulate mucin production which fortifies gut barrier functions (?), subsequently preventing gut inflammation (?). This phenomenon is likely explained by interactions between different bacterial taxa, through communication, cooperation, and competition (???). This means that gut bacteria exert different effects depending on which other bacteria are present in the gut. Different functions of the same bacterial species could also be explained by the fact that bacteria exert different activities based on their host's conditions, also known as phenotypic switching (??). Interestingly, some mRNAs have weak ribosome binding sites and are therefore poorly translated, while those with strong binding sites are easier to translate (?). This means that not all microbial mRNA detected by

metatranscriptomics may be involved in the expected metabolic processes, indicating that the interpretation of the results of these techniques must be done with caution.

Identifying microbial proteins (metaproteomics) and metabolites (metabolomics) might give a clearer picture of the role of gut bacteria in behaviour. Metaproteomics identifies levels of expressed proteins. The identification of these proteins is reliant on pipelines that process these data and match the peptides with online metagenomic databases to discover the most probable bacteria that might have expressed them (?). The reliance on these metagenomic databases is also a flaw, as they are dependent on the previously detected proteins. Hence, newly found peptides may not be in the database yet. Metabolomics is the study of metabolites in a biological sample, and allows for identification of key metabolites of specific pathways linked to a disease (?). However, as some metabolites are produced by different bacterial strains (?), it is difficult to disentangle which bacteria are related to the identified metabolites. Note that including metaproteomics, and metabolomics result in more variables and therefore more potential interactions to be investigated. Hence, it is extremely important that this type of research is properly powered.

All of the above supports the notion that identification of relative abundance is just a first step to understanding the role of gut bacteria in behaviour. Although all omics-techniques may have flaws, these techniques can get us closer to identifying causality in the microbiota-gut brain axis. A multi-omics approach could therefore lead to a better understanding on how gut microbiota may play a causal role in the relation between nutrition and behaviour (?).

Before validating the potential molecular mechanisms of bacteria, it is important to first isolate, culture, and characterise them. Although approximately only 20% of the human gut bacteria have been cultured so far (?), it might be possible to culture hundreds of gut bacterial strains in a short timespan in the near future, due to rapid developments in high-throughput cultivation approaches (?). Furthermore, besides

bacteria, the gut is also colonised by fungi, archaea, and viruses. Fungi and archaea have different functions and have been associated with host phenotype, such as gut-related diseases and gut motility, respectively (??). These microorganisms also interact with bacteria and their derived products (??). Viruses present in the gut interact and coexist with gut bacteria through lysogeny (i.e., integration of the virus' nucleic acid into the bacterial genome or formation of a viral replicon in the bacterial cytoplasm). This way, viruses directly impact gut microbiota composition and the immune system, possibly modulating drivers of health and disease (?). Identifying the function of individual micro-organisms may be challenging. However, considering the complex interactions between the host, bacteria, fungi, and archaea, it is extremely valuable to obtain a detailed view of these dynamic interactions before validating these pathways.

Lastly, *in vivo* and *in vitro* validation studies can help confirm the expected pathways that are likely involved in the microbiota-gut-brain axis (?). *In vitro* studies are studies outside of a (animal) body. For example, organoids, three-dimensional tissues cultures grown from stem cells, have been used more and more to model gut and microbial interactions (?). In these models, microbes or their derived metabolites are injected into gut organoids to determine interactions between the gut and the microbiota (?). *In vivo* studies model the potential causes of health outcomes, such as depression and anxiety, in animal models. These studies grant evidence for causal relations (??). For example, after transplanting microbiota of mice with high-anxiety into mice with low-anxiety, the behaviour of these recipient mice changed according to the donor's behavioural profile (?). Furthermore, transplantation of gut microbiota from humans with autism spectrum disorder into germ-free mice resulted in the induction of autistic behaviours in the mice (?). However, interpretation of these human microbiota-associated rodent studies must be done with caution. Overall, the majority of these studies do not attempt to gain insight in the mechanisms (e.g., which genes are up-, or down-regulated after the stool transplant), and they use a small number of human donors (?). In addition, studies

with null-results or negative outcomes are rarely published (?), and causal claims are overstated, also due to the fact that rodents are proxies for human diseases that do not occur naturally in rodents (e.g., what exactly are ‘autistic behaviours’ or other behaviours in rodents?) (??). Improving the experiments, and changing mindset and policies would aid in discovering true causality between gut microbiota composition and behaviour (?). All in all, the steps for turning correlational relations into causal relations are many and complex. Nonetheless, it is clear that gut microbiota research would benefit from applying repeated measures, identifying absolute gut bacterial abundances, applying a multi-omics approach, and validating the pathways in *in vitro* and *in vivo* studies, to confirm causal relations between the gut microbiota and the brain. This approach, in combination with more specific hypothesis formation, larger sample sizes, and rigorous data collection, storage, and processing, will create evidence that can become substantial enough to result in future clinical implications.

## **Maternal educational level: Key player contributing to child health**

Maternal educational level was found to be important when investigating early life nutrition and later child behavioural outcomes (**Chapter 2** and **Chapter 5**). Higher maternal educational level correlated with later breastfeeding cessation age (**Chapter 2**), better adolescent inhibitory control, higher adolescent diet quality, and more adolescent emotional eating behaviour (**Chapter 5**). A vast majority of previous literature, related to this thesis’ topic, included educational level in their analyses, and found it to impact their results (?????????). Despite educational level being determined differently in each country and culture, study results regarding relations between educational level and child health are consistent. Higher parental educational level is consistently positively related to child physical and mental health (???). There

are some potential suggested mechanisms behind this relation. Parental education was shown to relate to improved parenting abilities and marital quality (?), as well as improved maternal ability to manage finances, choose the qualitatively best child educational programs, and control family health (?). Furthermore, higher maternal educational level is usually accompanied by a higher income, allowing for provision of expensive healthier nutrition (?). One study also found that parental educational level affects child health through their own parental health and family living conditions (?). As such, maternal educational level appears to impact child health in different ways, making it a key variable to include in future research.

In the current thesis, we observed potential effects of maternal educational level within a generally highly educated sample. Since lower educated and higher educated families differ in their dietary intake (i.e., lower educated families have less healthy diets) (??), it is imperative to include and retain lower educated families in future studies. As achieving this goal is unfortunately a common challenge for scientific studies, previous research has reported on the barriers and strategies that improve the inclusion and retention rates of lower educated families (????). Generally, strategies to reduce participant burden (e.g., travel time, and flexible data collection methods) are most effective in retaining large sample sizes (?). To reduce the burden in lower educated families, a higher budget may be necessary (e.g., in the form of a higher incentive, or time and labor of the staff to allow for stepped-interventions and rapport-building between staff and participants) (???). Summarizing, future research on nutrition and behaviour should include lower educated families. By applying the abovementioned strategies, future studies can discover and obtain consistent results from a more diverse sample (e.g., inclusion of a wider variety of educational levels), allowing for generalization of the results.

## Assessment of child behaviour: challenges and future directions

The assessment of behaviour is reliant on behavioural tests, (semi-)naturalistic observations of behaviour, and questionnaires, all of which have been applied in all our studies. At different ages, different types of measures may be more suitable than others for characterizing behaviour. Indeed, we found changing relations depending on the measure used, and age assessed (in **Chapters 3**, and **4**, we found results for toddler behaviour assessed with parental questionnaires by the primary caregiver, and in **Chapter 5**, we found results for adolescent behaviour assessed with behavioural tasks). This could be due to the fact that toddlers spend a large part of their time together with parents. Furthermore, toddler behaviour during a behavioural task could be variable as it may be dependent on their hunger levels, sleep quality, and the examiner performing the tasks (e.g., sex, examiner-toddler interaction) (?). Adolescent behaviour is less affected by these factors (?). However, as children become adolescents, they become more independent and desire more privacy (?), resulting in parents having a less clear view on their adolescent's behaviour. Adolescent self-report on behaviour had not been assessed in our studies due to time and burden constraints. However, it could be very valuable to include adolescent self-reports next to behavioural tasks, as, commonly, literature finds equivocal correlations between behavioural tasks and questionnaires (?). Both methods are valuable but also have their biases, with questionnaires being prone to socially desirable answers (??), and behavioural tasks being a momentary assessment dependent on other factors, such as attention span (?). Hence, future research on toddler and adolescent behaviour ideally should include both behavioural tasks as well as (self-report) questionnaires. In case of time and/or budget restrictions, it may be advisable to assess toddler behaviour with parental questionnaires, and adolescent behaviour with behavioural tasks.

## Assessment of child dietary intake: challenges and future directions

Diet quality was determined by assessing the dietary intake with parental reports (**Chapter 2, 3 and 4**) and self-reports (**Chapter 5**). The most commonly used methods for dietary assessment are 24-hour recalls, food frequency questionnaires, and food records (?). Although keeping a food record is currently the most valid method for assessing total dietary intake (i.e., 'gold-standard'), the fact that the most commonly used dietary assessment methods are reliant on self-reports and parent reports, means that they are prone to memory bias as well as social desirability bias (??). This makes the assessment of dietary intake in a general population one of the largest challenges in nutritional sciences. Additionally, assessing dietary intake in specific age-groups within a general population has its own specific challenges. Toddlers cannot report their own dietary intake, hence, we are dependent on parental reports. It is a logical choice, since toddlers spend most of their time with their parents, and parents provide the toddler with nutrition, allowing them to know exactly what their child consumes. However, this also makes parent report highly subject to socially desirable answers, as it is the parent who is responsible for the toddler's dietary intake. In addition, there are moments when the parents do not know the dietary intake of their child, such as when it goes to kindergarten or is cared for by babysitters (which is often the case in the Netherlands (?)). This makes parental report still challenging. Regarding adolescent dietary intake, as children become more independent (?), the parent's view on the dietary intake of their adolescent child becomes less clear. This means that self-reports are more representative and reliable for assessing adolescent dietary intake. However, the multiple 24-hour recalls needed to obtain a reliable picture of diet quality cause a relatively high participant burden. As recruitment and retention of adolescents in studies is already challenging (?), a food frequency questionnaire,

which is less burdensome than three unannounced 24-hour recalls, is more appropriate for assessing habitual dietary intake in adolescents. Note that self-reported nutritional questionnaires are also prone to socially desirable answers, recall bias, and misreporting in adolescents (?). Fortunately, developments regarding the assessment of nutritional intake have been rising. Technology-based assessments, including image- and sensor-based technologies, are being developed and show promising results (???). Specifically, image-based technologies might be interesting for assessing dietary intake in the general population, as participants can simply take a picture of their food before and after the meal with a smartphone. This method reduces subject bias, burden, and provides a more accurate view on portion size and type of food, compared to 24-hour recalls, food frequency questionnaires, and food records. The largest challenge with this technology is for algorithms to accurately identify the nutritional value of the food on the image (?). More references, and thus, more time are necessary to improve this algorithm. All in all, dietary assessment methods are advancing, and technology-based assessments could aid in reducing the burden and improving the accuracy of reporting dietary intake. As the utilisation and development of technological image-based dietary assessment started roughly 10 years ago (??), it is likely that these technologies will be applied either as a stand-alone method, or in combination with traditional dietary assessment methods, in the foreseeable future. For the time being, the best way to assess dietary intake in toddlers is through parental reports. Specifically, multiple unannounced 24-hour dietary recall reports, although tedious, provide the most reliable data. Furthermore, adolescent dietary intake is most reliably assessed with a self-reported food frequency questionnaire.

## **Conclusion and future perspectives**

As reflected in this thesis, early life nutrition is an important life phase for future health and behaviour. We found evidence that supports the Lactocrine Programming

hypothesis: fucosylated HMOs are related to better EF in our study. Furthermore, the microbiota-gut-brain axis may be an important mediator between nutrition and behaviour as we found certain bacteria in early life and throughout the first three years of life to be related to better EF and IC in toddlerhood. To identify the likely causal role of gut microbiota on behaviour, recommendations for future research are: performing repeated measures, identifying absolute gut bacterial abundances, applying a multi-omics approach, validating the pathways in *in vitro* and *in vivo* studies, and replicating studies. Additionally, including lower educational levels is imperative as the role of maternal educational level was already shown to be important in our generally highly educated sample. A higher budget is necessary to aid the inclusion and retention of this target group. Lastly, the methods for assessing nutritional intake have their flaws. However, it is likely that technological image-based assessment methods will be applied more commonly in the foreseeable future. This will allow for accurate assessment of dietary intake in the general population, resulting in more accurate inferences on the relation between dietary intake and health outcomes.

The development of EF skills is important for many future outcomes, such as academic performance, socioemotional competence, and general health (??????). This thesis contributes to understanding the role of early life breastfeeding duration and HMO exposure on toddler EF, and the possible regulating role of gut microbiota on toddler EF. Replicating this thesis' results will help confirm the roles of early life nutritional predictors for future child health and behaviour. These studies would add to the body of literature that shows the importance of early life predictors for future healthy diet and behaviour. In turn, this would provide input for policy makers and health care institutions aiming to improve an infant's early life exposures.

# **Chapter 6**

## **Supplementary Materials**

## **Supplementary materials of chapter 2**

Supplementary Table 7.1. Correlations between mother and partner reports.

	1. BRIEF-P inh (M)	2. BRIEF-P inh (P)	3. BRIEF-P total (M)	4. BRIEF-P total (P)	5. REEF (M)	6. REEF (P)	7. BRIEF-A (M)	8. BRIEF-A (P)
1	-							
2	0.415**	-						
3	0.800**	0.539**	-					
4	0.248	0.857**	0.535**	-				
5	-0.426**	-0.279*	-0.461**	-0.259	-			
6	-0.182	-0.182	-0.181	-0.147	0.407**	-		
7	0.359*	0.366*	0.354**	0.318*	0.033	-0.067	-	
8	0.256	0.428**	0.324*	0.518*	-0.178	-0.049	0.385**	-

Correlations are denoted as  $r$ . BRIEF-P inh: Score of the inhibitory control scale of the BRIEF-P; BRIEF-P total: Total score of the BRIEF-P; (M): Questionnaire filled in by mother; (P): Questionnaire filled in by partner. \* indicates a  $p$ -value lower than 0.05, \*\* indicates a  $p$ -value lower than 0.01.

Supplementary Table 7.2. Correlations between potential confounding variables and independent and outcome variables.

	Maternal educational level	BRIEF-A-comp	Child Gender
<b>Breastfeeding data</b>			
Exclusive breastfeeding	0.191	0.126	-0.026
Breastfeeding cessation age	0.290*	-0.042	0.098
<b>Behavioural tasks</b>			
Flanker	0.106	-0.006	-0.289*
Whisper	-0.002	0.102	-0.124
Gift Wrap	0.063	-0.179	0.396**
Gift Delay	0.433***	-0.270*	0.140
Inhibitory control composite	0.217	-0.250*	0.132
<b>Questionnaires</b>			
BRIEF-P-inh	0.008	0.351**	0.157
BRIEF-P	-0.084	0.437***	-0.012
REEF	0.080	-0.019	0.021

Correlations are denoted as  $r$ . BRIEF-P-inh: Score of the inhibitory control scale of the BRIEF-P. BRIEF-A-comp: Composite score of the BRIEF-A filled in by mother and partner. Child gender: 1=boy, 2=girl. \* $p<0.05$ . \*\* $p<0.01$ . \*\*\* $p<0.001$ .

Supplementary Table 7.3. Parameter Estimates and bootstrapped Confidence Intervals for models 7 and 8.

	B	SE	Lower CI	Upper CI
<b>Model 7: Exclusive breastfeeding duration → diet quality score → reported executive functioning (BRIEF-P)</b>				
<b>Regression paths</b>				
Reported Executive functioning (BRIEF-P)				
Exclusive breastfeeding duration	-0.242	1.198	-2.590	2.107
Diet quality score	1.007	1.484	-1.902	3.917
Parental executive functioning	0.763***	0.056	0.653	0.873
Diet quality score				
Exclusive breastfeeding duration	0.173*	0.070	0.035	0.310
<b>Mediation effect</b>	0.174	0.260	-0.336	0.684
<b>Total effect</b>	0.695	1.083	-1.429	2.818
<b>Model 8: Breastfeeding cessation age → diet quality score → reported executive functioning (BRIEF-P)</b>				
<b>Regression paths</b>				
Reported Executive functioning (BRIEF-P)				
Breastfeeding cessation age	0.338	0.204	-0.061	0.738
Diet quality score	1.143	1.364	-1.531	3.817
Parental executive functioning	0.801***	0.081	0.642	0.960
Maternal educational level	-1.272	1.257	-3.736	1.191
Diet quality score				
Breastfeeding cessation age	0.154	0.131	-0.102	0.411
<b>Mediation effect</b>	0.177	0.223	-0.260	0.613
<b>Total effect</b>	0.044	1.123	-2.158	2.245

MLR estimator used to calculate parameter estimates, bootstrapping used to calculate bias-corrected confidence intervals. Model 7:  $\chi^2(3)=1.043$ ,  $p=0.307$ ; CFI=0.998, RMSEA=0.024, SRMR=0.032,  $n=67$ . Model 8:  $\chi^2(4)=1.817$ ,  $p=0.611$ , RMSEA=0.000, SRMR=0.046,  $n=67$ . \* $p<0.05$ . \*\*\* $p<0.001$ .

Supplementary Table 7.4. Parameter Estimates and bootstrapped Confidence Intervals for Exploratory Models 1, 2, 5, 6, 7, and 8.†

	B	SE	Lower CI	Upper CI	
<b>Regression paths</b>		Exploratory model 1: Exclusive breast-feeding duration → Diet quality score → Flanker			
<b>Mediation effect</b>					
<b>Total effect</b>					
<b>Regression paths</b>		Exploratory model 2: Breastfeeding cessation age → Diet quality score → Flanker			
<b>Mediation effect</b>					
<b>Total effect</b>					
<b>Regression paths</b>		Exploratory model 5: Exclusive breast-feeding duration → Diet quality score → Gift Wrap task			
<b>Mediation effect</b>					
<b>Total effect</b>					
<b>Regression paths</b>		Exploratory model 6: Breastfeeding cessation age → Diet quality score → Gift Wrap task			
<b>Mediation effect</b>					
<b>Total effect</b>					

Supplementary Table 7.4 (continued).

	Maternal educational level	0.091	0.059	-0.026	0.207
	Diet quality score				
	Breastfeeding cessation age	0.156	0.121	-0.082	0.393
<b>Mediation effect</b>		0.018	0.019	-0.020	0.056
<b>Total effect</b>		0.828***	0.174	0.487	1.169
<b>Regression paths</b>	Exploratory model 7: Exclusive breastfeeding duration → Diet quality score → Gift Delay task				
	Gift Delay task				
	Exclusive breastfeeding duration	1.260	1.414	-1.511	4.032
	Diet quality score	-1.790	2.187	-6.076	2.497
	Parental executive functioning	-0.441*	0.176	-0.788	-0.096
	Maternal educational level	6.195**	2.325	1.639	10.752
	Diet quality score				
	Exclusive breastfeeding duration	0.160*	0.068	0.027	0.294
<b>Mediation effect</b>		-0.287	0.399	-1.069	0.495
<b>Total effect</b>		6.726**	2.496	1.834	11.619
<b>Regression paths</b>	Exploratory model 8: Breastfeeding cessation age → Diet quality score → Gift Delay task				
	Gift Delay task				
	Breastfeeding cessation age	0.603	0.333	-0.049	1.256
	Diet quality score	-1.781	2.118	-5.933	2.371
	Parental executive functioning	-0.423*	0.167	-0.751	-0.096
	Maternal educational level	5.826*	2.255	1.406	10.247
	Diet quality score				
	Breastfeeding cessation age	0.153	0.125	-0.093	0.398
<b>Mediation effect</b>		-0.272	0.392	-1.040	0.497
<b>Total effect</b>		0.332	0.443	-0.537	1.200

MLR estimator used to calculate parameter estimates, bootstrapping used to calculate bias-corrected confidence intervals. Exploratory model 1:  $\chi^2(3)=0.696$ ,  $p=0.404$ , CFI=1.000, RMSEA=0.000, SRMR=0.035,  $n=52$ . Exploratory model 2:  $\chi^2(4)=1.592$ ,  $p=0.661$ ; CFI=1.000, RMSEA=0.000, SRMR=0.047,  $n=52$ . Exploratory model 5:  $\chi^2(2)=0.980$ ,  $p=0.613$ ; CFI=1.000, RMSEA=0.000, SRMR=0.034,  $n=65$ . Exploratory model 6:  $\chi^2(3)=2.079$ ,  $p=0.721$ ; CFI=1.000, RMSEA=0.000, SRMR=0.047,  $n=65$ . Exploratory model 7:  $\chi^2(4)=1.881$ ,  $p=0.598$ ; CFI=1.000, RMSEA=0.000, SRMR=0.045,  $n=66$ . Exploratory model 8:  $\chi^2(4)=1.765$ ,  $p=0.623$ , CFI=1.000, RMSEA=0.000, SRMR=0.044,  $n=66$ . \* $p<0.05$ . \*\* $p<0.01$ . \*\*\* $p<0.001$ .

†Model 3 (Exclusive breastfeeding duration → Diet quality score → Whisper) and Model 4 (Breastfeeding cessation age → Diet quality score → Whisper) could not be fitted; therefore no parameter estimates could be produced.

Supplementary Table 7.5. Parameter Estimates and bootstrapped Confidence Intervals for Exploratory Models 9a, 10a, 11a, 12a, and 14a.†

	B	SE	Lower CI	Upper CI
<b>Regression paths</b>				
Executive functioning (BRIEF-P) → Executive functioning (BRIEF-P)				
Executive functioning (BRIEF-P)				
Exclusive breastfeeding duration	0.647	0.872	-1.062	2.356
Vegetable intake	-0.391	0.239	-0.860	0.077
Parental executive functioning	0.363***	0.088	0.190	0.535
Vegetable intake → Executive functioning (BRIEF-P)				
Vegetable intake				
Exclusive breastfeeding duration	0.092	0.461	-0.812	0.996
Mediation effect	-0.036	0.185	-0.400	0.327
Total effect	0.974	0.892	-0.775	2.723
<b>Regression paths</b>				
Executive functioning (BRIEF-P) → Executive functioning (BRIEF-P)				
Executive functioning (BRIEF-P)				
Breastfeeding cessation age	0.341	0.197	-0.044	0.726
Vegetable intake	-0.367	0.232	-0.822	0.089
Parental executive functioning	0.378***	0.088	0.205	0.550
Maternal educational level	-1.004	1.141	-3.247	1.239
Vegetable intake → Executive functioning (BRIEF-P)				
Vegetable intake				
Breastfeeding cessation age	-0.033	0.108	-0.246	0.179
Mediation effect	0.012	0.040	-0.066	0.090
Total effect	-0.274	1.129	-2.486	1.939
<b>Regression paths</b>				
Executive functioning (BRIEF-P) → Executive functioning (BRIEF-P)				
Executive functioning (BRIEF-P)				
Exclusive breastfeeding duration	0.452	0.932	-1.374	2.278
Fruit intake	0.150	0.222	-0.285	0.584
Parental executive functioning	0.352***	0.087	0.182	0.522
Fruit intake → Executive functioning (BRIEF-P)				
Fruit intake				
Exclusive breastfeeding duration	1.215*	0.538	0.160	2.270
Mediation effect	0.178	0.291	-0.392	0.748
Total effect	0.981	0.889	-0.761	2.724
<b>Regression paths</b>				
Executive functioning (BRIEF-P) → Executive functioning (BRIEF-P)				
Executive functioning (BRIEF-P)				
Breastfeeding cessation age	0.338	0.201	-0.055	0.731
Fruit intake	0.132	0.202	-0.264	0.528
Parental executive functioning	0.362***	0.090	0.185	0.538

Supplementary Table 7.5. (continued).

Maternal educational level	-0.940	1.284	-3.457	1.576
Fruit intake				
Breastfeeding cessation age	0.107	0.110	-0.108	0.322
<b>Mediation effect</b>	0.014	0.029	-0.043	0.071
<b>Total effect</b>	-0.227	1.271	-2.718	2.265
<hr/>				
<b>Exploratory model 14a: Breastfeeding cessation age → Snack and Candy intake → Executive functioning (BRIEF-P)</b>				
<hr/>				
<b>Regression paths</b>				
Executive functioning (BRIEF-P)				
Breastfeeding cessation age	0.347	0.199	-0.043	0.736
Snack and Candy intake	-0.076	0.546	-1.146	0.994
Parental executive functioning	0.358***	0.096	0.170	0.545
Maternal educational level	-1.048	1.274	-3.546	1.449
Snack and Candy intake				
Breastfeeding cessation age	-0.075	0.043	-0.159	0.009
<b>Mediation effect</b>	0.006	0.042	-0.076	0.087
<b>Total effect</b>	-0.338	1.260	-2.808	2.132

MLR estimator used to calculate parameter estimates, bootstrapping used to calculate bias-corrected confidence intervals. Exploratory model 9a:  $\chi^2(3)=0.932$ ,  $p=0.334$ ; CFI=1.000, RMSEA=0.000, SRMR=0.033. Results based on  $n=67$ . Exploratory model 10a:  $\chi^2(3)=1.292$ ,  $p=0.863$ ; CFI=1.000, RMSEA=0.000, SRMR=0.038. Results based on  $n=67$ . Exploratory model 11a:  $\chi^2(3)=0.684$ ,  $p=0.408$ ; CFI=1.000, RMSEA=0.000, SRMR=0.025. Results based on  $n=67$ . Exploratory model 12a:  $\chi^2(3)=2.060$ ,  $p=0.725$ ; CFI=1.000, RMSEA=0.000, SRMR=0.049. Results based on  $n=67$ . Results based on  $n=66$ . Exploratory model 14a:  $\chi^2(3)=1.939$ ,  $p=0.747$ ; CFI=1.000, RMSEA=0.000, SRMR=0.049. Results based on  $n=67$ . \* $p<0.05$ . \*\*\* $p<0.001$ .

†Model 13a (Exclusive breastfeeding duration → Snack and Candy intake → Executive functioning (BRIEF-P)) could not be fitted; therefore no parameter estimates could be produced.

Supplementary Table 7.6. Parameter Estimates and bootstrapped Confidence Intervals for Exploratory Models 9b, 10b, 11b, 13b, and 14b.<sup>†</sup>

	B	SE	Lower CI	Upper CI	
<b>Regression paths</b>		Exploratory model 9b: Exclusive breastfeeding duration → Vegetable intake → Executive functioning (REEF)			
Executive functioning (REEF)					
Exclusive breastfeeding duration	-1.959	1.530	-4.958	1.041	
Vegetable intake	0.379	0.586	-0.769	1.528	
Maternal educational level	3.239	2.258	-1.186	7.665	
Vegetable intake					
Exclusive breastfeeding duration	0.077	0.461	-0.826	0.981	
<b>Mediation effect</b>		0.029	0.173	-0.310	0.368
<b>Total effect</b>		1.310	2.446	-3.484	6.103
<b>Regression paths</b>		Exploratory model 10b: Breastfeeding cessation age → Vegetable intake → Executive functioning (REEF)			
Executive functioning (REEF)					
Breastfeeding cessation age	-0.202	0.341	-0.870	0.466	
Vegetable intake	0.369	0.596	-0.799	1.538	
Maternal educational level	3.087	2.215	-1.255	7.429	
Vegetable intake					
Breastfeeding cessation age	-0.006	0.108	-0.218	0.206	
<b>Mediation effect</b>		-0.014	0.047	-0.107	0.079
<b>Total effect</b>		2.870	2.157	-1.358	7.099
<b>Regression paths</b>		Exploratory model 11b: Exclusive breastfeeding duration → Fruit intake → Executive functioning (REEF)			
Executive functioning (REEF)					
Exclusive breastfeeding duration	-2.547	1.713	-5.905	0.812	
Fruit intake	0.443	0.381	-0.304	1.191	
Maternal educational level	3.732	2.257	-0.692	8.156	
Fruit intake					
Exclusive breastfeeding duration	1.263**	0.470	0.341	2.185	
<b>Mediation effect</b>		0.560	0.588	-0.592	1.712
<b>Total effect</b>		1.746	2.383	-2.925	6.417
<b>Regression paths</b>		Exploratory model 13b: Exclusive breastfeeding duration → Snacks and candy intake → Executive functioning (REEF)			
Executive functioning (REEF)					
Exclusive breastfeeding duration	-1.943	1.599	-5.077	1.192	
Snacks and candy intake	0.163	0.805	-1.415	1.740	
Maternal educational level	3.296	2.199	-1.015	7.606	
Fruit intake					

Supplementary Table 7.6. (continued).

Exclusive breastfeeding duration	-0.310	0.209	-0.720	0.100
<b>Mediation effect</b>	-0.050	0.251	-0.543	0.442
<b>Total effect</b>	1.303	2.367	-3.336	5.941
<hr/>				
<b>Regression paths</b>				
Executive functioning (REEF)				
Breastfeeding cessation age	-0.230	0.367	-0.949	0.488
Snack and Candy intake	0.274	0.784	-1.263	1.811
Maternal educational level	3.176	2.169	-1.075	7.426
Snack and candy intake				
Breastfeeding cessation age	-0.076	0.049	-0.172	0.020
<b>Mediation effect</b>	-0.021	0.062	-0.142	0.100
<b>Total effect</b>	2.924	2.097	-1.186	7.035

MLR estimator used to calculate parameter estimates, bootstrapping used to calculate bias-corrected confidence intervals. Exploratory model 9b:  $\chi^2(2)=0.859$ ,  $p=0.651$ ; CFI=1.000, RMSEA=0.000, SRMR=0.034. Results based on  $n=67$ . Exploratory model 10b:  $\chi^2(3)=0.204$ ,  $p=0.651$ ; CFI=1.000, RMSEA=0.000, SRMR=0.016. Results based on  $n=67$ . Exploratory model 11b:  $\chi^2(3)=0.791$ ,  $p=0.374$ ; CFI=1.000, RMSEA=0.000, SRMR=0.034. Results based on  $n=67$ . Exploratory model 13b:  $\chi^2(2)=0.720$ ,  $p=0.698$ ; CFI=1.000, RMSEA=0.000, SRMR=0.032. Results based on  $n=67$ . Exploratory model 14b:  $\chi^2(3)=0.019$ ,  $p=0.889$ ; CFI=1.000, RMSEA=0.000, SRMR=0.005. Results based on  $n=67$ . \*\* $p<0.01$ .

†Model 12b (Breastfeeding cessation age → Fruit intake → Executive functioning (REEF)) could not be fitted; therefore no parameter estimates were produced.

## Supplementary materials of chapter 3

Supplementary Table 7.7. Associations between HMOs and HMO groups and measures of executive functioning including partially breastfed infants.

		Estimate (95% CI)	Standard error	p-value
<b>BRIEF-P</b>				
Model 1	Intercept	65.07 (40.01 - 90.12)***	12.52	0.00
	2'FL	-0.78 (-2.66 - 1.10)	0.94	0.41
	6'SL	-22.34 (-63.77 - 19.08)	20.69	0.28
	3'SL	34.57 (-11.013 - 80.15)	22.77	0.13
	BRIEF-A	0.20 (0.006 - 0.40)*	0.10	0.04
<b>REEF</b>				
Model 1	Intercept	166.97 (132.28 - 201.66)	17.34	0.00
	2'FL	3.87 (-0.19 - 7.93)†	2.03	0.06
	6'SL	-40.99 (-130.72 - 48.74)	44.84	0.36
	3'SL	1.18 (-97.01 - 99.36)	49.07	0.98
<b>Inhibitory control</b>				
Model 1	Intercept	1.01 (0.22 - 1.80)	0.40	0.01
	2'FL	0.01 (-0.05 - 0.07)	0.03	0.75
	6'SL	-0.94 (-2.25 - 0.37)	0.65	0.16
	3'SL	0.88 (-0.55 - 2.32)	0.72	0.22
	BRIEF-A	-0.01 (-0.01 - -0.002)*	0.003	0.01
<b>REEF</b>				
Model 2	Intercept	88.35 (-39.60 - 216.30)	63.97	0.17
	Fucosylated HMOs	2.19 (-0.44 - 4.82)	1.31	0.10
	Sialylated HMOs	1.94 (-29.79 - 33.67)	15.86	0.90
<b>Inhibitory control</b>				
Model 2	Intercept	1.54 (-0.57 - 3.65)	1.05	0.15
	Fucosylated HMOs	0.02 (-0.02 - 0.06)	0.02	0.29
	Sialylated HMOs	-0.27 (-0.73 - 0.19)	0.23	0.24
	BRIEF-A	-0.01 (-0.01 - -0.002)*	0.003	0.01

Note that the analyses were performed on data including partially breastfed infants,  $n=63$ . The REEF models did not include confounders as none of the potential confounders correlated with the REEF. The BRIEF-P is reverse coded to correspond with the other executive functions and inhibition measures (i.e., higher BRIEF-P scores indicate better executive functions). All HMOs and HMO groups mentioned in this table are presented as the Area Under the Curve.

† $p<0.1$ , \* $p<0.05$ , \*\*\* $p<0.001$ .

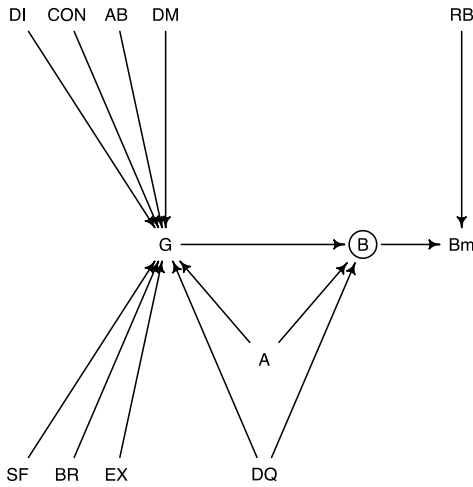
Supplementary Table 7.8. Multiple logistic regression results between the HMOs and HMO groups and the BRIEF-P including partially breastfed infants.

		Estimate (95% CI)	Standard error	p-value
<b>BRIEF-P</b>				
Model 1	Intercept	-2.79 (-7.51 -1.51)	2.25	0.23
	2'FL	-0.03 (-0.63 -0.47)	0.26	0.27
	6'SL	-10.36 (-26.00 - 1.86)	6.80	0.65
	3'SL	-12.84 (-44.72 - 11.80)	13.73	0.54
	BRIEF-A	0.03 (-0.02 - 0.10)	0.03	0.14
<b>BRIEF-P</b>				
Model 2	Intercept	3.31 (-10.17 -17.88)	6.97	0.64
	Fucosylated HMOs	-0.04 (-0.42 - 0.27)	0.16	0.27
	Sialylated HMOs	-1.16 (-7.71 - 5.07)	3.14	0.61
	BRIEF-A	0.03 (-0.01 - 0.09)	0.02	0.17

Note that the analyses were performed on data including partially breastfed infants,  $n=63$ . All HMOs and HMO groups mentioned in this table are presented as the Area Under the Curve. BRIEF-P coded as: 1, representing the high executive functions group and 0, representing the low executive functions group. Hence, positive values indicate a positive association between higher levels of HMOs and high executive functions.

## Supplementary materials of chapter 4

Gut microbiota → behaviour



**G:** relative abundance of the gut microbiota

**B:** behavioural score of problem behaviour, cognition  
and inhibitory control at age three (with missing values)

Bm: behavioural score of problem behaviour, cognition  
and inhibitory control at age three (without missing values)

RB: reasons for missingness

A: child age

DQ: dietary quality at age three

DI: diarrhea in the past one year

CON: constipation in the past one year

AB: antibiotic treatment in the past one year

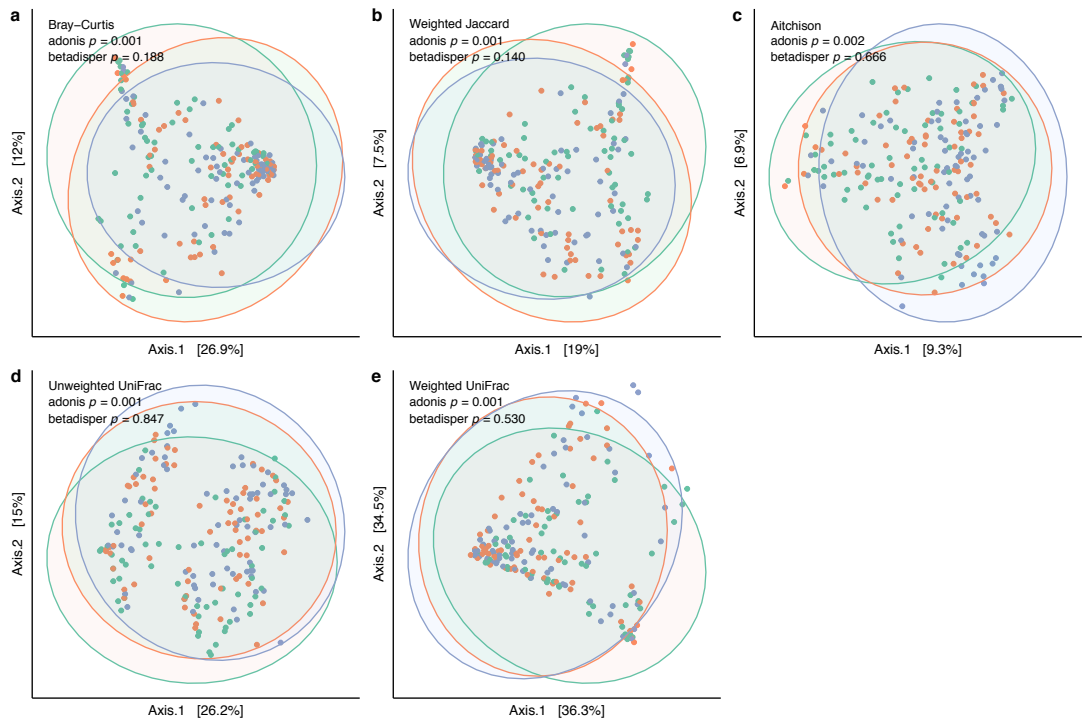
DM: delivery mode

SF: the first time when solid food was introduced

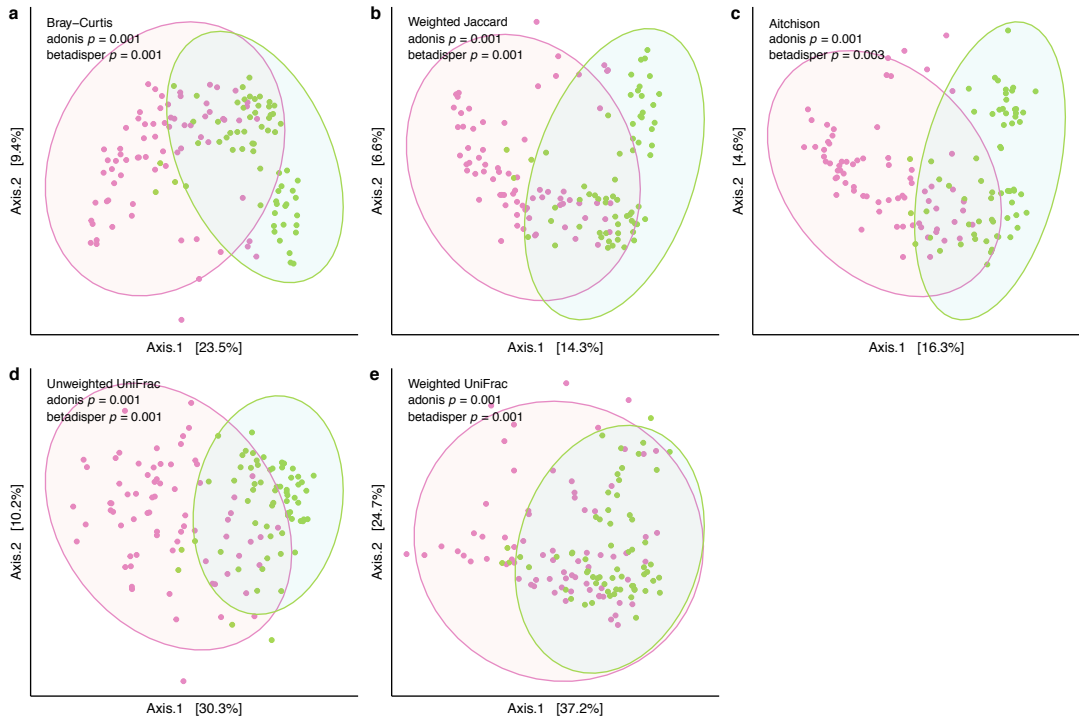
BR: breastfeeding duration

EX: exclusive breastfeeding duration

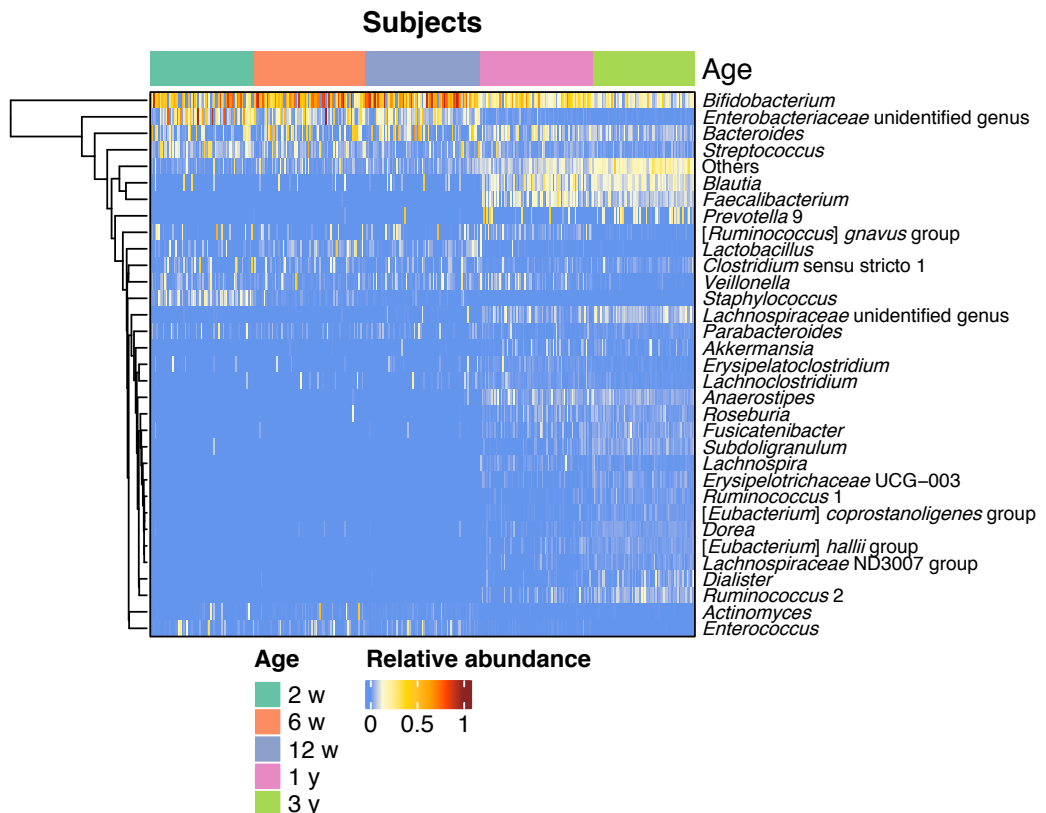
Supplementary Figure 7.1. Directed Acyclic Graph for determining confounders. Colors: black, predictors (G) and outcomes (B); grey, variables (Bm) and (RB) related to missingness; green, potential confounders that influence (G) and (B), including (A) and (DQ); orange, potential covariates of (G), including (DI), (CON), (AB), (DM), (SF), (BR), and (EX).



Supplementary Figure 7.2. Beta diversity of the gut microbiota at the age of two, six, and 12 weeks. (a-e) Principal coordinate plots of beta diversity, based on different pairwise dissimilarity (Bray-Curtis and weighted Jaccard) and distance (UniFrac and Aitchison) matrices, with points and ellipses colored by ages (Lake blue, two weeks; Orange, six weeks; Purple, 12 weeks).



Supplementary Figure 7.3. Beta diversity of the gut microbiota at the age of one and three years. (a-e) Principal coordinate plots of beta diversity, based on different pairwise dissimilarity (Bray-Curtis and weighted Jaccard) and distance (UniFrac and Aitchison) matrices, with points and ellipses colored by ages (Pink, one year; Grass green, three years).



Supplementary Figure 7.4. Heatmap showing relative abundances of the gut microbiota at the genus level over time. Bacteria with average relative abundances lower than 1% across the first three years, were assigned to 'Others'. Rows of bacteria were clustered based on Euclidean distance.

Supplementary Table 7.9. Kendall correlations between behavioural measures.

	CBCL (M) Internalizing	CBCL (M) Externalizing	CBCL (P) Internalizing	CBCL (P) Externalizing	SDQ (M) Internalizing	SDQ (M) Externalizing	SDQ (P) Internalizing	SDQ (P) Externalizing	BRIEF-P (M) Total Score	BRIEF-P (P) Total Score	REEF (M) Total Score	REEF (P) Total Score	Flanker	Gift Wrap	Gift Delay
(M) CBCL Externalizing	0.49*	-													
(P) CBCL Internalizing	0.4*	0.21	-												
(P) CBCL Externalizing	0.32*	0.29*	0.54*	-											
(M) SDQ Internalizing	0.4*	0.12	0.21	0.14	-										
(M) SDQ Externalizing	0.14	0.39*	-0.02	0.22	0	-									
(P) SDQ Internalizing	0.3*	0.17	0.34*	0.24	0.31*	-0.06	-								
(P) SDQ Externalizing	0.11	0.26	0.16	0.35*	0.15	0.32*	0.18	-							
(M) BRIEF-P Total Score	0.44*	0.53*	0.27	0.24	0.2	0.29*	0.18	0.22	-						
(P) BRIEF-P Total Score	0.32*	0.21	0.38*	0.37*	0.27	0.21	0.38*	0.23	0.39*	-					
(M) REEF Total Score	-0.19	-0.27*	-0.21	-0.18	-0.1	-0.16	-0.09	0.03	-0.34*	-0.21	-				
(P) REEF Total Score	0.02	-0.19	-0.03	-0.23	-0.01	-0.34*	-0.09	-0.25	-0.13	-0.13	0.24	-			
Flanker	-0.01	0.02	-0.18	-0.02	0.08	0.01	0.04	0.09	0.01	-0.16	0.07	0.04	-		
Gift Wrap	-0.07	-0.03	0.06	0.05	0	-0.09	-0.09	0.17	0.02	0.01	0.15	0.1	0.05	-	
Gift Delay	0.06	0.02	0.15	0.29*	0.14	-0.17	0.22	0.2	0.01	0	0.18	0.07	0.19	0.11	-
Whisper	-0.06	-0.04	-0.1	-0.09	-0.01	-0.1	-0.21	-0.21	-0.14	-0.23	0.21	0.19	0.11	-0.04	0.25*

M, Mother; P, Partner; CBCL, the Child Behavioral Checklist; SDQ, the Strengths and Difficulties Questionnaire; BRIEF-P, Behavior Rating Inventory of Executive Functions - Preschool; REEF, Ratings of Everyday Executive Functioning. Note that increased internalizing and externalizing scores refer to more corresponding behavioural problems. A higher score on the BRIEF-P indicates worse executive functions while a higher score on the REEF indicates better executive functions. Higher scores on the four behavioural tasks mean better performances in inhibitory control. \* indicates a p-value lower than 0.05.

Supplementary Table 7.10. Reliability of parental questionnaires.

Filler	Questionnaire	Behaviour	$\omega_{\text{total}}$	Cronbach's $\alpha$
Mother	CBCL	Internalizing	IC	0.83
		Externalizing	0.92	-
	SDQ	Internalizing	0.65	-
		Externalizing	0.74	-
Partner	BRIEF-P	Executive functions	0.94	-
		Executive functions	IC	0.96
	REEF	Internalizing	IC	0.83
		Externalizing	0.84	-
Partner	SDQ	Internalizing	0.65	-
		Externalizing	0.72	-
	BRIEF-P	Executive functions	IC	0.95
		Executive functions	IC	0.95

IC indicates the estimate was incalculable. Due to better ability at assessing reliability,  $\omega_{\text{total}}$  values were used as the first important estimates in determining reliability. For those subscales and questionnaires with incalculable  $\omega_{\text{total}}$ , Cronbach's  $\alpha$  values were computed as alternatives. All estimates were above 0.65, of which most of estimates were higher than 0.7, indicating good reliability of the scales.

Supplementary Table 7.11. Proportion of missing values in problem behaviour and executive functions.

	Proportion of missing values (%)				
	2w	6w	12w	1y	3y
CBCL Internalizing (M)	16.7	14.3	13.7	12.5	3.1
CBCL Externalizing (M)	16.7	14.3	13.7	12.5	3.1
SDQ Internalizing (M)	16.7	14.3	13.7	12.5	3.1
SDQ Externalizing (M)	16.7	14.3	13.7	12.5	3.1
BRIEF-P Total Score (M)	15.2	12.9	12.3	11.1	1.6
REEF Total Score (M)	16.7	14.3	13.7	12.5	3.1
Flanker	40.9	35.7	37	34.7	26.6
Whisper	19.7	17.1	17.8	15.3	6.2
Gift Wrap	21.2	20	19.2	16.7	6.2
Gift Delay	19.7	18.6	17.8	15.3	4.7

Notes. M, Mother; CBCL, the Child Behavioral Checklist; SDQ, the Strengths and Difficulties Questionnaire; BRIEF-P, Behavior Rating Inventory of Executive Functions - Preschool; REEF, Ratings of Everyday Executive Functioning.

Supplementary Table 7.12. Differentially abundant microbial taxa at the genus level over time with linear discriminant analysis (LDA) scores higher than 2.

Enriched age	Genus	LDA score
2 w	<i>Enterobacteriaceae</i> unidentified genus	4.93
2 w	<i>Streptococcus</i>	4.56
2 w	<i>Staphylococcus</i>	4.43
2 w	[ <i>Ruminococcus</i> ] <i>gnavus</i> group	4.3
2 w	<i>Enterococcus</i>	4.1
2 w	<i>Clostridium sensu stricto</i> 1	3.99
2 w	<i>Parabacteroides</i>	3.84
2 w	<i>Finegoldia</i>	2.49
2 w	<i>Negativicoccus</i>	2.3
6 w	<i>Lactobacillus</i>	4.31
6 w	<i>Actinomyces</i>	3.99
6 w	<i>Hungatella</i>	3.42
6 w	<i>Megasphaera</i>	3.4
6 w	<i>Candidatus Stoquefichus</i>	2.5
6 w	<i>Halomonas</i>	2.49
6 w	<i>Aeribacillus</i>	2.12
12 w	<i>Bifidobacterium</i>	5.3
12 w	<i>Bacteroides</i>	4.54
12 w	<i>Rothia</i>	2.85
12 w	<i>Varibaculum</i>	2.85
12 w	<i>Ruminiclostridium</i>	2.15
1 y	<i>Faecalibacterium</i>	4.69
1 y	<i>Anaerostipes</i>	4.32
1 y	<i>Veillonella</i>	4.23
1 y	<i>Akkermansia</i>	4.01
1 y	<i>Lachnospiraceae</i>	3.79
1 y	<i>Erysipelatoclostridium</i>	3.77
1 y	<i>Lachnospira</i>	3.75
1 y	[ <i>Eubacterium</i> ] <i>elicens</i> group	3.55
1 y	<i>Prevotella</i> 2	3.38
1 y	[ <i>Clostridium</i> ] <i>innocuum</i> group	3.38
1 y	<i>Flavonifractor</i>	3.2
1 y	<i>Sutterella</i>	3.16
1 y	<i>Tyzzerella</i> 4	3.09
1 y	<i>Lachnospiraceae</i> UCG-004	3.08
1 y	<i>Eggerthella</i>	2.98
1 y	<i>Parasutterella</i>	2.97
1 y	<i>Clostridioides</i>	2.67
1 y	<i>Tyzzerella</i> 3	2.6
1 y	CAG:352	2.54
1 y	<i>Lactococcus</i>	2.48

Supplementary Table 7.12 (continued).

3 y	<i>Blautia</i>	4.78
3 y	<i>Prevotella</i> 9	4.56
3 y	<i>Ruminococcus</i> 2	4.31
3 y	<i>Fusicatenibacter</i>	4.09
3 y	<i>Roseburia</i>	4.08
3 y	<i>Subdoligranulum</i>	4.06
3 y	<i>Dialister</i>	4.03
3 y	[ <i>Eubacterium</i> ] <i>hallii</i> group	3.88
3 y	<i>Erysipelotrichaceae</i> UCG-003	3.87
3 y	<i>Dorea</i>	3.85
3 y	<i>Lachnospiraceae</i> ND3007 group	3.79
3 y	<i>Ruminococcus</i> 1	3.74
3 y	<i>Lachnospiraceae</i> NK4A136 group	3.65
3 y	<i>Intestinibacter</i>	3.65
3 y	[ <i>Eubacterium</i> ] <i>coprostanoligenes</i> group	3.65
3 y	[ <i>Ruminococcus</i> ] <i>torques</i> group	3.58
3 y	<i>Ruminococcaceae</i> UCG-002	3.53
3 y	<i>Alistipes</i>	3.5
3 y	uncultured genus	3.49
3 y	<i>Christensenellaceae</i> R-7 group	3.45
3 y	<i>Romboutsia</i>	3.42
3 y	<i>Phascolarctobacterium</i>	3.41
3 y	<i>Butyrivibacter</i>	3.4
3 y	<i>Coprococcus</i> 2	3.4
3 y	uncultured bacterium	3.35
3 y	[ <i>Ruminococcus</i> ] <i>gauvreauii</i> group	3.33
3 y	<i>Barnesiella</i>	3.26
3 y	<i>Coprococcus</i> 3	3.25
3 y	<i>Prevotella</i> 7	3.2
3 y	<i>Senegaliimassilia</i>	3.14
3 y	<i>Coprococcus</i> 1	3.06
3 y	<i>Ruminococcaceae</i> UCG-013	3.02
3 y	<i>Holdemanella</i>	2.99
3 y	<i>Paraprevotella</i>	2.99
3 y	<i>Terrisporobacter</i>	2.98
3 y	[ <i>Eubacterium</i> ] <i>ventriosum</i> group	2.98
3 y	<i>Ruminococcaceae</i> NK4A214 group	2.94
3 y	<i>Sarcina</i>	2.93
3 y	<i>Ruminococcaceae</i> UCG-005	2.93
3 y	<i>Sellimonas</i>	2.9
3 y	[ <i>Eubacterium</i> ] <i>ruminantium</i> group	2.81
3 y	<i>Lachnospiraceae</i> UCG-001	2.81
3 y	<i>Ruminiclostridium</i> 6	2.8

Supplementary Table 7.12 (continued).

3 y	<i>Lachnospiraceae</i> FCS020 group	2.78
3 y	<i>Ruminococcaceae</i> UCG-014	2.76
3 y	<i>Ruminococcaceae</i> UCG-004	2.75
3 y	<i>Adlercreutzia</i>	2.67
3 y	<i>Lachnospiraceae</i> UCG-003	2.64
3 y	CAG:56	2.63
3 y	[ <i>Eubacterium</i> ] <i>xylanophilum</i> group	2.63
3 y	<i>Alloprevotella</i>	2.62
3 y	<i>Gordonibacter</i>	2.54
3 y	<i>Ruminiclostridium</i> 5	2.53
3 y	<i>Ruminococcaceae</i> UCG-003	2.52
3 y	<i>Turicibacter</i>	2.51
3 y	<i>Butyrivibrio</i>	2.5
3 y	Family XIII AD3011 group	2.45
3 y	<i>Odoribacter</i>	2.4
3 y	<i>Mollicutes</i> RF39 uncultured bacterium	2.4
3 y	<i>Oscillibacter</i>	2.36
3 y	<i>Anaeroplasma</i>	2.23
3 y	<i>Methanobrevibacter</i>	2.22
3 y	<i>Marvinbryantia</i>	2.15
3 y	<i>Butyricimonas</i>	2.1
3 y	<i>Ruminiclostridium</i> 9	2.09

Supplementary Table 7.13. Pearson correlations between actual and predicted results from random forest models.

Behaviour at age three	Age of the gut microbiota	Median of Pearson correlation coefficient	Permutation p-value	Adjusted permutation p-value
CBCL Internalizing (M)	2w	0.04	0.91	1.00
	6w	0.05	0.87	1.00
	12w	0.02	0.96	1.00
	1y	-0.09	0.80	1.00
	3y	-0.16	0.59	1.00
	2w	0.00	0.99	1.00
CBCL Externalizing (M)	6w	-0.33	0.32	1.00
	12w	0.13	0.71	1.00
	1y	0.09	0.78	1.00
	3y	-0.11	0.73	1.00
	2w	0.05	0.88	1.00
	6w	-0.03	0.91	1.00
SDQ Internalizing (M)	12w	0.28	0.37	1.00
	1y	-0.16	0.67	1.00
	3y	0.06	0.85	1.00
	2w	0.05	0.88	1.00
	6w	-0.29	0.37	1.00
	12w	0.10	0.78	1.00
SDQ Externalizing (M)	1y	0.02	0.94	1.00
	3y	0.14	0.67	1.00
	2w	0.12	0.70	1.00
	6w	0.07	0.85	1.00
	12w	0.10	0.77	1.00
	1y	0.06	0.82	1.00
BRIEF-P Total Score (M)	3y	-0.09	0.76	1.00
	2w	-0.15	0.65	1.00
	6w	-0.07	0.84	1.00
	12w	-0.15	0.66	1.00
	1y	-0.01	0.99	1.00
	3y	-0.11	0.74	1.00
REEF Total Score (M)	2w	-0.07	0.83	1.00
	6w	0.32	0.32	1.00
	12w	0.07	0.84	1.00
	1y	-0.17	0.63	1.00
	3y	0.07	0.83	1.00
	2w	0.09	0.82	1.00
Whisper	6w	-0.06	0.88	1.00
	12w	0.23	0.52	1.00
	1y	0.28	0.37	1.00
	3y	-0.03	0.93	1.00
	2w	0.02	0.94	1.00
	6w	0.25	0.39	1.00
Gift Wrap	12w	0.14	0.67	1.00

Supplementary Table 7.13 (continued).

	1y	-0.02	0.93	1.00
	3y	-0.37	0.23	1.00
Gift Delay	2w	-0.15	0.56	1.00
	6w	-0.09	0.89	1.00
	12w	0.00	1.00	1.00
	1y	0.32	0.32	1.00
	3y	0.04	0.91	1.00

N=1000 permutation tests were performed. FDR adjustments were conducted to the *p*-values.

Supplementary Table 7.14. Microbial taxa and alpha diversity with confident age-stratified relations to behavioural measures and taxa prevalence over time.

Type	Behaviour at age three	Taxa or alpha diversity	Prevalence at 2w	Prevalence at 6w	Prevalence at 12w	Prevalence at 1y	Prevalence at 3y	Prevalence >10% at all ages	Prevalence >10% only at the first three ages	Prevalence >10% only at the last two ages
genus	CBCL Internalizing	<i>Barnesiella</i>	0	1	0	7	50	no	no	no
genus	CBCL Internalizing	<i>Intestinibacter</i>	0	9	16	78	88	no	no	no
genus	CBCL Externalizing	<i>Barnesiella</i>	0	1	0	7	50	no	no	no
genus	CBCL Externalizing	<i>Butyrivibacoccus</i>	0	0	3	56	89	no	no	yes
genus	CBCL Externalizing	<i>Clostridium sensu stricto 1</i>	33	50	44	62	83	yes	no	no
genus	CBCL Externalizing	<i>Parabacteroides</i>	35	34	36	44	83	yes	no	no
genus	CBCL Externalizing	<i>Streptococcus</i>	94	93	88	90	88	yes	no	no
genus	SDQ Internalizing	[ <i>Ruminococcus</i> ] <i>torques</i> group	5	6	4	32	84	no	no	yes
genus	SDQ Internalizing	<i>Bifidobacterium</i>	79	87	93	99	100	yes	no	no
genus	SDQ Internalizing	<i>Blautia</i>	6	11	14	90	100	no	no	no
genus	SDQ Internalizing	<i>Ruminococcus 2</i>	0	0	0	39	94	no	no	yes
genus	SDQ Internalizing	<i>Sutterella</i>	8	10	12	46	61	no	no	no
genus	SDQ Externalizing	<i>Bifidobacterium</i>	79	87	93	99	100	yes	no	no
genus	SDQ Externalizing	<i>Butyrivibacoccus</i>	0	0	3	56	89	no	no	yes
genus	SDQ Externalizing	<i>Enterobacteriaceae</i> unidentified genus	89	93	97	68	31	yes	no	no
genus	SDQ Externalizing	<i>Halomonas</i>	12	11	12	0	0	no	yes	no
genus	SDQ Externalizing	<i>Oscillibacter</i>	0	0	0	4	22	no	no	no
genus	SDQ Externalizing	<i>Parabacteroides</i>	35	34	36	44	83	yes	no	no
genus	BRIEF-P	<i>Blautia</i>	6	11	14	90	100	no	no	no
genus	BRIEF-P	<i>Clostridium sensu stricto 1</i>	33	50	44	62	83	yes	no	no
genus	BRIEF-P	<i>Halomonas</i>	12	11	12	0	0	no	yes	no
genus	BRIEF-P	<i>Intestinibacter</i>	0	9	16	78	88	no	no	no
genus	BRIEF-P	<i>Ruminococcus 2</i>	0	0	0	39	94	no	no	yes
genus	BRIEF-P	<i>Streptococcus</i>	94	93	88	90	88	yes	no	no
genus	REEF	[ <i>Ruminococcus</i> ]	5	6	4	32	84	no	no	yes

Supplementary Table 7.14. (continued).

Supplementary Table 7.15. The multilevel Bayesian results of selected genera and alpha diversity with behavioural measures.

Behaviour at age three	Taxa or alpha diversity	Age of the gut microbiota	Rhat <1.01	Estimate	Estimate error	95% CI	95% CI excluding 0
CBCL Externalizing	<i>Clostridium sensu stricto</i> 1	2w, 6w, 12w, 1y, 3y	yes	0	0	[-0.01, 0.01]	no
CBCL Externalizing	<i>Parabacteroides</i>	2w, 6w, 12w, 1y, 3y	no	-	-	-	-
CBCL Externalizing	<i>Streptococcus</i>	2w, 6w, 12w, 1y, 3y	yes	0.03	0.02	[0, 0.07]	no
SDQ Internalizing	<i>Bifidobacterium</i>	2w, 6w, 12w, 1y, 3y	yes	0.09	0.07	[-0.04, 0.22]	no
SDQ Externalizing	<i>Bifidobacterium</i>	2w, 6w, 12w, 1y, 3y	yes	-0.04	0.07	[-0.17, 0.09]	no
SDQ Externalizing	<i>Enterobacteriaceae</i> unidentified genus	2w, 6w, 12w, 1y, 3y	yes	0.01	0.01	[-0.01, 0.03]	no
SDQ Externalizing	<i>Parabacteroides</i>	2w, 6w, 12w, 1y, 3y	no	-	-	-	-
BRIEF-P	<i>Clostridium sensu stricto</i> 1	2w, 6w, 12w, 1y, 3y	yes	0	0	[0, 0.01]	no
BRIEF-P	<i>Streptococcus</i>	2w, 6w, 12w, 1y, 3y	yes	0.05	0.02	[0.02, 0.09]	yes
REEF	<i>Parabacteroides</i>	2w, 6w, 12w, 1y, 3y	no	-	-	-	-
Flanker	<i>Bacteroides</i>	2w, 6w, 12w, 1y, 3y	no	-	-	-	-
Gift Wrap	<i>Veillonella</i>	2w, 6w, 12w, 1y, 3y	yes	0.01	0	[0, 0.02]	no
CBCL Internalizing	Chao1	2w, 6w, 12w, 1y, 3y	yes	-0.01	0.02	[-0.06, 0.04]	no
REEF	Chao1	2w, 6w, 12w, 1y, 3y	yes	0.04	0.03	[-0.01, 0.09]	no
Gift Wrap	Chao1	2w, 6w, 12w, 1y, 3y	yes	0.02	0.03	[-0.03, 0.07]	no
Gift Wrap	PD	2w, 6w, 12w, 1y, 3y	yes	0.05	0.03	[-0.01, 0.12]	no
CBCL Externalizing	<i>Parabacteroides</i>	2w, 6w, 12w	no	-	-	-	-
SDQ Externalizing	<i>Halomonas</i>	2w, 6w, 12w	no	-	-	-	-
SDQ Externalizing	<i>Parabacteroides</i>	2w, 6w, 12w	no	-	-	-	-
BRIEF-P	<i>Halomonas</i>	2w, 6w, 12w	no	-	-	-	-
REEF	<i>Halomonas</i>	2w, 6w, 12w	no	-	-	-	-
REEF	<i>Parabacteroides</i>	2w, 6w, 12w	no	-	-	-	-
Flanker	<i>Bacteroides</i>	2w, 6w, 12w	yes	0.01	0.01	[-0.01, 0.03]	no
CBCL Externalizing	<i>Butyrivibrio</i>	1y, 3y	yes	-0.01	0.08	[-0.17, 0.15]	no
CBCL Externalizing	<i>Parabacteroides</i>	1y, 3y	no	-	-	-	-
SDQ Internalizing	[ <i>Ruminococcus</i> ] torques group	1y, 3y	yes	-0.22	0.07	[-0.35, -0.07]	yes
SDQ Internalizing	<i>Ruminococcus</i> 2	1y, 3y	yes	-0.1	0.08	[-0.26, 0.05]	no
SDQ Externalizing	<i>Butyrivibrio</i>	1y, 3y	yes	-0.09	0.09	[-0.25, 0.08]	no
SDQ Externalizing	<i>Parabacteroides</i>	1y, 3y	yes	-0.04	0.03	[-0.09, 0.02]	no
BRIEF-P	<i>Ruminococcus</i> 2	1y, 3y	yes	-0.11	0.08	[-0.25, 0.04]	no
REEF	[ <i>Ruminococcus</i> ] torques group	1y, 3y	yes	-0.05	0.08	[-0.21, 0.09]	no
REEF	<i>Parabacteroides</i>	1y, 3y	yes	-0.01	0.03	[-0.06, 0.05]	no
Flanker	<i>Anaerostipes</i>	1y, 3y	yes	-0.05	0.09	[-0.23, 0.11]	no

Supplementary Table 7.15. (continued).

Flanker	<i>Bacteroides</i>	1y, 3y	yes	-0.07	0.08	[-0.23, 0.08]	no
Flanker	<i>Ruminococcaceae UCG-013</i>	1y, 3y	yes	0.1	0.1	[-0.09, 0.29]	no
Flanker	<i>Subdoligranulum</i>	1y, 3y	no	-	-	-	-
Gift Wrap	<i>Coprococcus 3</i>	1y, 3y	no	-	-	-	-
Gift Wrap	<i>Lachnospiraceae NK4A136 group</i>	1y, 3y	yes	-0.07	0.05	[-0.17, 0.01]	no
Gift Wrap	<i>Subdoligranulum</i>	1y, 3y	yes	-0.03	0.06	[-0.16, 0.06]	no

Notes. Multilevel Bayesian linear regression models were performed on taxa and alpha diversity over time. Relations in grey rows are confident with 95% CI excluding zero. Chains were regarded converged when Rhat values lower than 1.01. Models that did not meet the Rhat criteria under current settings were not considered in the present study. Given that *Parabacteroides* and *Bacteroides* did not meet the Rhat requirement in the pooled data of all five ages, we did extra trajectory analyses for them after splitting the data into two periods (2w, 6w, and 12w; 1y and 3y; grey coloured text).

Supplementary Table 7.16. Overview of the associations in our study in comparison with findings reported in literature.

Microbial taxa and alpha diversity	In the present study	Literature about problem behaviour or executive functions and inhibitory control	Other literature with similar findings	Other literature with divergent findings	Potential mechanisms
↑ <i>Parabacteroides</i> (2w)	↓ Externalizing behaviour ↑ Executive functions	NF	↓ <i>Parabacteroides</i> in children with ASD (?) (?) ↓ <i>Parabacteroides</i> in ADHD (?)	↑ <i>Parabacteroides</i> in children with ASD (?)	GABA
↑ <i>Parabacteroides</i> (1y)	↓ Externalizing behaviour	NF			
↑ <i>Ruminococcus</i> 2 (1y)	↓ Internalizing behaviour ↑ Executive functions	NF	↓ <i>Ruminococcus</i> 2 in MDD patients (?) (?)	↑ <i>Ruminococcaceae</i> in ADHD patients, and inattention (?)	Tryptophan/serotonin
↑ [Ruminococcus] <i>Torques</i> group (3y)	↓ Executive functions	NF			
↑ <i>Barnesiella</i> (3y)	↑ Internalizing and externalizing behaviour	NF	↑ <i>Barnesiella</i> in (constipated) ASD (?) (?)	↓ <i>Barnesiella</i> in ASD (?)	GABA
↑ <i>Butyrivibrio</i> (1y)	↓ Externalizing behaviour	NF	↑ <i>Butyrivibrio</i> in constipated ASD vs non-constipated ASD (?)		Butyrate
↑ <i>Butyrivibrio</i> (3y)	↑ Externalizing behaviour	NF	↓ <i>Butyrivibrio</i> in ASD (?)		
↑ <i>Streptococcus</i> (2w)	↑ Externalizing behaviour ↓ Executive	NF	↑ <i>Streptococcus</i> in ASD (?) ↑ <i>Streptococcus</i> in Bipolar disorder		GABA and tryptophan

Supplementary Table 7.16. (continued).

	functions	(?)			
↑ <i>Streptococcus</i> (12w)	↓ Executive functions	NF			
↑ <i>Clostridium sensu stricto</i> 1 (1y)	↑ Externalizing behaviour ↓ Executive functions	↑ <i>Clostridium</i> at 2.5 months with higher attention (?)	↑ <i>Clostridium</i> in ASD (?) (?)		Neurotoxins
↑ <i>Intestinibacter</i> (12w)	↑ Internalizing behaviour ↓ Executive functions	NF	↑ <i>Intestinibacter bartlettii</i> in children with neurodevelopmental disorders (?)		Neurotoxins
↑ <i>Bifidobacterium</i> (3y)	↑ Internalizing behaviour ↑ Externalizing behaviour	NF	↑ <i>Bifidobacterium</i> in MDD patients (?)	↓ <i>Bifidobacterium</i> in ASD (?) ↑ <i>Bifidobacterium</i> less ASD symptoms (?) ↓ <i>Bifidobacterium</i> in MDD patients (?) ↑ <i>Bifidobacterium longus</i> positive on ADHD (?) (?)	GABA, dopamine, and noradrenaline
↑ <i>Blautia</i> (3y)	↓ Internalizing behaviour ↑ Executive functions	NF	↓ <i>Blautia</i> in ASD patients (?)	↑ <i>Blautia</i> in MDD (?) ↑ <i>Blautia</i> with worse ADHD symptoms (?)	NF
↑ <i>Halomonas</i> (6w)	↑ Externalizing behaviour ↓ Executive functions	NF	↑ <i>Halomonas</i> in Alzheimers (?)		GABA and tryptophan

Supplementary Table 7.16. (continued).

↑ <i>Bacteroides</i> (6w)	↑ Inhibitory control	↑ <i>Bacteroides</i> with better cognition at 2 years (?) (?)		GABA
↑ <i>Subdoligranulum</i> (1y and 3y)	↓ Inhibitory control	NF	↓ <i>Subdoligranulum</i> in patients with anxiety (?)	NF
↑ <i>Anaerostipes</i> (1y)	↓ Inhibitory control	NF	↓ <i>Anaerostipes</i> in children with autism (?)	Butyrate
↑ <i>Lachnospiraceae</i> NK4A136 (1y)	↓ Inhibitory control	NF		NF
↑ <i>Ruminococcaceae</i> UCG-013 (1y)	↑ Inhibitory control	NF		NF
↑ <i>Sutterella</i> (1y)	↓ Inhibitory control	↑ <i>Sutterella</i> with better cognition at age three years (?)	↑ <i>Sutterella</i> in children with autism (?) (?)	NF
↑ <i>Coprococcus</i> 3 (1y)	↓ Inhibitory control	NF	↑ <i>Coprococcus</i> 3 in healthy patients compared to patients with anxiety disorder (?)	Tryptophan
↑ <i>Veillonella</i> (1y)	↑ Inhibitory control	↑ <i>Veillonella</i> with better cognition at five years (?)		Immune system, interleukin pathways
↑ Alpha diversity (2w)	↓ Internalizing behaviour	↑ Alpha diversity with less internalizing behaviour in boys (?)	↓ alpha diversity in ASD children (?) (??)  ↓ Alpha diversity in children above the clinical threshold for internalizing behaviour	No difference in alpha diversity between ASD patients and healthy controls (?)  GABA and norepinephrine

Supplementary Table 7.16. (continued).

↑ Executive functions	(?) ↑ alpha diversity and worse cognition (?)	↓ alpha diversity in ADHD (?)	No differences in alpha diversity between ADHD patients and healthy controls (?) (?) (?) (?)
-----------------------	---	----------------------------------	--

Notes. NF, Not Found (i.e., no comparable findings in the literature for behavioural problems or executive functions).

## **Supplementary materials of chapter 5**

Supplementary Table 7.17. Raw correlation coefficients between all measured variables.

	Sens 5w	Coop 5w	SP 12m	RA 12m	SP 2.5y	RA 2.5y	SP 10y	RA 10y	SP 14y	RA 14y	DQ	EE	BRIEF IC	GNG	STROOP
Sens 5w	-														
Coop 5w	0.86***	-													
SP 12m	0.17	0.10	-												
RA 12m	0.14	0.12	0.62***												
SP 2.5y	0.03	-0.01	0.06	-0.12	-										
RA 2.5y	0.05	-0.05	-0.04	-0.03	0.46***	-									
SP 10y	0.11	0.12	0.16	-0.01	0.15	0.14	-								
RA 10y	0.04	0.03	0.07	0.07	0.17*	0.19*	0.60***	-							
SP 14y	0.12	0.13	0.01	0.06	0.08	0.01	0.22*	0.20*	-						
RA 14y	0.15	0.14	0.08	0.19*	0.05	0.07	0.21*	0.18*	0.75***	-					
DQ	-0.05	-0.17*	-0.06	0.06	0.00	-0.02	-0.08	0.00	-0.04	-0.02	-				
EE	0.05	0.05	-0.05	-0.07	0.09	0.11	0.04	0.03	-0.07	-0.05	-0.03	-			
BRIEF IC	-0.07	-0.09	-0.08	-0.1	-0.11	0.02	-0.13	-0.11	-0.15	-0.09	-0.02	0.06	-		
GNG	0.21*	0.11	0.09	0.01	0.01	0.01	-0.03	-0.01	-0.01	0.06	-0.07	0.01	0.22**	-	
STROOP	-0.06	0.06	-0.20*	-0.14	0.05	0.00	-0.08	0.01	-0.08	-0.08	0.15	0.18*	-0.10	-0.15	-
Monetary Choice	0.04	0.09	-0.02	-0.13	0.00	0.06	0.06	0.03	-0.09	-0.15	-0.21*	0.00	-0.04	-0.04	-0.07

Sens = sensitivity, Coop = cooperation, SP = supportive presence, RA = respect for child autonomy, DQ = diet quality, EE = Emotional eating, BRIEF = Behavior Rating Inventory of Executive Functions, IC = inhibitory control, GNG = Go/No-Go. \* $p<0.05$ , \*\* $p<0.01$ , \*\*\* $p<0.001$ .

Supplementary Table 7.18. Mediation analyses estimates of model 1 and model 2 with diet quality as dependent variable.

Model description	Effect (beta)	SE	95% CI	
			LL	UL
<b>Model 1 Caregiving quality, IC BRIEF, Diet quality</b>				
Direct effect				
Caregiving quality 5w → Diet quality	-0.97	0.64	-2.22	0.29
Caregiving quality 12m → Diet quality	-0.20	1.15	-2.45	2.05
Caregiving quality 2.5y → Diet quality	-0.61	2.08	-4.68	3.46
Caregiving quality 10y → Diet quality	-0.97	1.40	-3.72	1.79
Caregiving quality 14y → Diet quality	-0.15	1.00	-2.10	1.81
IC BRIEF → Diet quality	-1.17	3.15	-7.34	4.99
Caregiving quality 5w → IC BRIEF	0.03	0.02	0.00	0.07
Caregiving quality 12m → IC BRIEF	0.00	0.03	-0.06	0.06
Caregiving quality 2.5y → IC BRIEF	0.03	0.06	-0.09	0.14
Caregiving quality 10y → IC BRIEF	-0.01	0.04	-0.08	0.07
Caregiving quality 14y → IC BRIEF	0.00	0.03	-0.05	0.06
Partial mediation				
Caregiving quality 5w → IC BRIEF → Diet quality	-0.04	0.10	-0.23	0.16
Caregiving quality 12m → IC BRIEF → Diet quality	0.00	0.04	-0.07	0.07
Caregiving quality 2.5y → IC BRIEF → Diet quality	-0.03	0.11	-0.24	0.18
Caregiving quality 10y → IC BRIEF → Diet quality	0.01	0.05	-0.09	0.11
Caregiving quality 14y → IC BRIEF → Diet quality	0.00	0.03	-0.07	0.06
Full mediation				
Caregiving quality 5w → IC BRIEF → Diet quality ← Caregiving quality 5w	-1.00	0.63	-2.24	0.24
Caregiving quality 12m → IC BRIEF → Diet quality ← Caregiving quality 12m	-0.20	1.15	-2.45	2.05
Caregiving quality 2.5y → IC BRIEF → Diet quality ← Caregiving quality 2.5y	-0.64	2.08	-4.70	3.43
Caregiving quality 10y → IC BRIEF → Diet quality ← Caregiving quality 10y	-0.96	1.40	-3.71	1.80
Caregiving quality 14y → IC BRIEF → Diet quality ← Caregiving quality 14y	-0.15	1.00	-2.11	1.80
<b>Model 2 Caregiving quality, IC composite, Diet quality</b>				
Direct effect				
Caregiving quality 5w → Diet quality	-0.88	0.58	-2.02	0.25
Caregiving quality 12m → Diet quality	-0.17	1.20	-2.52	2.18
Caregiving quality 2.5y → Diet quality	-1.18	1.94	-4.97	2.62
Caregiving quality 10y → Diet quality	-1.17	1.23	-3.58	1.23
Caregiving quality 14y → Diet quality	-0.51	0.86	-2.19	1.18
IC composite → Diet quality	5.22*	2.34	0.64	9.80
Caregiving quality 5w → IC composite	-0.04	0.02	-0.08	0.01
Caregiving quality 12m → IC composite	-0.06	0.04	-0.14	0.02
Caregiving quality 2.5y → IC composite	0.03	0.08	-0.12	0.18
Caregiving quality 10y → IC composite	-0.04	0.05	-0.13	0.06
Caregiving quality 14y → IC composite	0.00	0.04	-0.07	0.08
Partial mediation				

Supplementary Table 7.18. (continued).

Caregiving quality 5w → IC composite → Diet quality	-0.19	0.16	-0.50	0.11
Caregiving quality 12m → IC composite → Diet quality	-0.30	0.24	-0.78	0.18
Caregiving quality 2.5y → IC composite → Diet quality	0.15	0.39	-0.62	0.91
Caregiving quality 10y → IC composite → Diet quality	-0.20	0.26	-0.70	0.31
Caregiving quality 14y → IC composite → Diet quality	0.03	0.19	-0.35	0.40
<b>Full mediation</b>				
Caregiving quality 5w → IC composite → Diet quality	-1.08	0.59	-2.24	0.08
← Caregiving quality 5w				
Caregiving quality 12m → IC composite → Diet quality	-0.47	1.21	-2.84	1.90
← Caregiving quality 12m				
Caregiving quality 2.5y → IC composite → Diet quality	-1.03	1.97	-4.90	2.84
← Caregiving quality 2.5y				
Caregiving quality 10y → IC composite → Diet quality	-1.37	1.22	-3.76	1.01
← Caregiving quality 10y				
Caregiving quality 14y → IC composite → Diet quality	-0.48	0.89	-2.23	1.27
← Caregiving quality 14y				

Note that the BRIEF is reverse scored to align with our inhibitory control measures. Hence higher scores on the BRIEF indicate better inhibitory control. SE: Standard Effect, CI: Confidence interval, LL: Lower limit, UL: Upper limit, IC: Inhibitory control, BRIEF: Behavior Rating Inventory of Executive Functions, 5w: five weeks, 12m: 12 months, 2.5y: 2.5 years, 10y: 10 years, 14y: 14 years, \* $p<0.05$ .

Supplementary Table 7.19. Mediation analyses estimates of model 3 and model 4 with emotional eating as dependent variable.

Model description	Effect (beta)	SE	95% CI	
			LL	UL
<b>Model 3 Caregiving quality, IC BRIEF, Emotional Eating</b>				
Direct effect				
Caregiving quality 5w → Emotional Eating	0.25	0.33	-0.41	0.90
Caregiving quality 12m → Emotional Eating	-0.36	0.58	-1.49	0.77
Caregiving quality 2.5y → Emotional Eating	1.03	1.07	-1.07	3.13
Caregiving quality 10y → Emotional Eating	0.00	0.74	-1.45	1.46
Caregiving quality 14y → Emotional Eating	-0.78	0.53	-1.82	0.25
IC BRIEF → Emotional Eating	-0.17	1.68	-3.46	3.13
Caregiving quality 5w → IC BRIEF	0.03	0.02	0.00	0.06
Caregiving quality 12m → IC BRIEF	-0.01	0.03	-0.06	0.05
Caregiving quality 2.5y → IC BRIEF	0.02	0.05	-0.09	0.12
Caregiving quality 10y → IC BRIEF	-0.02	0.04	-0.09	0.05
Caregiving quality 14y → IC BRIEF	0.00	0.03	-0.05	0.05
Partial mediation				
Caregiving quality 5w → IC BRIEF → Emotional Eating	0.00	0.05	-0.10	0.09
Caregiving quality 12m → IC BRIEF → Emotional Eating	0.00	0.01	-0.02	0.03
Caregiving quality 2.5y → IC BRIEF → Emotional Eating	0.00	0.03	-0.06	0.05
Caregiving quality 10y → IC BRIEF → Emotional Eating	0.00	0.03	-0.06	0.06
Caregiving quality 14y → IC BRIEF → Emotional Eating	0.00	0.01	-0.01	0.01
Full mediation				
Caregiving quality 5w → IC BRIEF → Emotional Eating ← Caregiving quality 5w	0.24	0.33	-0.41	0.89
Caregiving quality 12m → IC BRIEF → Emotional Eating ← Caregiving quality 12m	-0.36	0.58	-1.49	0.77
Caregiving quality 2.5y → IC BRIEF → Emotional Eating ← Caregiving quality 2.5y	1.03	1.07	-1.07	3.13
Caregiving quality 10y → IC BRIEF → Emotional Eating ← Caregiving quality 10y	0.01	0.74	-1.44	1.46
Caregiving quality 14y → IC BRIEF → Emotional Eating ← Caregiving quality 14y	-0.78	0.53	-1.82	0.25
<b>Model 4 Caregiving quality, IC composite, Emotional Eating</b>				
Direct effect				
Caregiving quality 5w → Emotional Eating	0.29	0.33	-0.36	0.94
Caregiving quality 12m → Emotional Eating	-0.30	0.58	-1.43	0.83
Caregiving quality 2.5y → Emotional Eating	1.01	1.07	-1.08	3.10
Caregiving quality 10y → Emotional Eating	0.05	0.74	-1.40	1.50
Caregiving quality 14y → Emotional Eating	-0.79	0.53	-1.82	0.24
IC composite → Emotional Eating	1.33	1.29	-1.20	3.85
Caregiving quality 5w → IC composite	-0.04	0.02	-0.08	0.01

Supplementary Table 7.19. (continued).

Caregiving quality 12m → IC composite	-0.05	0.04	-0.12	0.03
Caregiving quality 2.5y → IC composite	0.02	0.07	-0.12	0.15
Caregiving quality 10y → IC composite	-0.03	0.05	-0.12	0.06
Caregiving quality 14y → IC composite	0.00	0.03	-0.06	0.07
Partial mediation				
Caregiving quality 5w → IC composite → Emotional Eating	-0.05	0.06	-0.16	0.06
Caregiving quality 12m → IC composite → Emotional Eating	-0.06	0.08	-0.22	0.09
Caregiving quality 2.5y → IC composite → Emotional Eating	0.02	0.09	-0.16	0.21
Caregiving quality 10y → IC composite → Emotional Eating	-0.04	0.08	-0.19	0.11
Caregiving quality 14y → IC composite → Emotional Eating	0.01	0.05	-0.08	0.10
Full mediation				
Caregiving quality 5w → IC composite → Emotional Eating ← Caregiving quality 5w	0.24	0.33	-0.41	0.89
Caregiving quality 12m → IC composite → Emotional Eating ← Caregiving quality 12m	-0.36	0.58	-1.49	0.77
Caregiving quality 2.5y → IC composite → Emotional Eating ← Caregiving quality 2.5y	1.03	1.07	-1.07	3.13
Caregiving quality 10y → IC composite → Emotional Eating ← Caregiving quality 10y	0.01	0.74	-1.44	1.46
Caregiving quality 14y → IC composite → Emotional Eating ← Caregiving quality 14y	-0.78	0.53	-1.82	0.25

Note that the BRIEF is reverse scored to align with our inhibitory control measures. Hence higher scores on the BRIEF indicate better inhibitory control. CI: Confidence interval, LL: Lower limit, UL: Upper limit, IC: Inhibitory control, BRIEF: Behavior Rating Inventory of Executive Functions, 5w: five weeks, 12m: 12 months, 2.5y: 2.5 years, 10y: 10 years, 14y: 14 years.

Supplementary Table 7.20. Mediation analyses estimates of Exploratory model 1, 2 and 3 with diet quality as dependent variable.

Model description	Effect (beta)	SE	95% CI	
			LL	UL
<b>Exploratory model 1 Caregiving quality, STROOP, Diet quality</b>				
Direct effect				
Caregiving quality 5w → Diet quality	-1.10	0.64	-2.36	0.1
Caregiving quality 12m → Diet quality	0.33	1.19	-2.00	2.66
Caregiving quality 2.5y → Diet quality	-0.73	2.11	-4.86	3.4
Caregiving quality 10y → Diet quality	-0.79	1.42	-3.58	2.0
Caregiving quality 14y → Diet quality	-0.31	1.01	-2.29	1.6
STROOP → Diet quality	0.28	0.22	-0.14	0.70
Caregiving quality 5w → STROOP	0.08	0.26	-0.43	0.59
Caregiving quality 12m → STROOP	-1.21*	0.47	-2.13	-0.29
Caregiving quality 2.5y → STROOP	0.61	0.85	-1.05	2.28
Caregiving quality 10y → STROOP	-0.03	0.58	-1.16	1.10
Caregiving quality 14y → STROOP	-0.22	0.41	-1.02	0.58
Partial mediation				
Caregiving quality 5w → STROOP → Diet quality	0.02	0.07	-0.12	0.17
Caregiving quality 12m → STROOP → Diet quality	-0.34	0.29	-0.91	0.23
Caregiving quality 2.5y → STROOP → Diet quality	0.17	0.27	-0.36	0.70
Caregiving quality 10y → STROOP → Diet quality	-0.01	0.16	-0.32	0.31
Caregiving quality 14y → STROOP → Diet quality	-0.06	0.12	-0.30	0.18
Full mediation				
Caregiving quality 5w → STROOP → Diet quality ← Caregiving quality 5w	-1.08	0.65	-2.35	0.19
Caregiving quality 12m → STROOP → Diet quality ← Caregiving quality 12m	-0.01	1.17	-2.30	2.28
Caregiving quality 2.5y → STROOP → Diet quality ← Caregiving quality 2.5y	-0.56	2.11	-4.70	3.59
Caregiving quality 10y → STROOP → Diet quality ← Caregiving quality 10y	-0.80	1.43	-3.60	2.01
Caregiving quality 14y → STROOP → Diet quality ← Caregiving quality 14y	-0.37	1.01	-2.36	1.62
<b>Exploratory Model 2 Caregiving quality, Go/No-Go, Diet quality</b>				
Direct effect				
Caregiving quality 5w → Diet quality	-1.01	0.66	-2.30	0.28
Caregiving quality 12m → Diet quality	0.00	1.17	-2.28	2.29
Caregiving quality 2.5y → Diet quality	-0.53	2.11	-4.67	3.61
Caregiving quality 10y → Diet quality	-0.81	1.43	-3.61	1.99
Caregiving quality 14y → Diet quality	-0.35	1.01	-2.33	1.64
Go/No-Go → Diet quality	-0.16	0.27	-0.70	0.37
Caregiving quality 5w → Go/No-Go	0.43*	0.21	0.03	0.84
Caregiving quality 12m → Go/No-Go	0.07	0.37	-0.66	0.80
Caregiving quality 2.5y → Go/No-Go	0.16	0.68	-1.17	1.48
Caregiving quality 10y → Go/No-Go	-0.07	0.46	-0.96	0.83
Caregiving quality 14y → Go/No-Go	0.16	0.32	-0.48	0.80
Partial mediation				

Supplementary Table 7.20. (continued).

Caregiving quality 5w → Go/No-Go → Diet quality	-0.07	0.12	-0.31	0.17
Caregiving quality 12m → Go/No-Go → Diet quality	-0.01	0.06	-0.14	0.11
Caregiving quality 2.5y → Go/No-Go → Diet quality	-0.03	0.12	-0.26	0.21
Caregiving quality 10y → Go/No-Go → Diet quality	0.01	0.08	-0.14	0.16
Caregiving quality 14y → Go/No-Go → Diet quality	-0.03	0.07	-0.16	0.11
<b>Full mediation</b>				
Caregiving quality 5w → Go/No-Go → Diet quality	-1.08	0.65	-2.35	0.19
← Caregiving quality 5w				
Caregiving quality 12m → Go/No-Go → Diet quality	-0.01	1.17	-2.30	2.28
← Caregiving quality 12m				
Caregiving quality 2.5y → Go/No-Go → Diet quality	-0.56	2.11	-4.70	3.59
← Caregiving quality 2.5y				
Caregiving quality 10y → Go/No-Go → Diet quality	-0.80	1.43	-3.60	2.01
← Caregiving quality 10y				
Caregiving quality 14y → Go/No-Go → Diet quality	-0.37	1.01	-2.36	1.62
← Caregiving quality 14y				
<b>Exploratory model 3 Caregiving quality, Monetary choice, Diet quality</b>				
<b>Direct effect</b>				
Caregiving quality 5w → Diet quality	-0.97	0.63	-2.21	0.28
Caregiving quality 12m → Diet quality	-0.24	1.15	-2.49	2.01
Caregiving quality 2.5y → Diet quality	-0.79	2.07	-4.85	3.27
Caregiving quality 10y → Diet quality	-0.43	1.41	-3.19	2.33
Caregiving quality 14y → Diet quality	-0.72	1.00	-2.69	1.25
Monetary choice → Diet quality	-5.51*	2.29	-10.01	-1.01
Caregiving quality 5w → Monetary choice	0.02	0.02	-0.03	0.07
Caregiving quality 12m → Monetary choice	-0.04	0.04	-0.13	0.04
Caregiving quality 2.5y → Monetary choice	-0.04	0.08	-0.20	0.11
Caregiving quality 10y → Monetary choice	0.07	0.05	-0.04	0.17
Caregiving quality 14y → Monetary choice	-0.06	0.04	-0.14	0.01
<b>Partial mediation</b>				
Caregiving quality 5w → Monetary choice → Diet quality	-0.12	0.14	-0.39	0.16
Caregiving quality 12m → Monetary choice → Diet quality	0.23	0.26	-0.27	0.74
Caregiving quality 2.5y → Monetary choice → Diet quality	0.23	0.44	-0.64	1.10
Caregiving quality 10y → Monetary choice → Diet quality	-0.37	0.33	-1.02	0.28
Caregiving quality 14y → Monetary choice → Diet quality	0.35	0.25	-0.15	0.85
<b>Full mediation</b>				
Caregiving quality 5w → Monetary choice → Diet quality ← Caregiving quality 5w	-1.08	0.65	-2.35	0.19
Caregiving quality 12m → Monetary choice → Diet quality ← Caregiving quality 12m	-0.01	1.17	-2.30	2.28
Caregiving quality 2.5y → Monetary choice → Diet quality ← Caregiving quality 2.5y	-0.56	2.11	-4.70	3.59

Supplementary Table 7.20. (continued).

Caregiving quality 10y → Monetary choice → Diet quality ← Caregiving quality 10y	-0.80	1.43	-3.60	2.01
Caregiving quality 14y → Monetary choice → Diet quality ← Caregiving quality 14y	-0.37	1.01	-2.36	1.62

SE: Standard Effect, CI: Confidence interval, LL: Lower limit, UL: Upper limit, 5w: five weeks, 12m: 12 months, 2.5y: 2.5 years, 10y: 10 years, 14y: 14 years, \* $p<0.05$ .

Supplementary Table 7.21. Mediation analyses estimates of Exploratory model 4, 5 and 6 with emotional eating as dependent variable.

Model description	Effect (beta)	SE	95% CI	
			LL	UL
<b>Exploratory model 4 Caregiving quality, STROOP, Emotional eating</b>				
Direct effect				
Caregiving quality 5w → Emotional eating	0.22	0.33	-0.42	0.87
Caregiving quality 12m → Emotional eating	-0.15	0.59	-1.30	1.00
Caregiving quality 2.5y → Emotional eating	0.97	1.06	-1.12	3.05
Caregiving quality 10y → Emotional eating	0.04	0.73	-1.40	1.48
Caregiving quality 14y → Emotional eating	-0.73	0.52	-1.75	0.30
STROOP → Emotional eating	0.16	0.11	-0.05	0.38
Caregiving quality 5w → STROOP	0.13	0.26	-0.37	0.63
Caregiving quality 12m → STROOP	-1.33*	0.45	-2.20	-0.46
Caregiving quality 2.5y → STROOP	0.32	0.83	-1.30	1.95
Caregiving quality 10y → STROOP	-0.11	0.57	-1.23	1.01
Caregiving quality 14y → STROOP	-0.26	0.40	-1.06	0.53
Partial mediation				
Caregiving quality 5w → STROOP → Emotional eating	0.02	0.04	-0.07	0.11
Caregiving quality 12m → STROOP → Emotional eating	-0.22	0.16	-0.53	0.10
Caregiving quality 2.5y → STROOP → Emotional eating	0.05	0.14	-0.22	0.33
Caregiving quality 10y → STROOP → Emotional eating	-0.02	0.09	-0.20	0.17
Caregiving quality 14y → STROOP → Emotional eating	-0.04	0.07	-0.18	0.10
Full mediation				
Caregiving quality 5w → STROOP → Emotional eating ← Caregiving quality 5w	0.25	0.33	-0.40	0.89
Caregiving quality 12m → STROOP → Emotional eating ← Caregiving quality 12m	-0.37	0.58	-1.50	0.76
Caregiving quality 2.5y → STROOP → Emotional eating ← Caregiving quality 2.5y	1.02	1.07	-1.08	3.12
Caregiving quality 10y → STROOP → Emotional eating ← Caregiving quality 10y	0.02	0.74	-1.43	1.48
Caregiving quality 14y → STROOP → Emotional eating ← Caregiving quality 14y	-0.77	0.53	-1.80	0.26
<b>Exploratory Model 5 Caregiving quality, Go/No-Go, Emotional eating</b>				
Direct effect				
Caregiving quality 5w → Emotional eating	0.24	0.34	-0.42	0.90
Caregiving quality 12m → Emotional eating	-0.36	0.58	-1.49	0.77
Caregiving quality 2.5y → Emotional eating	1.03	1.07	-1.07	3.13
Caregiving quality 10y → Emotional eating	0.01	0.74	-1.44	1.46
Caregiving quality 14y → Emotional eating	-0.79	0.53	-1.82	0.25
Go/No-Go → Emotional eating	0.01	0.14	-0.27	0.29
Caregiving quality 5w → Go/No-Go	0.39*	0.19	0.01	0.77

Supplementary Table 7.21. (continued).

Caregiving quality 12m → Go/No-Go	0.04	0.34	-0.62	0.70
Caregiving quality 2.5y → Go/No-Go	0.13	0.63	-1.10	1.37
Caregiving quality 10y → Go/No-Go	-0.19	0.43	-1.04	0.67
Caregiving quality 14y → Go/No-Go	0.09	0.31	-0.52	0.69
<b>Partial mediation</b>				
Caregiving quality 5w → Go/No-Go → Emotional eating	0.00	0.06	-0.11	0.11
Caregiving quality 12m → Go/No-Go → Emotional eating	0.00	0.01	-0.01	0.01
Caregiving quality 2.5y → Go/No-Go → Emotional eating	0.00	0.02	-0.04	0.04
Caregiving quality 10y → Go/No-Go → Emotional eating	0.00	0.03	-0.05	0.05
Caregiving quality 14y → Go/No-Go → Emotional eating	0.00	0.01	-0.02	0.02
<b>Full mediation</b>				
Caregiving quality 5w → Go/No-Go → Emotional eating ← Caregiving quality 5w	0.24	0.33	-0.41	0.89
Caregiving quality 12m → Go/No-Go → Emotional eating ← Caregiving quality 12m	-0.36	0.58	-1.49	0.77
Caregiving quality 2.5y → Go/No-Go → Emotional eating ← Caregiving quality 2.5y	1.03	1.07	-1.07	3.13
Caregiving quality 10y → Go/No-Go → Emotional eating ← Caregiving quality 10y	0.01	0.74	-1.45	1.46
Caregiving quality 14y → Go/No-Go → Emotional eating ← Caregiving quality 14y	-0.78	0.53	-1.82	0.25

**Exploratory model 6 Caregiving quality, Monetary choice, Emotional eating**

<b>Direct effect</b>				
Caregiving quality 5w → Emotional eating	0.25	0.33	-0.40	0.90
Caregiving quality 12m → Emotional eating	-0.37	0.58	-1.50	0.76
Caregiving quality 2.5y → Emotional eating	1.03	1.07	-1.07	3.12
Caregiving quality 10y → Emotional eating	0.03	0.74	-1.42	1.49
Caregiving quality 14y → Emotional eating	-0.81	0.53	-1.85	0.24
Monetary choice → Emotional eating	-0.42	1.19	-2.74	1.91
Caregiving quality 5w → Monetary choice	0.03	0.02	-0.02	0.07
Caregiving quality 12m → Monetary choice	-0.02	0.04	-0.10	0.06
Caregiving quality 2.5y → Monetary choice	0.00	0.08	-0.15	0.15
Caregiving quality 10y → Monetary choice	0.05	0.05	-0.05	0.15
Caregiving quality 14y → Monetary choice	-0.06	0.04	-0.13	0.01
<b>Partial mediation</b>				
Caregiving quality 5w → Monetary choice → Emotional eating	-0.01	0.03	-0.08	0.05
Caregiving quality 12m → Monetary choice → Emotional eating	0.01	0.03	-0.05	0.07
Caregiving quality 2.5y → Monetary choice → Emotional eating	0.00	0.03	-0.06	0.06
Caregiving quality 10y → Monetary choice	-0.02	0.06	-0.14	0.10

Supplementary Table 7.21. (continued).

→ Emotional eating				
Caregiving quality 14y → Monetary choice	0.03	0.07	-0.12	0.17
→ Emotional eating				
<b>Full mediation</b>				
Caregiving quality 5w → Monetary choice	0.24	0.33	-0.41	0.89
→ Emotional eating ← Caregiving quality 5w				
Caregiving quality 12m → Monetary choice	-0.36	0.58	-1.49	0.77
→ Emotional eating ← Caregiving quality 12m				
Caregiving quality 2.5y → Monetary choice I	1.03	1.07	-1.07	3.12
→ Emotional eating ← Caregiving quality 2.5y				
Caregiving quality 10y → Monetary choice	0.01	0.74	-1.44	1.46
→ Emotional eating ← Caregiving quality 10y				
Caregiving quality 14y → Monetary choice	-0.78	0.53	-1.81	0.25
→ Emotional eating ← Caregiving quality 14y				

SE: Standard Effect, CI: Confidence interval, LL: Lower limit, UL: Upper limit, 5w: five weeks, 12m: 12 months, 2.5y: 2.5 years, 10y: 10 years, 14y: 14 years, \* $p<0.05$ .

Supplementary Table 7.22. Exploratory mediation models with the caregiving scores combined.

Model description	Effect (beta)	SE	95% CI	
			LL	UL
<b>Exploratory model 7 Caregiving quality composite, IC BRIEF, Diet quality</b>				
Direct effect				
Caregiving quality composite → Diet quality	-3.99	2.66	-9.20	1.21
IC BRIEF → Diet quality	-1.54	3.13	-7.68	4.60
Caregiving quality composite → IC BRIEF	0.08	0.07	-0.07	0.22
Partial mediation				
Caregiving quality composite → IC BRIEF → Diet quality	-0.12	0.26	-0.64	0.40
Full mediation				
Caregiving quality composite → IC BRIEF → Diet quality ← Caregiving quality composite	-4.11	2.65	-9.30	1.08
<b>Exploratory model 8 Caregiving quality composite, IC composite, Diet quality</b>				
Direct effect				
Caregiving quality composite → Diet quality	-3.46	2.41	-8.18	1.26
IC composite → Diet quality	5.46*	2.33	0.91	10.02
Caregiving quality composite → IC composite	-0.12	0.10	-0.31	0.08
Partial mediation				
Caregiving quality composite → IC composite → Diet quality	-0.65	0.63	-1.89	0.60
Full mediation				
Caregiving quality composite → IC composite → Diet quality ← Caregiving quality composite	-4.11	2.44	-8.89	0.67
<b>Exploratory model 9 Caregiving quality composite, IC BRIEF, Emotional eating</b>				
Direct effect				
Caregiving quality composite → Emotional eating	-0.41	1.39	-3.13	2.31
IC BRIEF → Emotional eating	0.07	1.69	-3.24	3.37
Caregiving quality composite → IC BRIEF	0.04	0.07	-0.10	0.17
Partial mediation				
Caregiving quality composite → IC BRIEF → Emotional eating	0.00	0.06	-0.12	0.13
Full mediation				
Caregiving quality composite → IC BRIEF → Emotional eating ← Caregiving quality composite	-0.41	1.39	-3.12	2.31
<b>Exploratory model 10 Caregiving quality composite, IC composite, Emotional eating</b>				
Direct effect				
Caregiving quality composite → Emotional eating	-0.22	1.40	-2.95	2.52
IC composite → Emotional eating	1.27	1.30	-1.28	3.81
Caregiving quality composite → IC composite	-0.15	0.09	-0.32	0.03
Partial mediation				
Caregiving quality composite → IC composite → Emotional eating	-0.19	0.22	-0.63	0.25

Supplementary Table 7.22. (continued).

Full mediation

Caregiving quality composite → IC composite →	-0.50	1.38	-3.20	2.21
Emotional eating ← Caregiving quality composite				

Note that the BRIEF is reverse scored to align with our inhibitory control measures. Hence higher scores on the BRIEF indicate better inhibitory control. \* $p<0.05$ , CI: Confidence interval, LL: Lower limit, UL: Upper limit, IC: Inhibitory control, BRIEF: Behavior Rating Inventory of Executive Functions.

# **Chapter 7**

## **Appendices**

Nederlandse samenvatting

Research data management statement

Acknowledgements

Curriculum Vitae

Donders Graduate School

## Nederlandse samenvatting

Dit proefschrift bevat cross-sectionele en longitudinale onderzoeken die verbanden tussen voeding en gedrag onderzochten. Voor gedrag is er onder andere specifiek gekeken naar executieve functies en inhibitievermogen. Executieve functies zijn belangrijke processen die plaatsvinden in het brein om doelgerichte handelingen zo efficiënt mogelijk uit te voeren. Hierbij kan men bijvoorbeeld denken aan het bakken van een taart: wanneer de oven wordt aangezet voordat het beslag wordt gemaakt, dan is de oven al op temperatuur wanneer het beslag klaar is. Inhibitie, ofwel het vermogen om impulsen te beheersen, speelt een belangrijke rol in deze executieve functies.

De onderzochte verbanden in dit proefschrift reiken van het vroege leven tot de adolescentie. De darmbacterie-brein as, ofwel de communicatieroute tussen de darmbacteriën en het brein, is een belangrijk mechanisme dat de verwachte verbanden zou kunnen verklaren. Het eerste doel van dit proefschrift was om de relaties te onderzoeken tussen borstvoedingsfactoren en gedrag bij peuters. Het tweede doel was om de relaties te onderzoeken tussen darmbacteriën en gedrag bij peuters. Het derde doel was om de rol van de kwaliteit van de zorg van de moeder, meerdere keren gemeten tussen geboorte van het kind en de adolescentie, in het voedingsgedrag van adolescenten te onderzoeken.

In **hoofdstuk 2** is onderzocht of de lengte van de borstvoedingsperiode, ofwel borstvoedingsduur, het inhibitievermogen van een peuter voorspelt. Vervolgens is onderzocht of de dieetkwaliteit van een peuter een tussenrol speelt in deze voorspelling. In de eerste drie jaren na de bevalling, hebben moeders de borstvoedingsduur bijgehouden. Op driejarige leeftijd is het inhibitievermogen van het kind in kaart gebracht met behulp van vier verschillende gedragstaken. Ook zijn er vragenlijsten bij beide ouders afgenummerd om het gedrag van het kind in kaart te brengen. De voedingsvragenlijst over de voedingsinname van de peuters is ingevuld door één van de ouders. Er is geen bewijs

gevonden voor een verband tussen borstvoedingsduur en inhibitievermogen. Resultaten van voorgaand onderzoek op dit onderwerp liepen al uiteen, waarschijnlijk onder meer door het gebruik van verschillende meetmethoden. Net als voorgaand onderzoek wees ons onderzoek wel uit dat langere borstvoedingsduur een betere dieetkwaliteit van de peuters voorspelt. Het is echter niet duidelijk wat het mechanisme achter dit verband is. Hoe belangrijk moeders gezonde voeding vinden is mogelijk een belangrijke speler in dit verband.

In **hoofdstuk 3** is er onderzocht of humane melk oligosachariden (HMOs), de executieve functies en het inhibitievermogen van peuters voorspelt. HMOs zijn complexe suikers die aanwezig zijn in moedermelk. Moeders hebben hiervoor op twee, zes en 12 weken een kleine hoeveelheid melk verzameld. Van deze melk is de HMO-samenstelling geanalyseerd. Dezelfde meetmethoden benoemd in hoofdstuk 2 zijn gebruikt om executieve functies en inhibitie bij de peuters te meten. Resultaten lieten zien dat hoge niveaus van gefucosyleerde HMOs gerelateerd zijn aan betere executieve functies bij peuters. Er is geen bewijs gevonden voor een verband tussen gesialyleerde HMOs en executieve functies bij peuters. Onze resultaten wat betreft gefucosyleerde HMOs komen overeen met voorgaand soortgelijk onderzoek in dieren en mensen. Onze resultaten over gesialyleerde HMOs komen gedeeltelijk overeen met soortgelijke studies. Dit komt omdat er uiteenlopende resultaten zijn gevonden in voorgaand onderzoek. Deze verschillen zijn te verklaren door het gebruik van verschillende onderzoeksmethoden en de leeftijden waarop het gedrag van de kinderen is gemeten. Dit is het eerste onderzoek bij mensen dat HMOs heeft gemeten op drie tijdstippen binnen de eerste drie maanden. Replicatie van dit onderzoek is daarom belangrijk.

In **hoofdstuk 4** zijn de relaties tussen darmbacteriën en executieve functies (inclusief inhibitievermogen) van peuters onderzocht. Dezelfde meetmethoden benoemd in hoofdstuk 2 zijn gebruikt om de executieve functies en inhibitie te meten. Op twee, zes en 12 weken en op één en drie jaar, is de compositie van de darmbacteriën van

het kind geanalyseerd. Er zijn verbanden gevonden tussen hogere niveaus van *Streptococcus*, [*Ruminococcus*] *Torques* groep, *Clostridium sensu stricto* 1, *Intestinibacter*, en *Halomonas* en verminderde executieve functies bij peuters. Een hoger niveau van *Bacteroides*, *Parabacteroides*, *Ruminococcus* 2, en *Blautia* en een hogere diversiteit aan verschillende soorten darmbacteriën bleken gerelateerd aan betere executieve functies. Hogere niveaus van *Bacteroides*, *Ruminococcaceae* UCG-013 en *Veillonella* voorspelden betere inhibitievermogen. Hogere niveaus van *Subdoligranulum*, *Lachnospiraceae* NK4A136, *Anaerostipes*, *Sutterella* en *Coprococcus* 3 voorspelden verminderde inhibitievermogen in peuters. Resultaten van voorgaande onderzoeken overlappen gedeeltelijk met de bevindingen van dit proefschrift. Zo heeft eerder onderzoek ook een verband gevonden tussen *Bacteroides* en beter inhibitievermogen. Er zijn echter ook verbanden gevonden die niet in voorgaand onderzoek naar voren kwamen. Verschillen tussen de resultaten van ons onderzoek en eerder onderzoek komt mede doordat er sprake is van verschillende leeftijden en gedragsmaten die zijn onderzocht. Meer (replicatie) onderzoek is nodig om de gevonden relaties te bevestigen en de bewijskracht te versterken.

In **hoofdstuk 5** zijn de voorspellers van de kwaliteit van voeding van adolescenten onderzocht. Kwaliteit van zorg van de moeder is onderzocht op de kinderleeftijden van vijf weken, 12 maanden, twee-en-een-half jaar, 10 jaar en 14 jaar. Dit is onderzocht aan de hand van video's van interacties tussen moeder en kind die door onafhankelijke beoordelaars scores hebben gekregen. Voedingsinname en emotie-eten van adolescenten is middels zelfrapportage verzameld. Verder is het inhibitievermogen van de adolescent gemeten met behulp van drie gedragstaken en een vragenlijst die is ingevuld door de moeder. Er is geen bewijs gevonden voor maternale zorgkwaliteit en inhibitievermogen of dieetkwaliteit. Wel is er bewijs gevonden voor een verband tussen betere inhibitievermogen en betere dieetkwaliteit bij adolescenten. Toekomstig onderzoek zou (zelf)rapportage en objectieve observaties moeten combineren om een beter beeld te

krijgen over kwaliteit van de zorg van moeders (en partners) en hoe dat relateert aan het gedrag van adolescenten (voedingsinname en inhibitievermogen). Langlopende en experimentele onderzoeken zijn nodig om de richting van de verbanden te achterhalen.

Samenvattend, specifieke suikers in moedermelk en bepaalde darmbacteriën voorspellen betere executieve functies bij peuters. Tevens is er een verband gevonden tussen het inhibitievermogen en de dieetkwaliteit van een adolescent. Ondanks dat deze bevindingen geen oorzakelijke verbanden kunnen aantonen, wijzen de resultaten erop dat voeding in het vroege leven en de darmbacteriën mogelijk een rol spelen in de executieve functies en het inhibitievermogen van peuters. Daarnaast suggereren de resultaten dat er samenspel is tussen inhibitievermogen en voedingsinname tijdens adolescentie.

Belangrijkste bevindingen van dit proefschrift:

- Langere borstvoedingsduur voorspelt niet het inhibitievermogen van een peuter, maar wel betere dieetkwaliteit van de peuter op de leeftijd van drie jaar.
- Hogere concentraties van gefucusyleerde HMOs in moedermelk voorspellen betere executieve functies op peuterleeftijd.
- We vonden geen bewijs voor een verband tussen gesialyleerde HMOs in moedermelk en executieve functies op peuterleeftijd.
- Hogere niveaus van de darmbacterieën *Streptococcus*, [*Ruminococcus*] *Torques* groep, *Clostridium sensu stricto* 1, *Intestinibacter*, en *Halomonas* zijn gerelateerd aan verminderde executieve functies in peuters.
- Hogere niveaus van de darmbacterieën *Bacteroides*, *Parabacteroides*, *Ruminococcus* 2 en *Blautia* en hogere diversiteit aan verschillende soorten darmbacteriën zijn gerelateerd aan betere executieve functies in peuters.
- Hogere niveaus van de darmbacterieën *Bacteroides*, *Ruminococcaceae* UCG-013 en *Veillonella* voorspellen beter inhibitievermogen in peuters.

- Hogere niveaus van de darmbacterieën *Subdoligranulum*, *Lachnospiraceae* NK4A136, *Anaerostipes*, *Sutterella* en *Coprococcus* 3 voorspellen verminderd inhibitievermogen in peuters.
- Beter inhibitievermogen van adolescenten is gerelateerd aan betere dieetkwaliteit.
- Er is geen bewijs gevonden dat de zorgkwaliteit van de moeder tijdens de kindertijd de inhibitie en dieetkwaliteit van adolescenten voorspelt.

## Research Data Management Statement

### Ethics

The BINGO and BIBO study were conducted in accordance with the 1964 Declaration of Helsinki and its later amendments. No formal objections were made against the study protocol of the BINGO study (ECSW2014-1003-189, and ECSW-2018-034) and the BIBO study (SW2017-1303-497, SW2017-1303-498, and ECSW-2018-067) by the ethics committee of the Social Science faculty of the Radboud University, Nijmegen, the Netherlands. A written informed consent was obtained from all participants regarding the use and storage of their data. Participants were informed that they may decide to discontinue the study at any moment, without giving a reason. This research was supported by the European Union's Horizon 2020 Eat2beNice grant (728018 to C. de Weerth and A. Arias Vásquez), a Jacobs Foundation Advanced Research Fellowship (to C. de Weerth), and a Netherlands Organization for Scientific Research VENI grant (016.195.197 to R. Beijers), VIDI grant (575-25-009 to C. de Weerth) and VICI grant (016.Vici.185.038 to C. de Weerth).

### FAIR principles

#### 1. Findable

All data from the BINGO and BIBO study, including the raw, cleaned, and master data are stored at the secure network drive of the Donders Institute for Brain, Cognition, and Behavior. The pseudonymization key is included in a subfolder of the BINGO and BIBO folder. Physical data, indicating paper data, are stored in the locked archive of the department of Cognitive Neuroscience at the Donders Institute for Brain, Cognition, and Behavior.

#### 2. Accessible

The data and research documentation are only accessible to researchers involved in the BINGO and/or BIBO project, and to the Developmental Psychobiology (DPB) lab

manager. The data are not freely available since we did not ask participants for consent to store their data in a public online depository. Researchers may ask for permission for the re-use of the data with a methodologically sound proposal. The proposal to access the BINGO and/or BIBO should be directed to carolina.deweert@radboudumc.nl. If approved, data requestors need to sign a data transfer agreement or research collaboration agreement, depending on the level of collaboration. The anonymous processed data will be shared with the collaborator, and researchers are asked to analyze the data and/or publish the results within two years.

### **3. Interoperable**

Documentation on the set-up of the BINGO and BIBO study can be found in the BINGO and BIBO folder and published papers. Results are reproducible and interpretable as the data, documentation files, and R scripts for the papers described in the current thesis are stored at the secure network drive of the Donders Institute for Brain, Cognition, and Behavior.

### **4. Reusable**

All data will be stored for at least 15 years from moment of data collection and can be reused within this period, as stated in the informed consent forms.

### **Privacy**

The privacy of the BINGO and BIBO study participants was guaranteed by pseudonymization. The pseudonymization key that linked the code to personal data was stored on the secure network drive of the Donders Institute for Brain, Cognition, and Behavior in separate folders for the BINGO and BIBO studies. This key is only accessible to the DPB lab manager, and researchers that are involved in the project depending on their role. To contact participants for new measurement waves, the pseudonymization key was not destroyed since the BINGO study is halted, and may continue, and the BIBO study is currently ongoing. If data is shared, no personal data (e.g., addresses, videos with participant faces) will be shared.

## Acknowledgements

It is difficult to describe how I feel about everyone who has been with me in this journey towards getting my doctorate degree. However, I will do my best to put my feelings into words!

First and foremost, thank you **Carolina** for giving me the opportunity to perform research in your lab! Although you might be notoriously famous for your “RBF” ;), I felt that it did not represent how you are as a promotor and a person. Your compassionate guidance and commitment to the improvement of your students have shaped me into the scientist that I am today. Your eye for detail, scientific knowledge, and critical thinking showed me that I have had a professional and experienced promotor on my side. I am fortunate to have had you as my mentor, or rather, a science mom. :)

**Roseriet**, as my co-promotor, you have been a gigantic help throughout this entire journey. Details on projects were easy for you to remember, which made me feel at ease knowing that you were extremely involved in all phases of my PhD track. Your meticulous mind and pragmatic thinking were a great combination of skills that helped me make important decisions. Thank you! Both you and Carolina are hard workers, and you both have also taught me the value of work-life balance. I think I have grown the most in my life during the years that I was under both your supervision, on a professional as well as personal level.

**Alejandro**, as my co-promotor, you've been supportive of me since the start of my PhD track. Although our contact was limited, your support came at the right times when situations seemed challenging, or even gloomy. I am grateful for the opportunities you facilitated for me to engage with colleagues both within and beyond the Radboud community. The experience in Rome was unforgettable.

Major gratitude goes to **every single participant of the BINGO and BIBO study!** The completion of this dissertation would have been impossible without your commitment, excitement, and dedication. BINGO was such a wonderful first experience with human data collection! Every single toddler was a pleasure to work with. During the COVID pandemic, my life took a somber turn as I missed the human interactions.

I therefore felt truly fortunate to have the opportunity to visit all BIBO participants, with each one of you adding an extra touch of sunshine to my life.

Thanks to the other co-authors of my papers, **Henk Schols**, **Fangjie Gu**, **Clara Belzer**, and **Hauke Smidt**, whose expertise and input were extremely valuable in guiding our research and in understanding what our data was showing us and how it could be interpreted. Special thanks go to **Jeanne de Vries** and **Corine Perenboom** for their advice and help regarding the assessment of dietary intake.

My PhD journey started at the Developmental Psychology department at the Radboud University in the first 2 years. I have had warm interactions with many who are already continuing their professional journey. **Christine**, your initiation of the BINGO study set the stage for an incredible journey. Thank you so much! **Bonnie**, your quirkiness was refreshing. You showed me that being yourself is the strongest asset one can express. **Pamela**, you are a kind-hearted colleague whose calmness and knowledge were inspirational. **Kelly**, as you always provided a listening ear, your kindness never went unnoticed. It was always good to see you. **Maartje**, of the few interactions that we've had, you struck me as a kind and gentle person. Thanks for handing BIBO over to me :) **Anouk**, thank you for your advice and knowledge about executive functions, and the shared stories. I would also like to thank **Yvonne van den Berg**, **Toon Cillessen**, **Bill Burk**, **Tessa Lansu**, **Remco**, **Sterre**, **Nicole**, **Jesse**, **Ilja**, **Nina**, **Lisan**, and **Geert** for making me feel welcome at the department at the Radboud University (and thanks to the latter 3 for being my brief tennis partners!). I also want to thank **Brianna**, **Daria**, and **Esther** for including me in their activities during the first year of my PhD (I still remember the tasty pumpkin bread!). Special thanks to **Julian** who helped me create a behavioural task in Psychopy for the BIBO study. **Peiying**, I always felt so comfortable with you talking about anything, and I had a lot of fun playing tennis with you! Hope you're doing well! **Kris**, thank you for your major support during this PhD journey!

My PhD journey continued at the Radboudumc. As our lab expanded, I had the pleasure of encountering many kind and intelligent people. **Irene**, my Paronymph, you were the first person that I felt connected to in our new-forming lab. Your presence, your humour, and your accent (:P) made me smile! I am delighted that we could share

our hardships and learnings in the past years. :) **Hellen**, my Paranympth, radiates a contagious brightness. I loved our conversations about science, sustainability, and more personal topics. I admire you and have learned invaluable lessons from our chats. :) **Yang**, my precious colleague and co-author, collaborating on our microbiota paper was a pleasure (despite the challenges we encountered!). Your admirable strength and kindness shine through, and I cherish the conversations we shared. Wishing you all the best in China! **Kathi**, it was so nice to have you as a colleague because of your bright and kind personality. I was happy to hear that you are pursuing something you truly enjoy. **Nicole**, you are the gentlest and kindest person I know. I very much enjoyed our random dinners together, and your BIBO knowledge tests, haha! I wish you all the best for your PhD! **Henrik**, you are intelligent, with a sense of humour and a down-to-earth nature. I am very thankful that I could always ask you microbiota-related questions and receive the most well-constructed answers. **Stefania**, you are such an intelligent and passionate person, and that makes you shine! It was so nice collaborating with you on our caregiving paper :) **Nina**, I can always count on you being at the office ;) I enjoyed our chats (and rants :P) about our PhD lives during lunch. **Evie**, I admire your strong, righteous, and gentle personality. It was always a pleasure to chat with you :) **Ana**, though we were situated in different buildings, it was always good to see you in our lab meetings and at other meet ups :) **Marjorie** and **Dafna**, we have not seen each other that much, but it was always fun and pleasant to chat with you!

Other colleagues, students, and research assistants have played a major role in my PhD trajectory! Special thanks to **Jana**, **Rosa**, and **Ilse** who spent a large amount of time helping me with the home visits, and data coding for BINGO and BIBO! You made my data collection time so much smoother, and much more fun! Thank you **Anna**, for your help setting up the BIBO 12.5 years round. It was a reassurance knowing that we had a brain expert by our side :). **Timothy**, thanks for your help with programming BIBO's curiosity task! Thank you **Els**, **Lisanne**, **Eefje**, **Annefleur**, **Ismay**, **Noortje**, **Hilde**, **Jasmijn**, **Danique**, and **Lonnieke** for your help with picking up samples, processing samples, preparing materials and/or entering and coding data for BINGO and BIBO, and the great conversations! Thanks to **Sofia** for helping with

the creation of the BIBOOK ;D It was such a comforting feeling to have you all by my side!

Other people walking around at the Donders were a major part of how I experienced my work life. **Vab, Casper** (/former Nijmegen tennis partner), **Carolina** (/moving partner), **Alejandro, Mariana, Sevgi, Lea, James, Emma** (/coffee break partner), **Michael, Claire, Angelos, and Shery** you have all been such great mood-makers during my time at the CNS department. Thank you all for the cosy lunches, shared food, and good/random/silly conversations. :) **Jo** and **Kübra**, two of my former 'Best Office Ever' mates, together with Irene, were such pleasant office mates to be around! Thanks for tolerating my phone calls to participants ;) I really enjoyed our dinners together. Let's do that again sometime! Of course, I want to thank **Erna, Inge, Annemarie**, and **Ellen** at the secretary! You have always been there to help me out. And thanks to **Nino** for your help with my administrative things (e.g., reminding me to fill in my hours hehe). Thanks to **Andrea** and **Max** from Betty and Mora for the tasty fresh Italian lunches I could always count on!

I would like to thank everyone outside the Radboud who has supported me during my PhD journey. To **Nard**, the first to believe in this PhD adventure, thank you for your unwavering belief and support! **Olga**, our conversations have helped me get through my darker days, thank you! **Dewi**, our annual life updates feel like a comforting tradition. I'm grateful to have you capturing my major life event. **Marjolein**, I loved our catch-ups every so often. Your empathy always made me feel comfortable to talk to you about everything. **Ivy Mok**, I enjoyed our chats and rants about life! I hope you are doing well.

I would like to thank **my colleagues at Danone Nutricia Research**, as the end my PhD journey partly overlapped with my start at this company within this amazing team. From the first moment, I felt very welcomed by everyone. All of your interest in my PhD research has made me feel recognised and extra proud. So thank you all, and especially **Raka, Nana, Elly, Loret**, and **Evelien**.

My most heartfelt gratitude goes to the closest people in my life, people who know best how this entire PhD journey impacted me. **Aaron**, we met quite close to the start

of my PhD and our conversations have been a constant source of comfort. **Ivy**, from elementary school age to adulthood, our occasional contact is a cherished comfort I can always count on. **Liselotte**, since the age of 12, you have always been by my side. I think we both have grown a lot. Thanks for hearing out about my PhD (and other) struggles and joys these past 6 years. **Maga**, throughout the challenges during this PhD, you have been my rock. Thank you for always being there. Of course, I want to thank **my parents** for being patient with me, and hearing out all my experiences during the past 6 years (and my entire life!). I'm excited to bring the first Doctor's title into the family. **Nishant**, you've been there with me at the end of my PhD journey, and have helped me tremendously in ways I cannot describe. Thank you for your unwavering support and love. I love you all!

Thank you all! Dank jullie wel! 謝謝大家!

## Curriculum Vitae

Yvonne Willemsen was born in Wageningen on December 6th, 1992. She obtained her Bachelor's degree of Nutrition and Dietetics, at the Hogeschool Arnhem en Nijmegen in Nijmegen, minoring in infant and child nutrition. To understand the science behind what was taught during her Bachelor's studies, she continued studying Nutrition and Health at Wageningen University & Research, where she completed two specializations: Molecular Nutrition & Toxicology and Nutritional Physiology & Health Status. For both these specializations, her theses focused on toddler, and child nutrition. Within this Master's track, she also did her internship at TNO where she wrote a review on gut microbiota, antibiotics use in early life, and its relations with obesity development. All these previous experiences contributed to her growing interest in the interactions between gut microbiota, nutrition, and health. She was granted an ideal fitting PhD position at the Radboud University (RU) and the Radboudumc (RUMC) in Nijmegen. Under the supervision of Prof. dr. Carolina de Weerth (RUMC), Dr. Roseriet Beijers (RU) and Dr. Alejandro Arias Vásquez (RUMC), she conducted research on (early life) nutrition, gut microbiota, and behaviour as described in this thesis.



## Donders Graduate School for Cognitive Neuroscience

For a successful research Institute, it is vital to train the next generation of young scientists. To achieve this goal, the Donders Institute for Brain, Cognition and Behaviour established the Donders Graduate School for Cognitive Neuroscience (DGCN), which was officially recognised as a national graduate school in 2009. The Graduate School covers training at both Master's and PhD level and provides an excellent educational context fully aligned with the research programme of the Donders Institute.

The school successfully attracts highly talented national and international students in biology, physics, psycholinguistics, psychology, behavioral science, medicine and related disciplines. Selective admission and assessment centers guarantee the enrolment of the best and most motivated students.

The DGCN tracks the career of PhD graduates carefully. More than 50% of PhD alumni show a continuation in academia with postdoc positions at top institutes worldwide, e.g., Stanford University, University of Oxford, University of Cambridge, UCL London, MPI Leipzig, Hanyang University in South Korea, NTNU Norway, University of Illinois, North Western University, Northeastern University in Boston, ETH Zürich, University of Vienna etc. Positions outside academia spread among the following sectors: specialists in a medical environment, mainly in genetics, geriatrics, psychiatry and neurology. Specialists in a psychological environment, e.g. as specialist in neuropsychology, psychological diagnostics or therapy. Positions in higher education as coordinators or lecturers. A smaller percentage enters business as research consultants, analysts or head of research and development. Fewer graduates stay in a research environment as lab coordinators, technical support or policy advisors. Upcoming possibilities are positions in the IT sector and management position in pharmaceutical industry. In general, the PhDs graduates almost invariably continue with high-quality positions that play an important role in our knowledge economy.

For more information on the DGCN as well as past and upcoming defenses please visit: <http://www.ru.nl/donders/graduate-school/phd/>

